TU Delft Delft University of Technology

MSc Project Steel Structures:

High Strength Steel Structures – FEM Validation Experiments

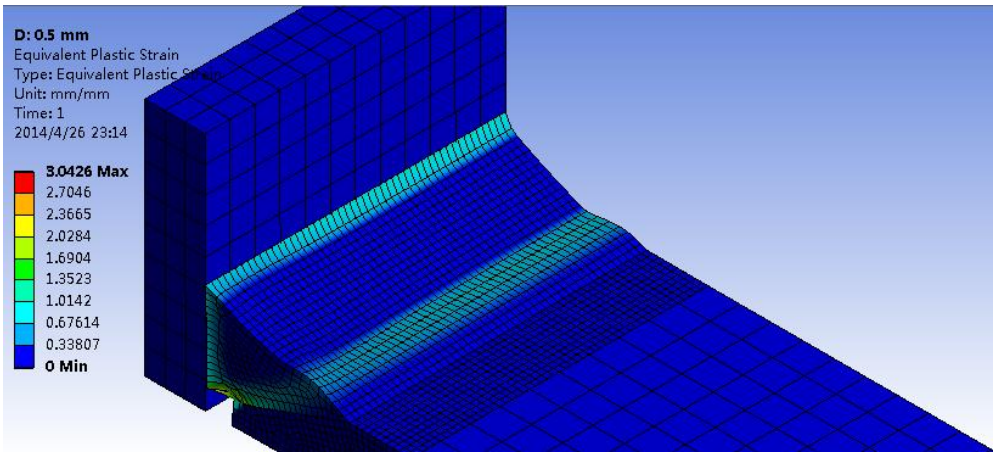

Yang Chen

Faculty CITG, Delft University of Technology

Delft, the Netherlands, 2014

Contents

Notations

A_0 – original cross sectional area

A_1 – deformed cross sectional area

E – modulus of elasticity

F – reaction force

K – strength coefficient

l – specimen length

n – exponent in Ramberg Osgood relation

np – strain hardening exponent

R_e – yield strength

R_u – ultimate strength

α_m – ratio of failure strain to ultimate strain

α_s – coefficient in parabolic relation of engineering stress strain based on the position of ultimate stress and failure stress

β_m – ratio of failure stress to ultimate stress

δ – longitudinal deformation

ε – strain

ε_{eng} – engineering strain

$\varepsilon_{eq,p}$ – equivalent plastic strain

ε_f – failure strain

ε_0 – characteristic failure strain

ε_{true} – true strain

ε_u – ultimate tensile strain

σ – stress

σ_{eng} – engineering stress

σ_{eq} – equivalent Von Mises stress

σ_h – hydrostatic stress

σ_{true} – true stress

v – Poisson ratio

List of figures

List of tables

1. Introduction

1.1 Background

Due to economic and technical advances, high strength steel (HSS) structures are more and more used. However, the fabrication and design of HSS structures need special attention and existing codes are lack of relevant design criterion (EN 1993-1-12 only gives additional rules to steel grades S500 to S690). Therefore a research project called *Integrity High Strength Steel Structures, IHSSS*, was carried out by TNO and Delft University of Technology for the investigation of the applicability of HSS with yield strength up to 1100 MPa.

Normally, HSS has a high yield to tensile strength ratio which means that the deformation capacity will be lower in connections and structural parts with (bolt) holes or other area reducing effects (e.g. fatigue cracks). Furthermore, for HSS, especially the one has yield strength as high as 1100 MPa, it cannot always be welded with overmatched weld material. Therefore the deformation capacity of these joints may be limited due to failure of the weld before yielding in the connection members occur. Because of these reasons, the safety of the structure is declined and the application of a fully plastic design for HSS is restricted. Therefore the deformation capacity of joints in HSS structures is essential and has been investigated in this project.

In the IHSSS research project, experiments had been carried out on three types of welded joints (Cross plate, X-joint with low stress concentration factor (SCF) and X-joint with high SCF). However, the FEM validation analyses had only been carried out for a limited number of joints. As a continuation on the basic FE-analyses, it is proposed to carry out validation analyses on other joint geometries.

1.2 Goal of the research

Based on the former research performed by TNO, the behavior of a welded joint of HSS can be nicely simulated by FEM. The aim of this master project is to continue the basic FE-analyses, cross comparison the FEM results with a modern commercial FEM software and carry out validation analyses on other joint types performed in the experiments. Then try to finalize a method to accurately predict both strength and deformation capacity for different types of (undermatched) welded joints for HSS by using FEM software.

1.3 Ductile failure criteria [7]

Ductile failure can be defined as a situation in which the plastic strains become too large. Therefore, this strain level is considered as the failure criterion. Obviously, failure depends on the material itself and the stress state (e.g. tension versus shear). High tensile stresses in all directions (high triaxiality) will result in a low deformation capacity. Previous researches show that the failure criterion of Lemaitre [1] provides decent results for high strength steel.

According to Lemaitre, failure occurs when the equivalent ("Von Mises") plastic strain ($\varepsilon_{eq.p}$) exceeds the failure strain (ε_f).

The material is described by the Poisson's ratio v (=0.3 for steel) and the characteristic failure strain ε_0 (taken 1.0 in this report).

Whether the stress-state is either one-dimensional or three-dimensional has a substantial influence. Therefore, triaxiality is introduced by including the hydrostatic pressure (σ_h) and the equivalent stress (σ_{eq}).

Therefore, Lemaitre describes the failure criterion for the equivalent plastic strain as follows [8]:

$$\varepsilon_f = \frac{\varepsilon_0}{\frac{9}{2}\cdot\frac{1-2\nu}{1+\nu}\cdot\left(\frac{\sigma_h}{\sigma_{eq}}\right)^2 + 1} \tag{1.1}$$

In which the hydrostatic pressure σ_h equals:

$$\sigma_h = \frac{1}{3}\cdot(\sigma_1 + \sigma_2 + \sigma_3) \tag{1.2}$$

Whereas the equivalent, stress equals:

$$\sigma_{eq} = \sqrt{\sigma_1^2 + \sigma_2^2 + \sigma_3^2 - \sigma_1\sigma_2 - \sigma_2\sigma_3 - \sigma_3\sigma_1} \tag{1.3}$$

And σ_h/σ_{eq} is the so-called triaxiality, the allowable plastic strain decreases with increasing triaxiality.

In previous analyses research, ε_0 values ranging from 0.4 to 1.0. These values were based on literature and can be regarded as a scatter band for ε_0 values in several steels. And the results showed that in general the overall deformation capacity does not vary much for the ε_0 values used [8].

Lemaitre's failure criterion can be visualized in Figure 1.1 [8]. By introducing triaxiality, Lemaitre's criterion can give a better prediction than a one-dimensional failure criterion.

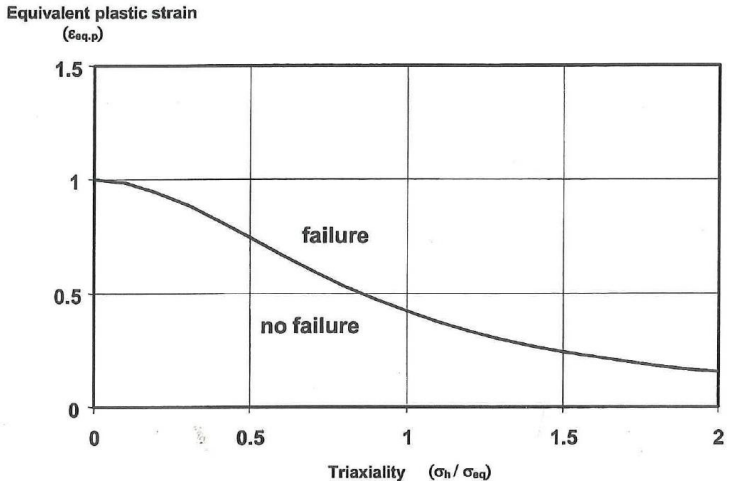

Figure 1.1: Failure criterion of Lemaitre with a characteristic failure strain

1.4 Approach

The approaches which are used in this report to solve the problem are listed as follows.

1) Literature study;
2) Study ANSYS;
3) Determine material behavior and input data for FE-analyses;
4) Model and simulate connections for Specimen series B;
5) Model and simulate connections for Specimen series C;
6) Compare the results and make conclusions.

2. Test overview

2.1 Joint geometry

The geometry tested in the experimental part must be practical and serve as a basis for the modeling at the same time. Therefore 3 different joints with and without an SCF are tested in the program.

The following geometry types are chosen (Figure 2.1-Figure 2.3) [3]:

- Type A: Cross plate connection with fillet welds loaded in shear
- Type B: X-joint with load carrying full penetration welds with low SCF
- Type C: X-joint with load carrying full penetration welds with high SCF

In type A the weld is loaded in shear. So there will be unequal stress distribution along the weld and at the end of the plates there is an SCF. In type B there are load carrying full penetration welds and there is no SCF along the weld. In type C there are also load carrying penetration welds. Due to the rotated connection of the transverse plate on each side of the connecting plate there is a high SCF along the weld.

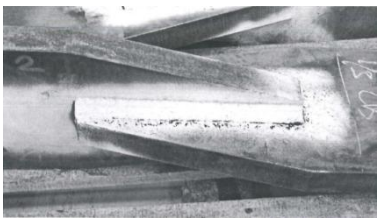

Figure 2.1: Cross plate connection (Specimen type A)

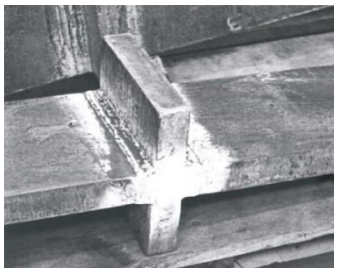

Figure 2.2: X-joint with low SCF (Specimen type B)

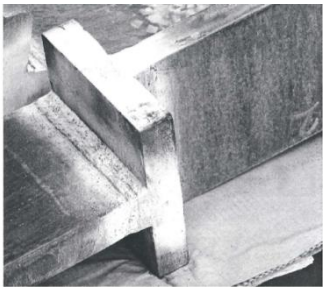

Figure 2.3: X-joint with high SCF (Specimen type C)

2.2 Test parameters

The variables to be investigated in the test program are:

- Specimen type (A, B and C, connection A will not be investigated in this report);
- Test type (static, fatigue and ratcheting, the latter two will not be investigated in this report);
- Material thickness (10/12 and 40 mm);
- Base material strength (690 and 1100 MPa);
- Relative weld strength (overmatched, only for S690 base material and undermatched, for both S690 and S1100 base materials).

A review of the test program including 48 tests is shown in Table 2.1 [4]. Each test series includes specimens of type A, B and C.

Table 2.1: Test plan

Test Series	Number of tests	Re base / MPa	Re weld / MPa	Plate/mm	Parameter
I/VII *	12	690	900	12/4	Reference
II	9	690	900	40	Thickness
III/VIII *	12	690	490	12/4	Under matched
IV	9	1100	900	10	High strength
V	6	1100	900	40	Thickness/ High strength

*: Results for A-type test specimens from Series I and A-type test specimens from Series III were included, even though these test specimens presented wrong fabrication. Series VII and VIII are substitutes of those specimens, and are also presented.

2.3 Static test procedure

In the static tests the specimens will be loaded until failure occurs. The tests will be displacement controlled in order to get a stable curve to failure. The main result will be a load-deformation curve (Figure 2.4) [3]. The strain gauges will be fixed on the specimen at specific locations for detailed information. As given in Figure 2.4, it is expected that for an overmatched weld the failure load and the deformation capacity will be higher.

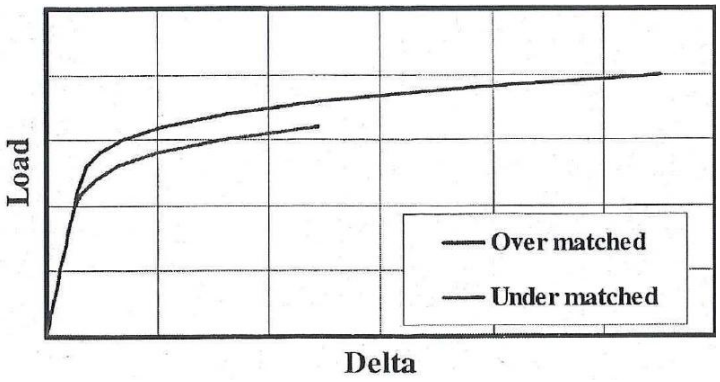

Figure 2.4: Static test

2.4 Test rig and measurements

Two servo hydraulic test rigs are available to load test specimen to failure. The capacity of these rigs are 600kN respectively 10000kN (Figure 2.5) [3]. Deformation of the weld and deformation of the whole connection of all test specimens can be locally tested by displacement transducers. Single strain gauges are used to measure the nominal stress in the connection plates. Strip strain gauges are used to obtain information about the strain development at the hot spot stress location of the welded connection. A typical example is shown in Figure 2.6 [3].

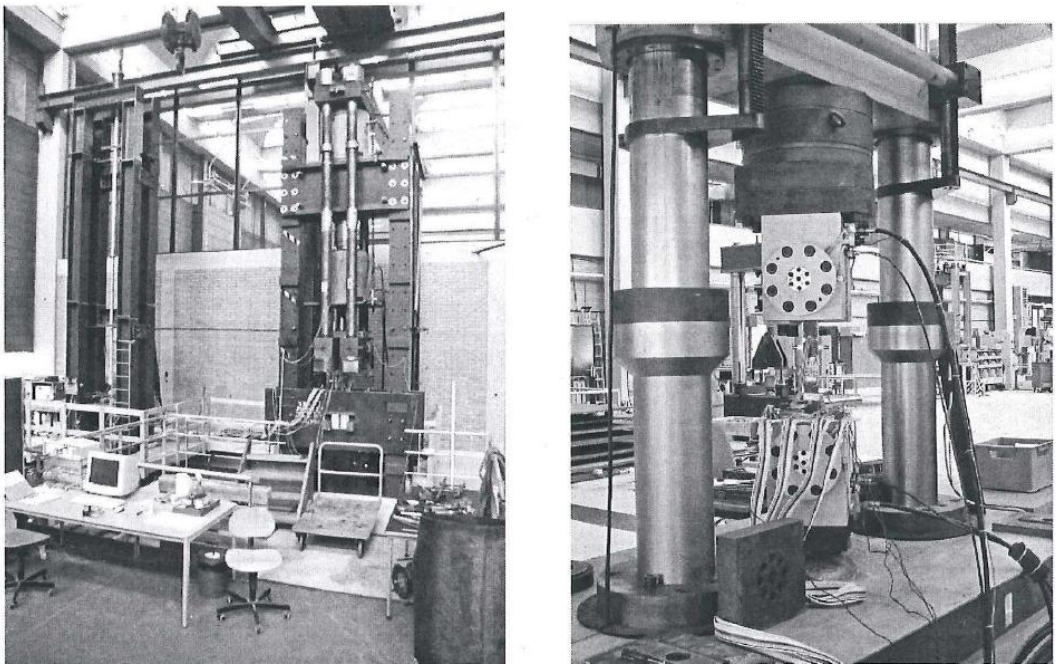

Figure 2.5: 10.000kN (left fig.) and 600kN (right fig.) test rig

Locally means that the measuring length includes the weld and the transverse plate (LVDT_1 and LVDT_2). The measuring length for the overall measurements is about 10 times the plate thickness (LVDT_3 and LVDT_4). Single strain gauges are used to measure the nominal stress in the connection plates. Strip strain gauges are used to obtain information about the strain development at the hot spot stress location of the welded connection.

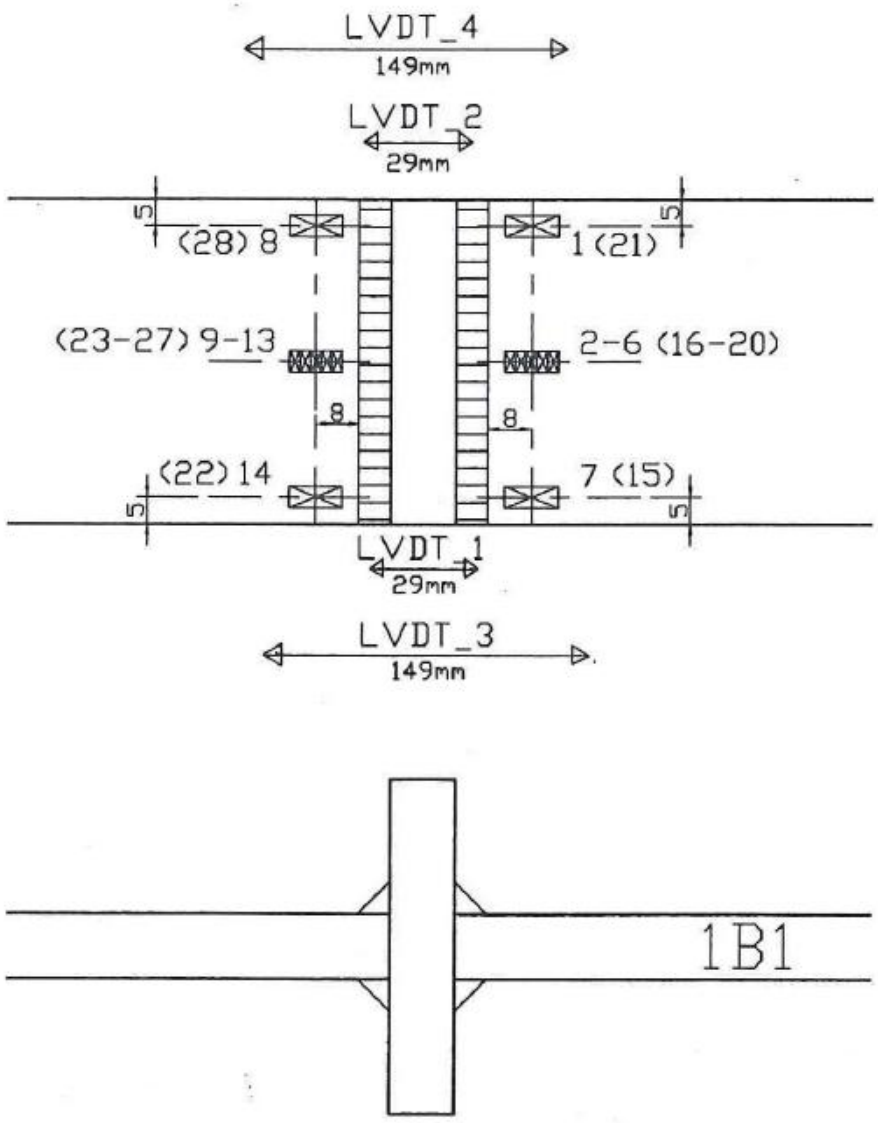

Figure 2.6: Instrumentation with strain gauges and displacement transducers

3. Material properties

3.1 Material specification

There are two parent materials (S690 and S1100) in the overall project. For the S690 material, there are both undermatched and overmatched welds. For the S1100 only undermatched weld is available. Real material properties like R_e, R_m and ε_u are available and used in developing the material input for FE-analyses. All the initial material properties are adopted from the TNO report [8], and given in Table 3.1.

Table 3.1: Material specifications

Specimen	Plate/weld	T [mm]	S [Mpa] O/U	R_e [Mpa]	R_m [Mpa]	ε_u [-]	K [Mpa]	np [-]
1	Plate	12	690	757	820	18%	1060	0.07
	Weld	Overmatched		864	1079	15%	1300	0.045
2	Plate	40	690	792	835	16.1%	1050	0.06
	Weld	Overmatched		864	1079	15%	1300	0.045
3	Plate	12	690	757	820	18%	1060	0.07
	Weld	Undermatched		500	600	15%	732	0.05
4	Plate	10	1100	1179	1432	11%	1500	0.003
	Weld	Undermatched		728	777	15%	950	0.05
5	Plate	40	1100	1106	1325	11%	1375	0.0001
	Weld	Undermatched		931	1061	14%	1250	0.037

Table 3.1 represents actual material behaviors under material tests and the load-displacement relation has been scaled into engineering stress-strain.

In order to perform geometrical and physical non-linear FE-analyses, ANSYS requires the so called true stress strain curve as an input. This curve is based on the material specifications described in Table 3.1 (parameters K and np will be used later in creating the true stress strain curve in the FE-analyses). In simulations of this report, same procedure and assumptions to make the curve will be used based on [8], and the elastic modulus E is taken as 210000 N/mm^2.

3.2 Material properties

3.2.1 Stress strain relation

As the first step, a simple stress strain relation is adopted. In this section, the same procedure and assumption based on [7] is used to create the material stress strain curve. S690 12 mm plate material properties from Table 3.1 are numerically simulated in this section. The engineering stress strain curve is generated from Ramberg-Osgood relation:

$$\varepsilon_{eng} = \frac{\sigma_{eng}}{E} + 0.002\left(\frac{\sigma_{eng}}{R_e}\right)^n \tag{3.1}$$

Where substitution of ultimate strength point (R_m at 1/3 εu) can result the parameter n.

Then based on engineering stress strain curves, true stress strain curves can be theoretically determined. ε_{eng} and σ_{eng} are taken from Equation 3.1.

$$\varepsilon_{true}=\ln(1+\varepsilon_{eng}) \tag{3.2}$$

$$\sigma_{true}=\sigma_{eng}(1+\varepsilon_{eng}) \tag{3.3}$$

The resulting stress strain curves are shown in Figure 3.1.

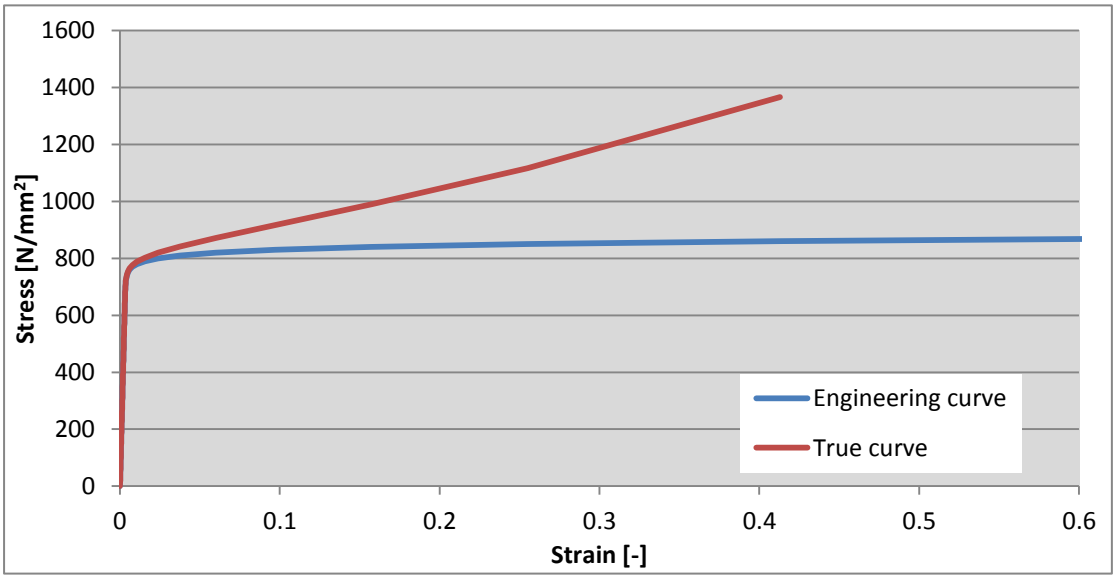

Figure 3.1: Visualization of the characteristic material data for S690

To validate the true stress strain curves obtained from previous work and test the nonlinear analysis of the numerical software, tensile simulations are performed using the commercial FE-software, ANSYS Workbench. These simulations are done in both 2D and 3D.

A very simple random size rectangular bar is tested. The analyses represent respectively plane stress, plane strain and 3D-full situation. Due to the symmetry of geometry and loading, only one-eighth of the material specimen is modeled (Figure 3.2).

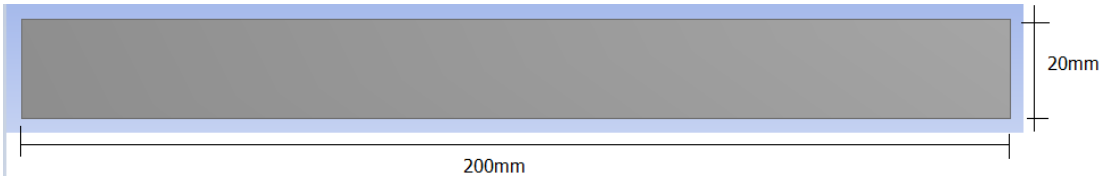

(a)

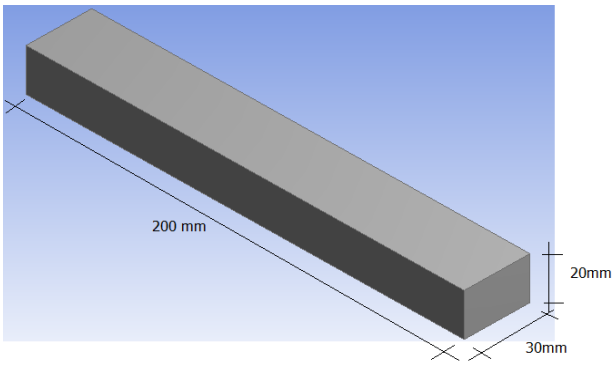

(b)

Figure 3.2: Geometry of simple coarse simulation
(a) 2D geometry, (b) 3D geometry

To include material nonlinearity, the true stress strain curve is used as the input. The isotropic hardening rule is chosen for materials. More details about hardening rule can be found in Appendix A.

For ANSYS, the input data requires both linear elastic material properties (black line, E & v) and metal plastic hardening data (red line, stress and plastic strain relation) (Figure 3.3, Figure 3.4):

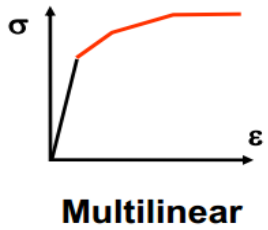

Figure 3.3: Multilinear isotropic hardening material input in ANSYS

For plastic hardening part, the plastic strain can be calculated from Equation 3.4.

$$\varepsilon_{plastic} = \varepsilon - \frac{\sigma}{E} \tag{3.4}$$

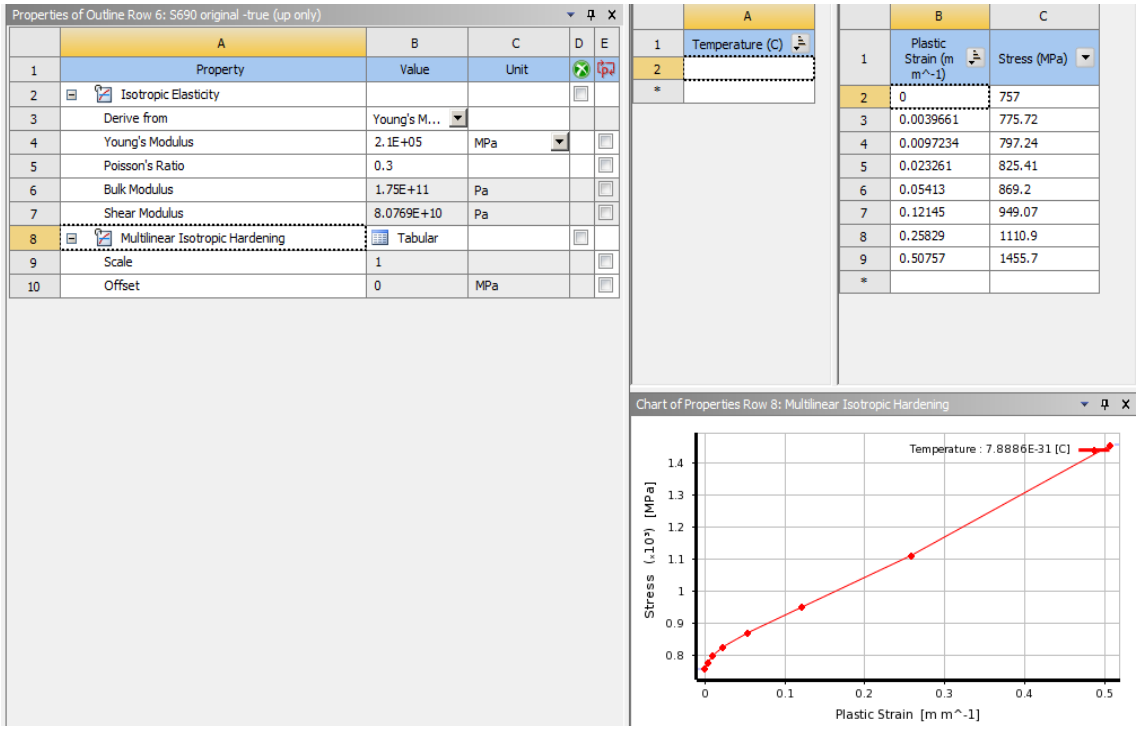

Figure 3.4: Material input

The mesh is automatically generated and there is no preference for the size of elements, SOLID 186 (20 nodes brick) element is used in all the analyses. In the analyses, large deflection is activated. The calculation procedure and time stepping method are program controlled. The boundary conditions are only applied in the area of symmetry. Finally, for the loading, displacement control is used where this load is increased gradually for each sub-step, and the total longitudinal displacement is given as 30 mm (Figure 3.5). In these analyses necking doesn't happen.

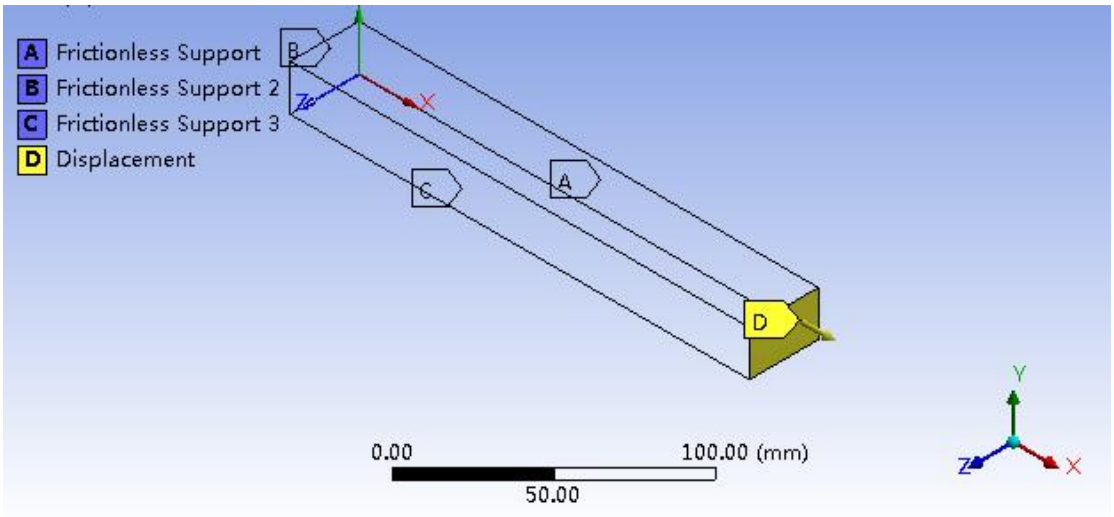

Figure 3.5: Boundary conditions

The "Frictionless Support" in ANSYS is used to restrain normal displacement, so it could be used on symmetrical area.

The resulting load-displacement curves are presented in Figure 3.6.

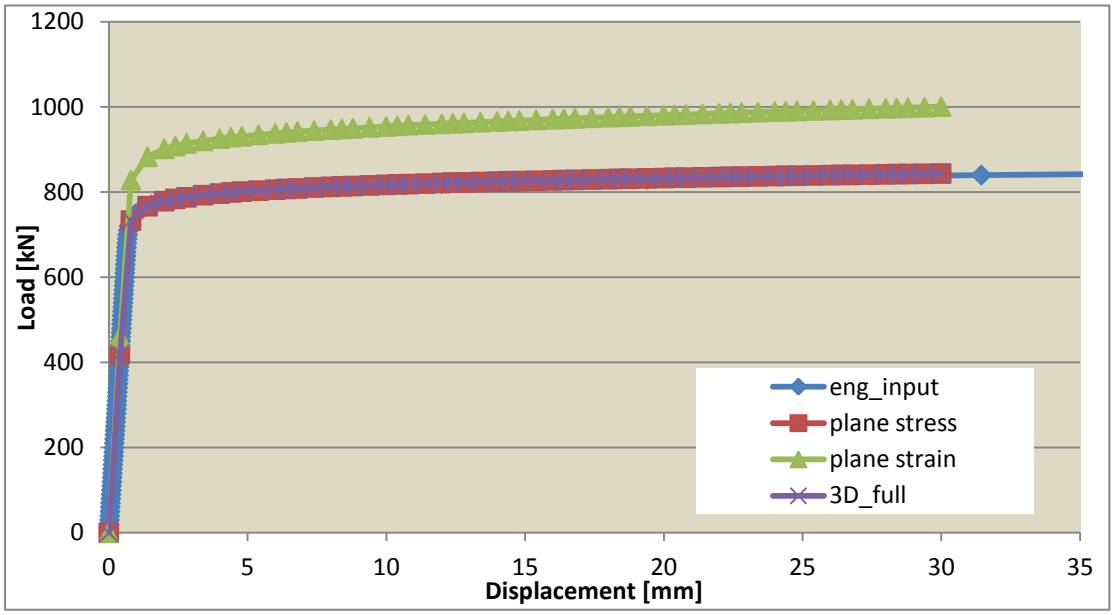

Figure 3.6: Load-displacement comparison

From Figure 3.6 it can be seen that:

1. In the elastic range the plane strain analysis is stiffer than the other analyses because lateral contraction is restricted;
2. The plane stress situation and 3D full situation are in good agreement with the engineering input data;
3. Because of the limitation of the material input and the geometry without imperfection, necking doesn't happen.

It is concluded that for this specific geometry and material input the plane stress and 3D full analyses can provide good results.

3.2.2 Modified stress strain relation

Then a more sophisticated stress strain relation is used to simulate a more realistic material behavior. This time a downward part is added to engineering stress strain relation after the stress reaches R_m. In this section, the same procedure and assumption based on [8] is used to create the material stress strain curve. The input data can be generated from the following steps.

Firstly, 3 points will be constructed based on Table 3.1. The first point is R_e positioned at strain ε_e. The second point is R_m at the assumed strain of one third of ε_u. The last one is the failure stress (approximately 0.6 R_m) at ε_u. The results are presented in Figure 3.7.

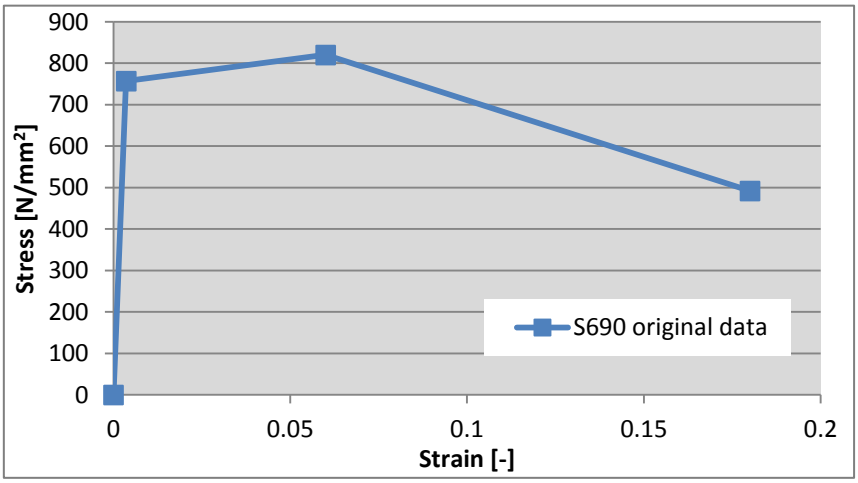

Figure 3.7: Visualization of the characteristic material data for S690 12mm plate

Then based on Figure 3.7, the engineering stress strain curve can be made. The steps to create this curve are described as follows.

1) Before the yield point, use the linear elastic relation.

$$\varepsilon_{eng} = \frac{\sigma_{eng}}{E} \tag{3.5}$$

2) The upward part of the curve can also be approximated by the Ramberg-Osgood relation.

$$\varepsilon_{eng} = \frac{\sigma_{eng}}{E} + 0.002\left(\frac{\sigma_{eng}}{R_e}\right)^n \tag{3.6}$$

Where substitution of R_m and 1/3 ε_u can result the parameter n.

3) The downward part can be approximated by a parabolic relation.

$$\sigma_{eng} = Rm - \alpha_s\left(\varepsilon_{eng} - \frac{\varepsilon_u}{3}\right)^2 \tag{3.7}$$

Where

$$\alpha_s = \frac{R_m(1-\beta_m)}{\varepsilon_u^2(1-\alpha_m)^2}$$

α_m=1/3; β_m=0.6

Finally, the true stress strain curve can be created based on engineering curve. The steps are as follows.

1) Before the yield point, same with the engineering curve (Eq. 3.5).

2) For the upward part, the true curve can be theoretically determined from the engineering curve. ε_{eng} and σ_{eng} are taken from Equation 3.6.

$$\varepsilon_{true}=\ln(1+\varepsilon_{eng}) \tag{3.8}$$

$$\sigma_{true}=\sigma_{eng}(1+\varepsilon_{eng}) \tag{3.9}$$

3) For the downward part a formula called Power Law is used to generate the true stress strain curve.

$$\sigma_{true}=K\varepsilon_{true}^{np} \tag{3.10}$$

Theoretically, parameters K and np can be determined by an iterative approach with the following steps:

1. Make an assumption for K and np in the Power Law;
2. Execute an FE-analysis resembling a tensile test;
3. Adapt the initial assumption for K and np to the outcome of the FE-analysis and start again at step 1 for the next iteration step.

In this section, the K and np are directly adopted from Table 3.1. The resulting stress strain curves are shown in Figure 3.8.

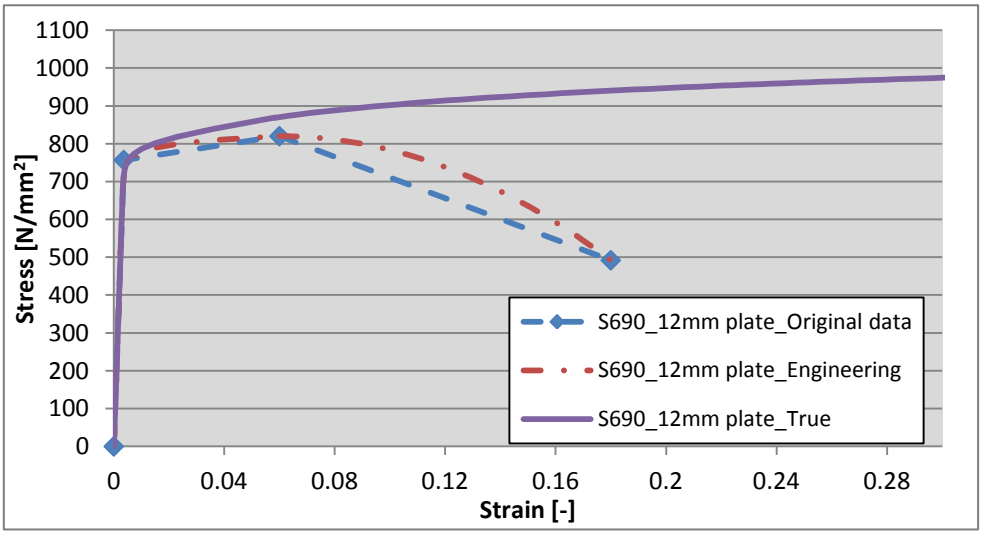

Figure 3.8: Resulting stress strain curves, S690 12mm plate

A flow chart to generate modified stress strain curves is given in Figure 3.9.

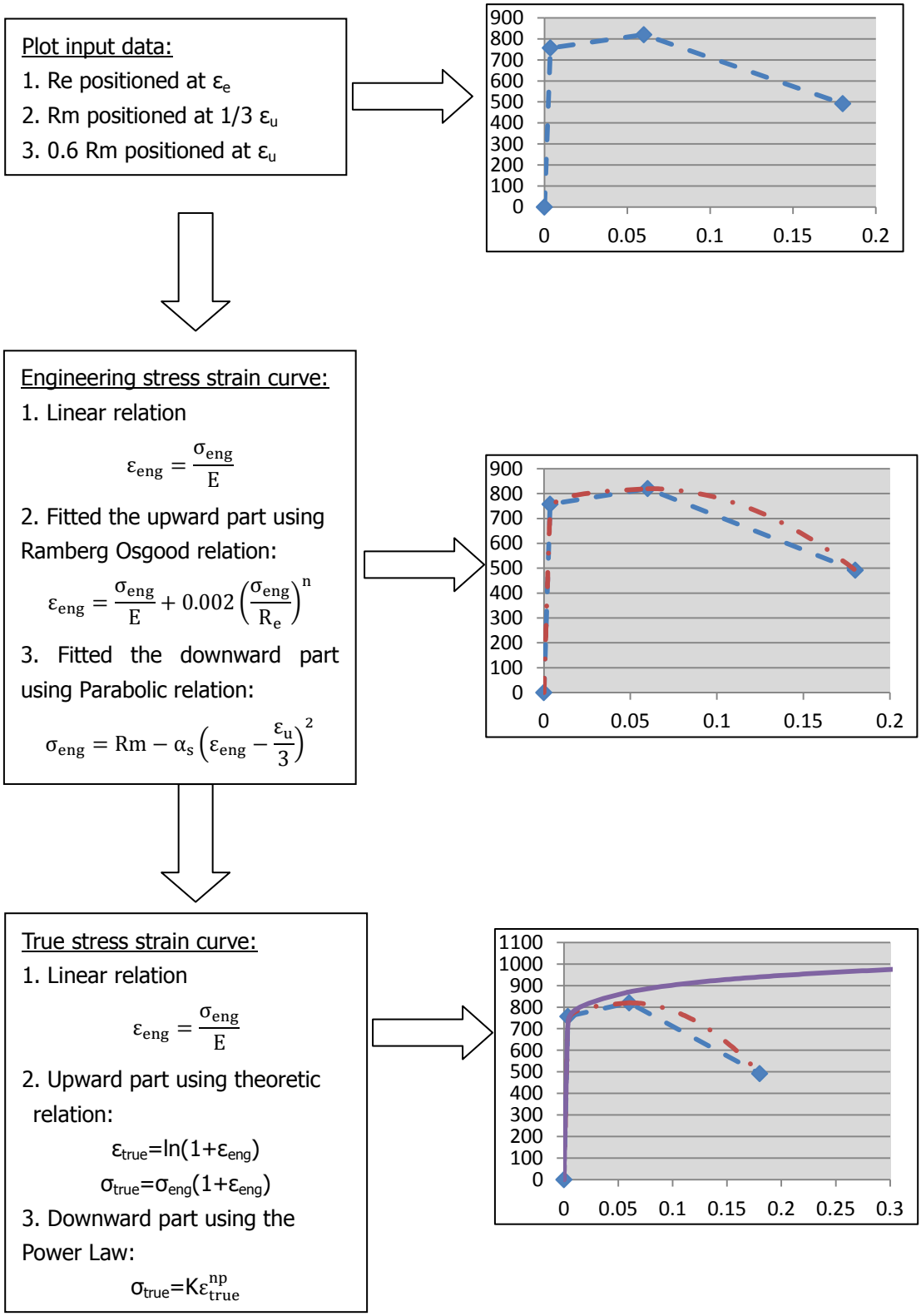

Figure 3.9: Flow chart for creating the modified true stress strain curve

The comparison of true stress strain curve input used in Section 3.2.1 and the modified curve based on S690 plate material is visualized in Figure 3.10.

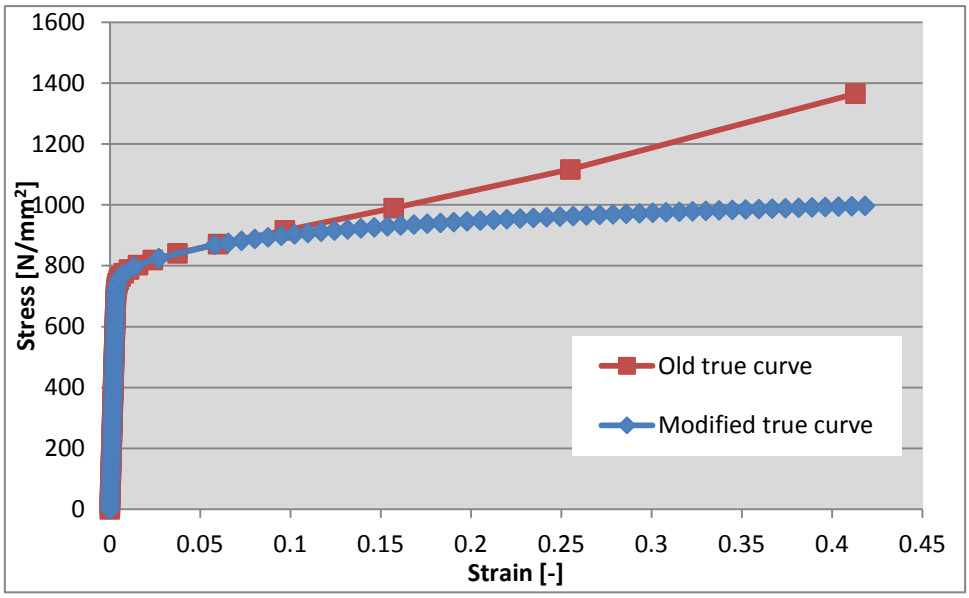

Figure 3.10: Comparison of true stress strain input

3.2.3 Tensile test simulation (without necking)

To validate the modified true stress strain curves obtained from the former section, tensile tests are performed as well.

The same geometries and boundary conditions as Section 3.2.1 are tested (Figure 3.11). The analyses also represent respectively plane stress, plane strain and 3D situation. The mesh is automatically generated.

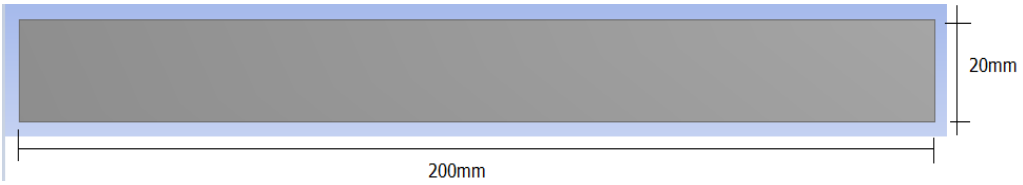

(a)

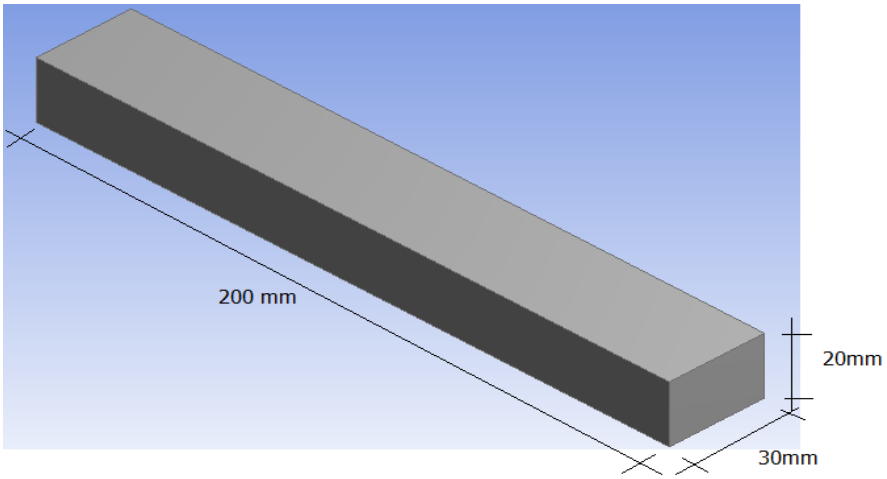

(b)

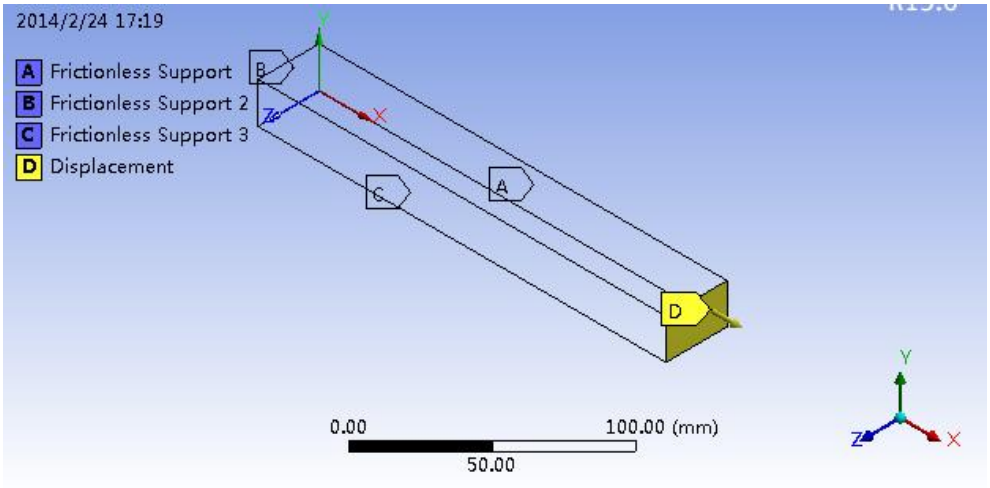

(c)

Figure 3.11: Simulation setup

(a) 2D geometry, (b) 3D geometry, (c) boundary conditions

The reaction force (F) has been scaled to the nominal engineering stress σ (=F/A_0, A_0 is the cross sectional area of the specimen before the test) in order to compare the results with engineering material inputs. Figure 3.12 presents the FEM results as well as the 12 mm S690 plate material engineering input.

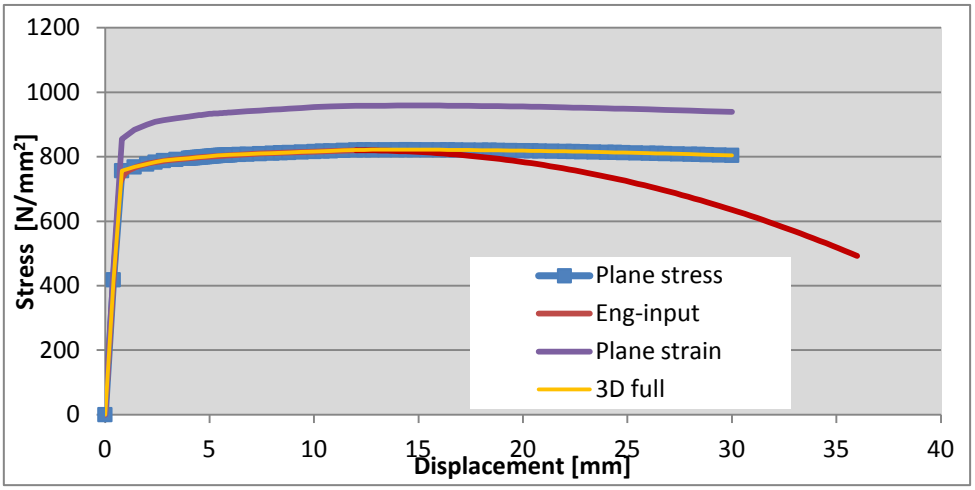

Figure 3.12: Comparison of engineering material input and FEM result, without necking

From Figure 3.12 we can see that

1) Same as before, in the elastic range the plane strain analysis is stiffer than the other analyses because lateral contraction is restricted;

2) The plane stress situation and 3D full situation are still in good agreement, but since necking doesn't happen (because of there is no imperfection in geometry), they no longer fitting the engineering input.

True stress strain relation has also been compared to have a more direct and accurate comparison.

The deformed cross sectional area (A_1) can be calculated from following steps (in order to have a clear demonstration, the necking model from next section is shown here).

1) Exporting nodal deformation of the outlines of required cross section

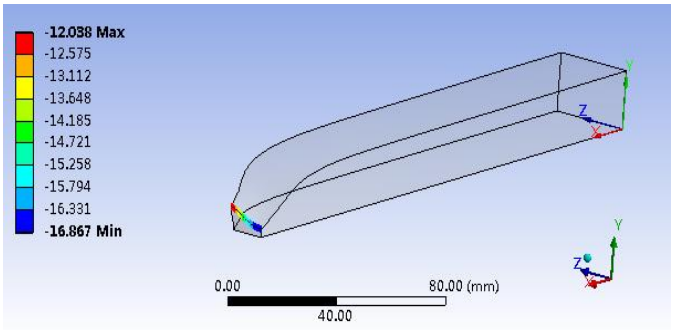

(a)

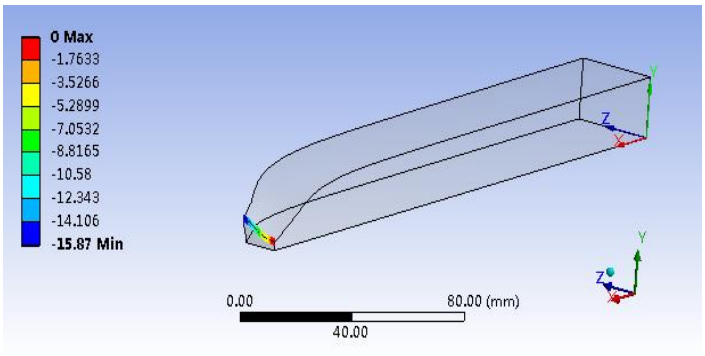

(b)

Figure 3.13: Outline deformation, upper line

(a)uy, (b)uz

2) Calculate the nodal coordinates after deformation
3) Put the coordinates into AutoCAD, plot a closed figure (Figure 3.14)

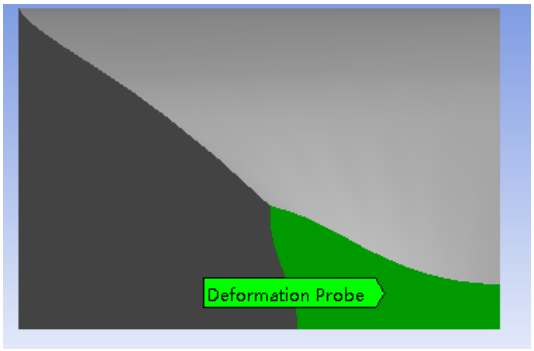

(a)

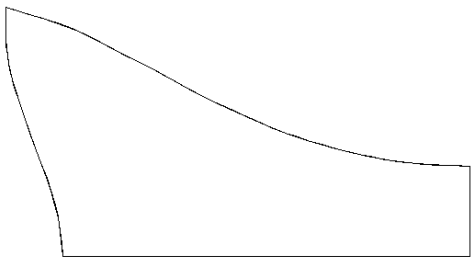

(b)

Figure 3.14: Comparison of the shapes at the required cross section

(a) FEM results, (b) Plot in AutoCAD

4) AutoCAD can calculate the area automatically.

The reaction force (F) has been scaled to the true stress σ_{true} (=F/A_1) and the nominal true strain is calculated from longitudinal displacement over original length (=δ/L).

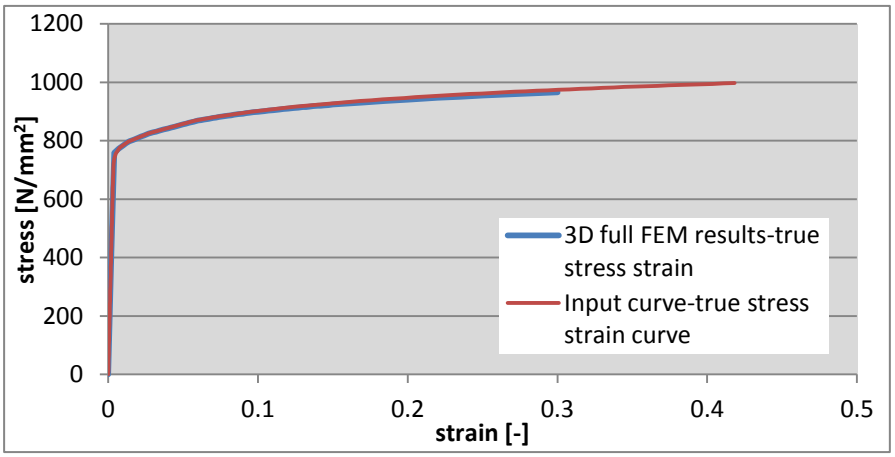

Figure 3.15: True stress strain comparison

From Figure 3.15 we can see that the 3D full simulation result is in good agreement with the true stress strain input.

It is concluded that 3D full analyses provide good results when necking doesn't happen.

3.2.4 Tensile test simulation (with necking)

3.2.4.1 General simulation

Then the specimen under necking situation is tested. In order to have necking in the appropriate part of the tensile test specimen, an imperfection is introduced to the geometry. This is done by reducing 2% of the height of the specimen part where the necking is expected to occur, the reduction is gradually over the whole length. And the boundary conditions are still like the ones used before (Figure 3.16).

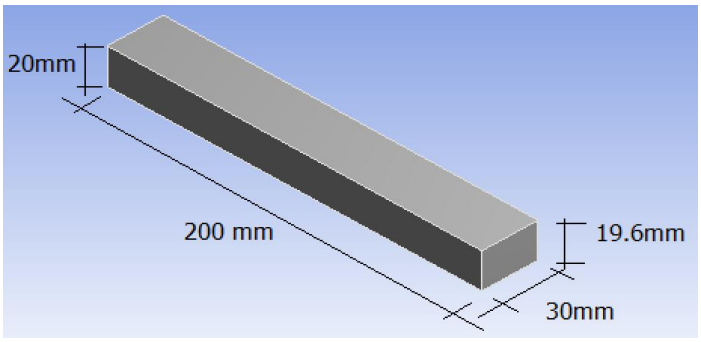

(a)

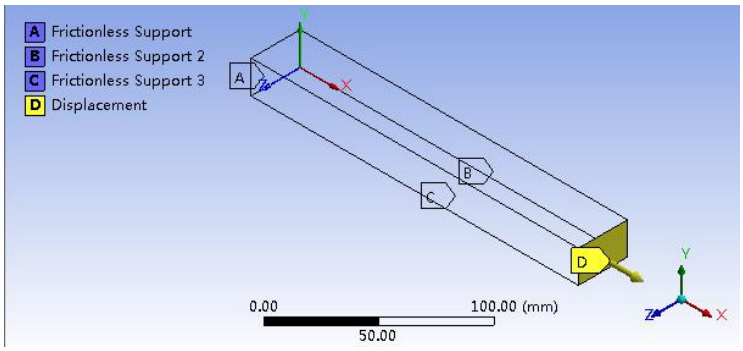

(b)

Figure 3.16: 3D necking simulation specimen
(a) Geometry, (b) boundary conditions

The material input is still the true stress strain curve generated from Section 3.2.2. In this general simulation the mesh is automatically generated (relatively coarse). The results are present in Figure 3.17.

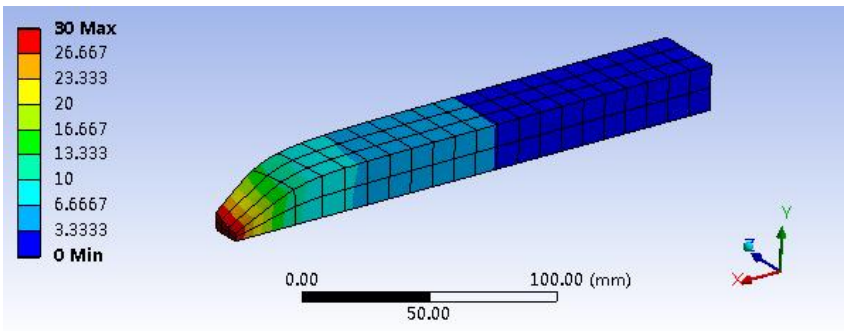

(a)

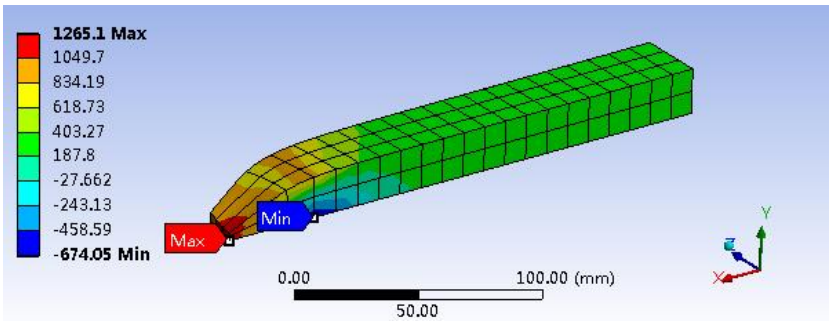

(b)

Figure 3.17: Necking phenomena

(a) Directional deformation, (b) normal stress (longitudinal direction)

From Figure 3.17 we can see that the necking phenomena actually occur after calculating.

The minimum normal stress happens somewhere behind the necking area. However, the minimum stress value is -674 MPa, which means that a small part of the specimen is under compression, while the whole specimen is under axial tension. This phenomenon is confirmed by another FEM software, Abaqus. One possible reason is that the given displacement in the simulation is too large and the 'static analysis' is no longer applicable. In reality, the specimen will fail before having such a large deformation.

The reaction force has also been scaled to the nominal engineering stress σ and compared with engineering input (Figure 3.18).

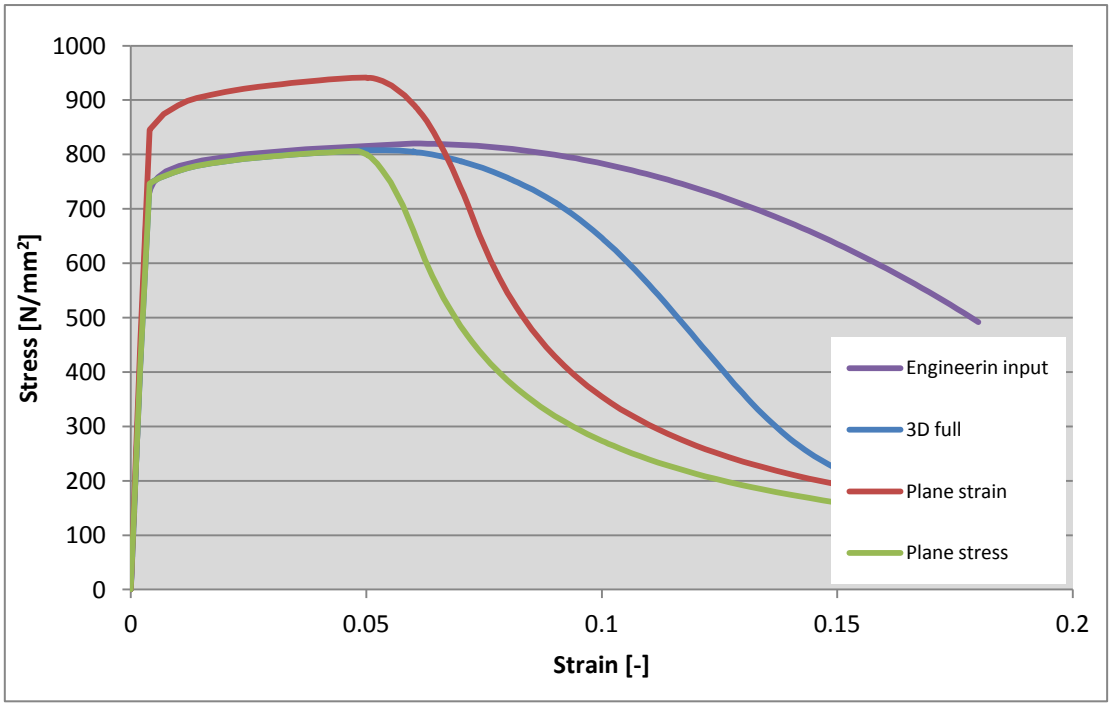

Figure 3.18: Comparison of engineering material input and FEM result, with necking

From Figure 3.18 we can see that:

1) Same as before, in the elastic range the plane strain analysis is stiffer than the other analyses;
2) The resulting engineering stress goes down after necking in all analytic situations, but they all drop much quicker than material input;
3) 3D-full analysis gives the closest result to material input;
4) None of the analyses give the result in accordance with the material input.

Then true stress strain relation has also been compared in 3D-full analysis situation (Figure 3.19). The way to get cross sectional area and determine the true stress strain has been described in Section 3.2.3.

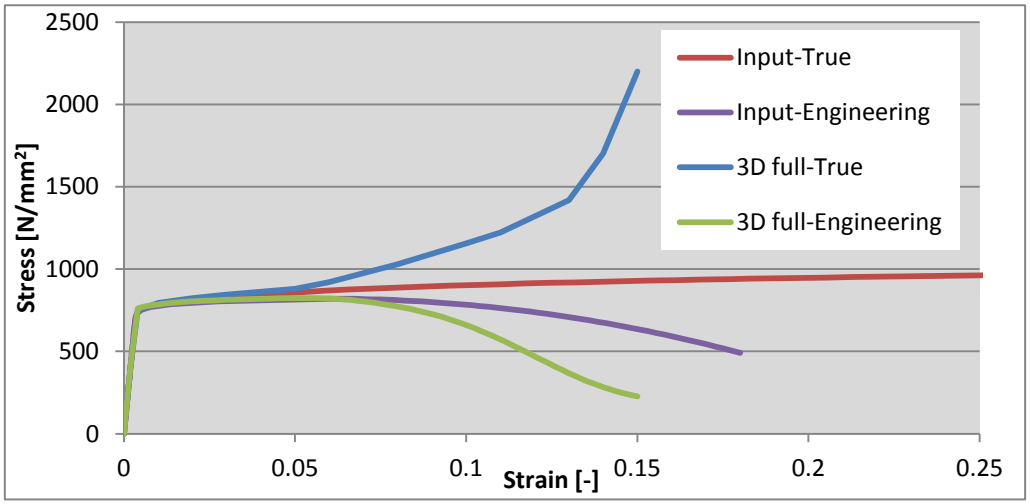

Figure 3.19: Comparison of 3D full FEM results and material input

From Figure 3.19 we can see that the FEM resulting true stress strain doesn't match the input data anymore. This is because after necking, some of the elements will be highly distorted and the nodal stress strain relation will be complicated within the element (localized plastic strain at necking area can be more than 1, Figure 3.20). This means that the true stress strain can't be simply determined from the way described in Section 2.2.3. In ANSYS only the micro nodal equivalent stress strain relation follows the actual input data, but not the macro structural reaction. So for specimen under necking, the comparison has to be made based on engineering results.

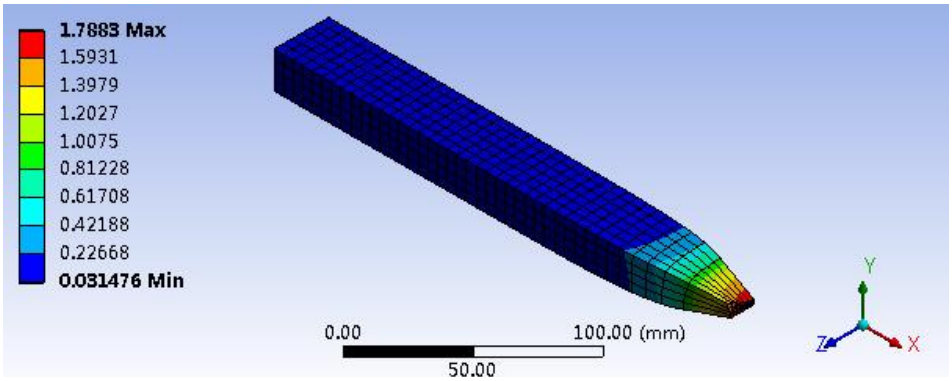

Figure 3.20: Equivalent plastic strain

3.2.4.2 Boundary condition (cross-sectional area) simulation

In order to find why the difference in Figure 3.18 happens, more simulations are made. Firstly, the influence of boundary condition is tested. Every simulation setup is the same as Section 3.2.4.1 except boundary conditions.

In total four analyses are made with various restraints on the lower (y=0) surface in Y-direction and on right (z=0) surface in the Z-direction. The x=0 end is fixed in the longitudinal direction (X-direction). This means that the "real cross-section" of the geometry is according to the values given in Table 3.2.

Table 3.2: Boundary condition simulation information

Geometry	Restraint y=0 surface in Y-direction	Restraint z=0 surface in Z-direction	Resulting "real cross section" due to the symmetry conditions
I	No	No	20 mm x 30 mm
II	Yes	No	40 mm x 30 mm
III	No	Yes	20 mm x 60 mm
IV	Yes	Yes	40 mm x 60 mm

So, the cross section II and III are twice the cross section of the I geometry and the cross section IV is four times the cross section of the A geometry. The boundary condition, directional deformation, longitudinal normal stress are shown as follows (Figure 3.21-Figure 3.24).

1) Geometry I

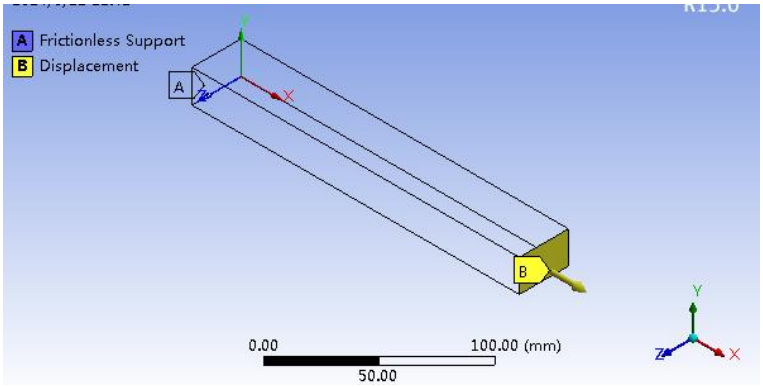

(a)

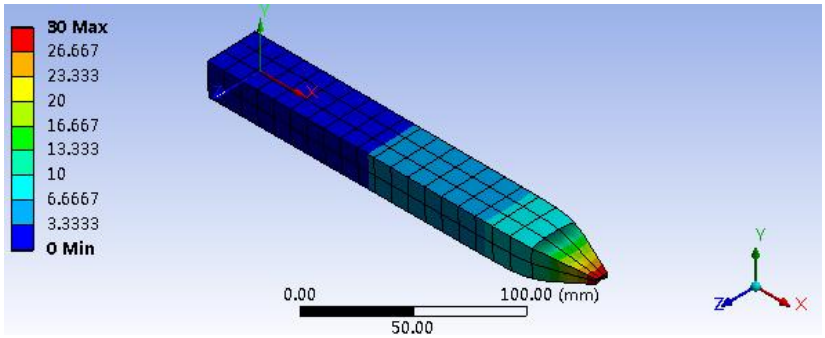

(b)

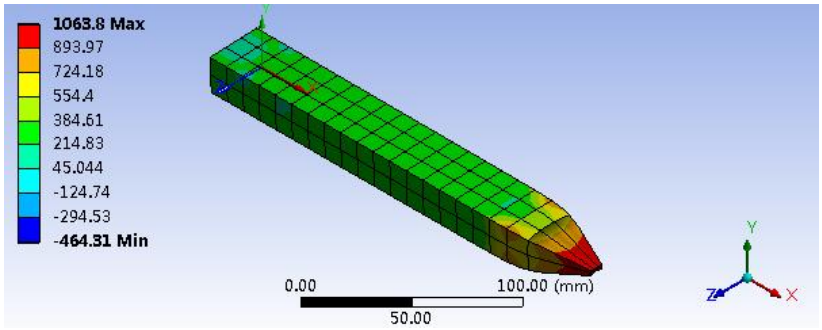

(c)

Figure 3.21: Geometry I

(a) Boundary condition, (b) directional deformation, (c) normal stress

2) Geometry II

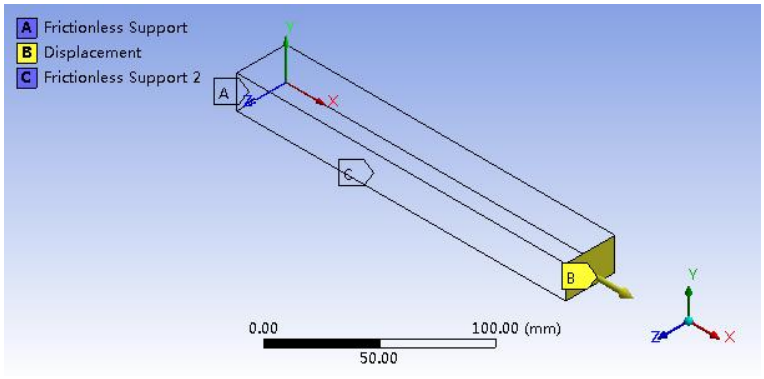

(a)

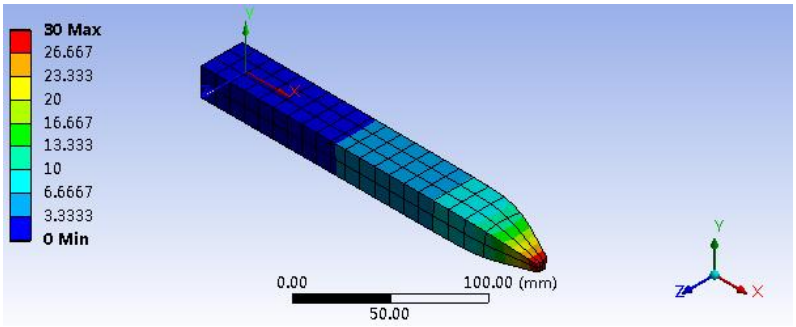

(b)

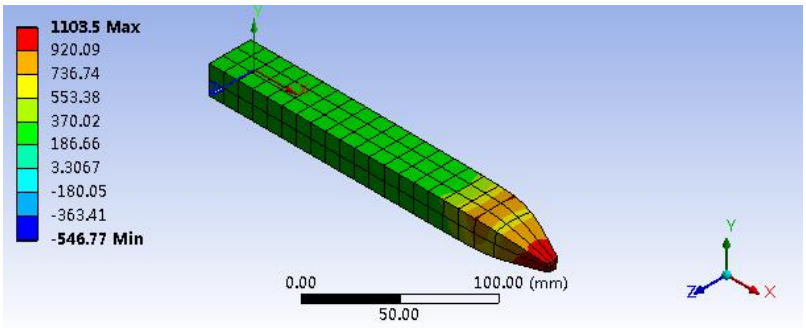

(c)

Figure 3.22: Geometry II

(a) Boundary condition, (b) directional deformation, (c) normal stress

3) Geometry III

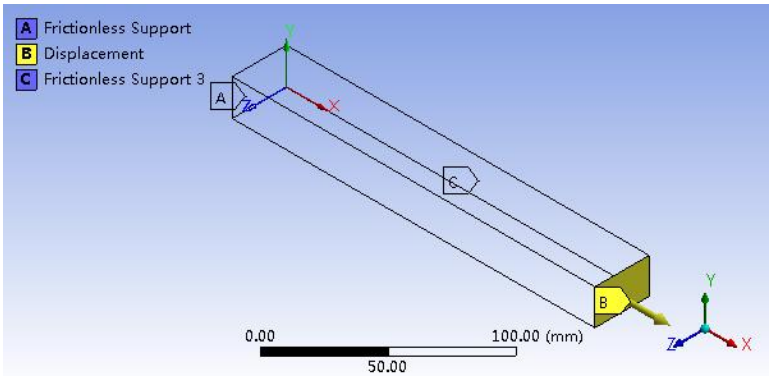

(a)

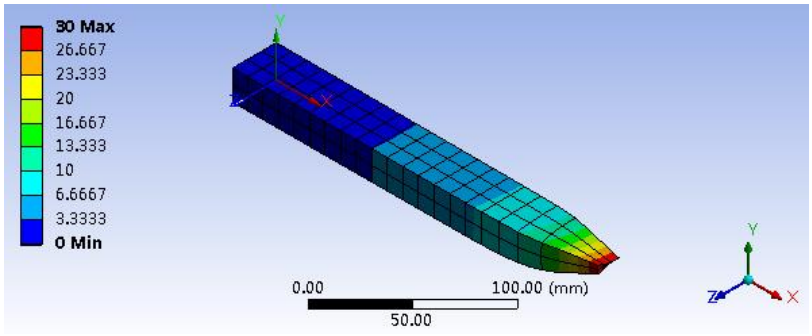

(b)

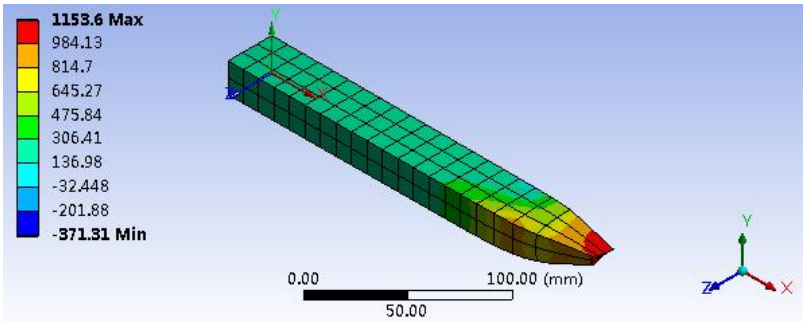

(c)

Figure 3.23: Geometry III

(a) Boundary condition, (b) directional deformation, (c) normal stress

4) Geometry IV

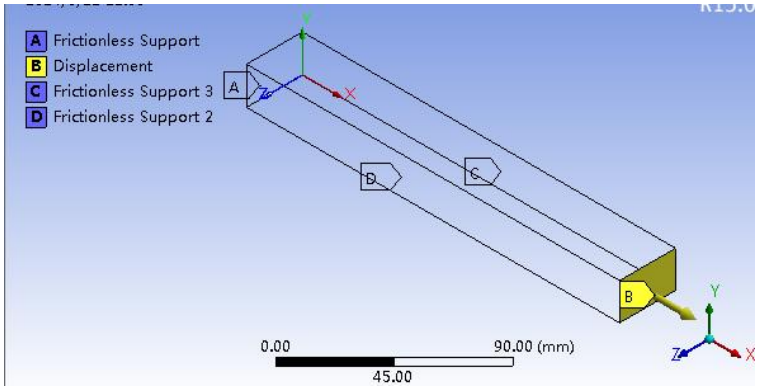

(a)

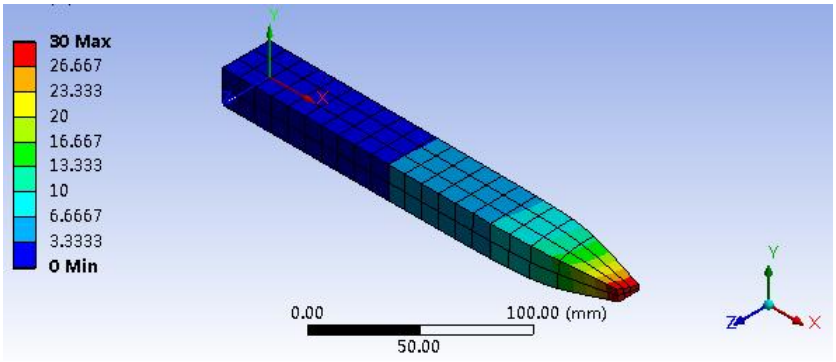

(b)

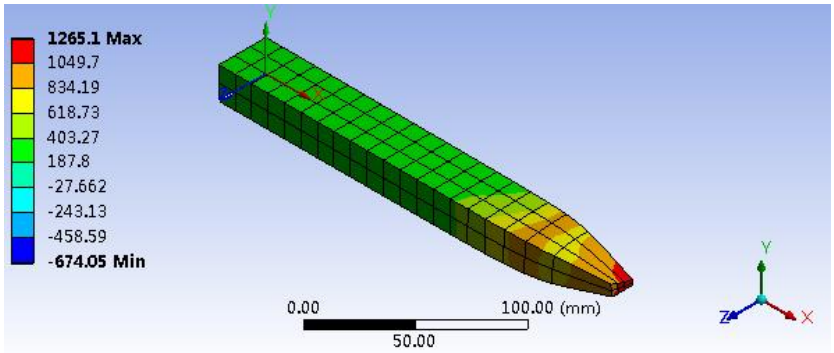

(c)

Figure 3.24: Geometry IV

(a) Boundary condition, (b) directional deformation, (c) normal stress

The load-displacement comparison is shown in Figure 3.25.

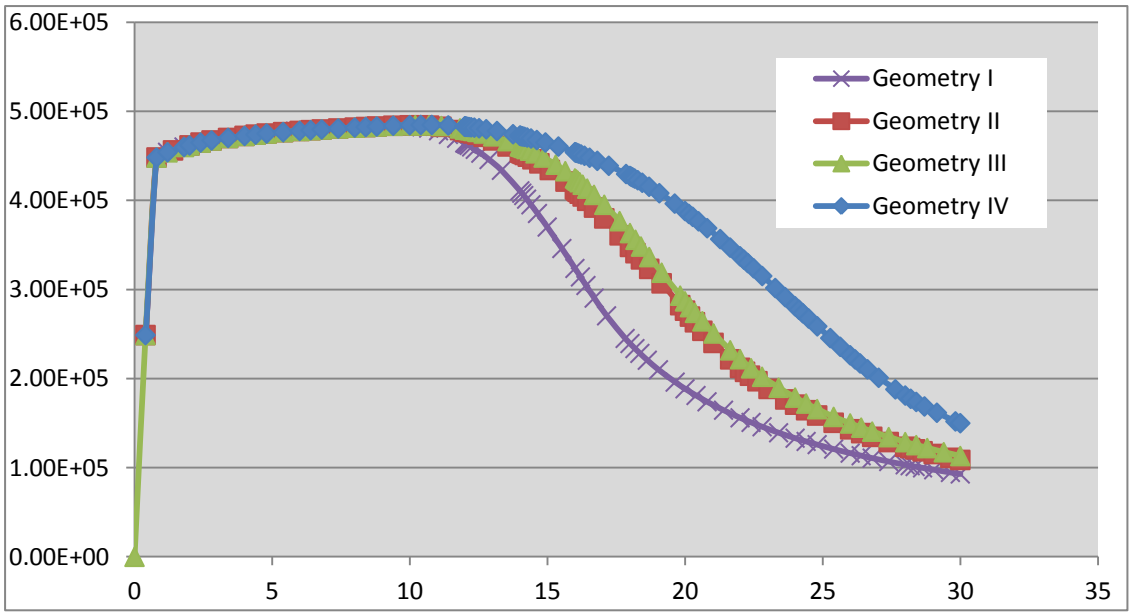

Figure 3.25: Load-displacement comparison

During the necking process geometry with a larger cross-section will have a stiffer behavior due to the fact that in the center of the cross section a more plane strain situation will occur. This is in accordance with the simulation results.

3.2.4.3 Element size test

The influence of element size has also been tested. Every simulation setup is the same as Section 3.2.4.1 except the element size.

There are three different element sizes tested in this section, resulting: 120 elements, 960 elements and 4690 elements. The directional deformation, normal stress as well as the mesh of specimen are shown as follows (Figure 3.26-Figure 3.28).

1) 120 elements (element size: 10 mm)

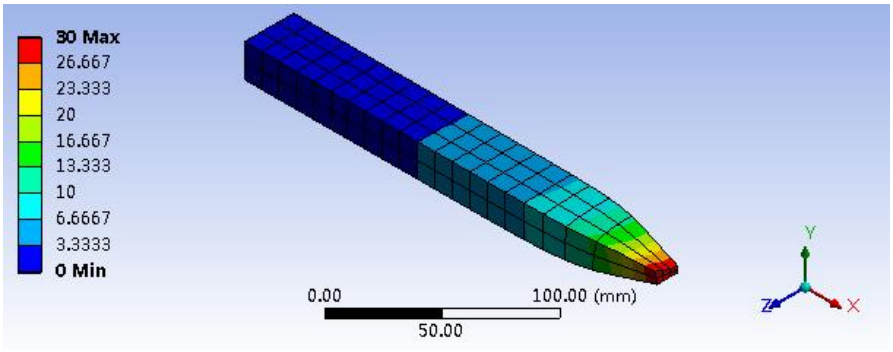

(a)

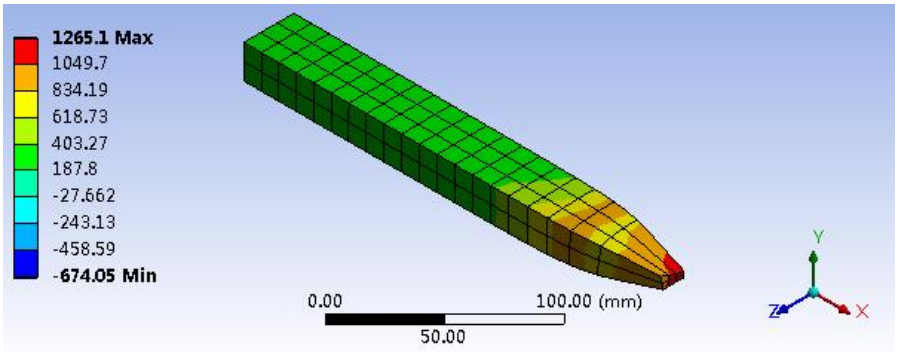

(b)

Figure 3.26: FEM results of 120 elements
(a) Directional deformation, (b) normal stress

2) 960 elements (element size: 5 mm)

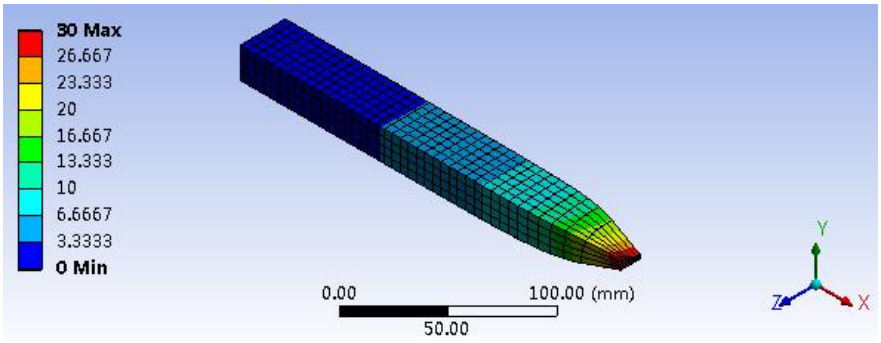

(a)

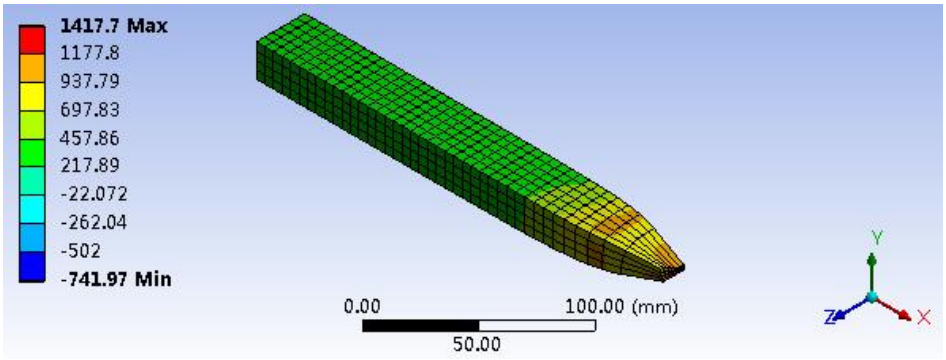

(b)

Figure 3.27: FEM results of 960 elements

(a) Directional deformation, (b) normal stress

3) 4690 elements (element size: 3 mm)

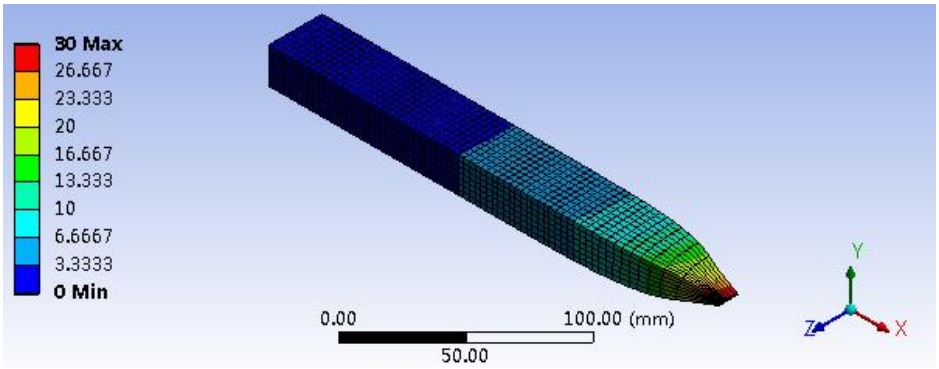

(a)

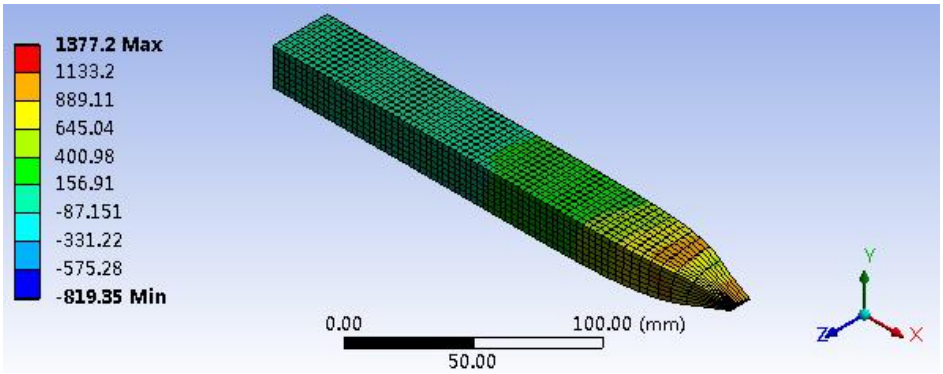

(b)

Figure 3.28: FEM results of 4690 elements

(a) Directional deformation, (b) normal stress

The load-displacement comparison is given in Figure 3.29.

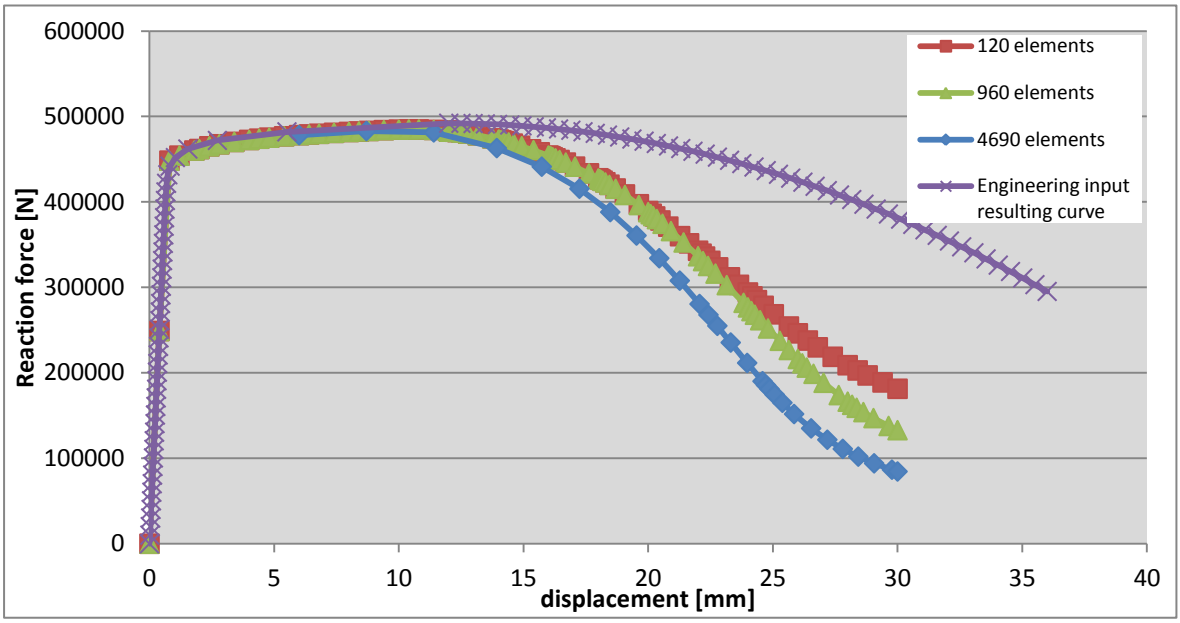

Figure 3.29: Load-displacement comparison

It can be seen that for large directional deformation, the reaction forces have obvious differences with different element sizes. It is well known that the smaller the elements the more pronounced the influence of stress concentrations and other irregularities are present in the results of analyses, so the influence of necking is more pronounced.

3.2.5 Calibrated true stress strain input data

From Section 3.2.4.2 and 3.2.4.3 it is obvious that both the cross sectional area and element size can affect the FEM simulation results. So the difference in Figure 3.18 might because of different simulative geometry and element size used in the simulation.

To prove this, another series of simulation are made.

3.2.5.1 Geometry & element size

The geometry used in actual specimen experiments is adopted this time (12 mm x 60 mm) and this geometry is also similar to the one used in TNO report [8] when determine parameter K and np in Table 3.1.

Due to the symmetry of the geometry, one eighth of the specimen is modeled (Figure 3.30), boundary conditions are shown in Figure 3.31 and an example of the result is present in Figure 3.32.

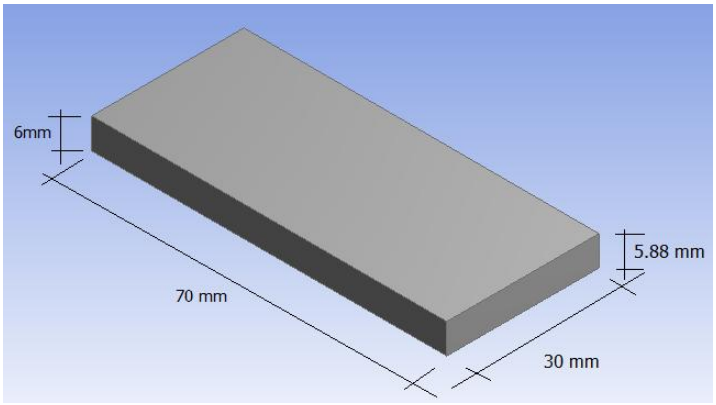

Figure 3.30: Simulation geometry

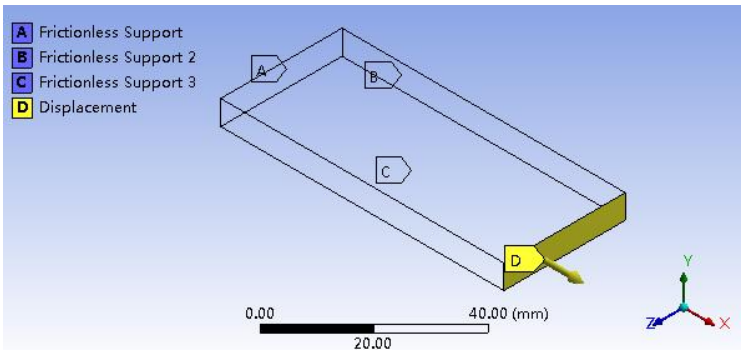

Figure 3.31: Boundary conditions

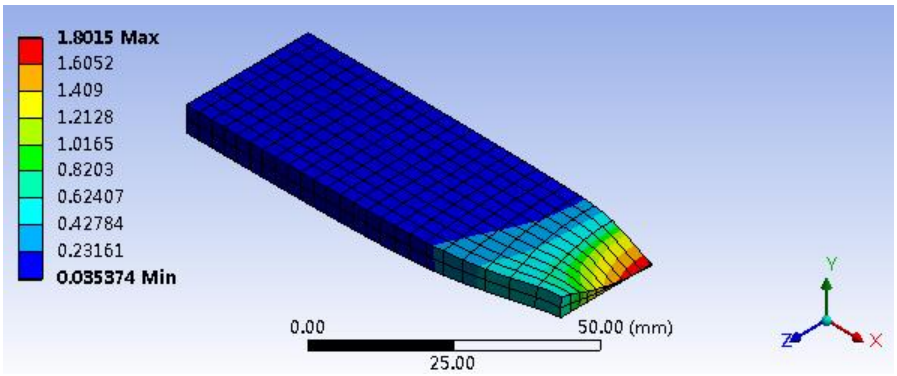

Figure 3.32: Tensile test analysis, example, deformed shape and equivalent plastic strains (3mm)

The influence of element size is also tested and the overall comparison is shown in Figure 3.33. From this figure, it can be seen that the FEM resulting engineering stress strain is close to the calculated engineering input and the relatively coarse mesh (which is more similar to the case in TNO report [8]) gives a closer result.

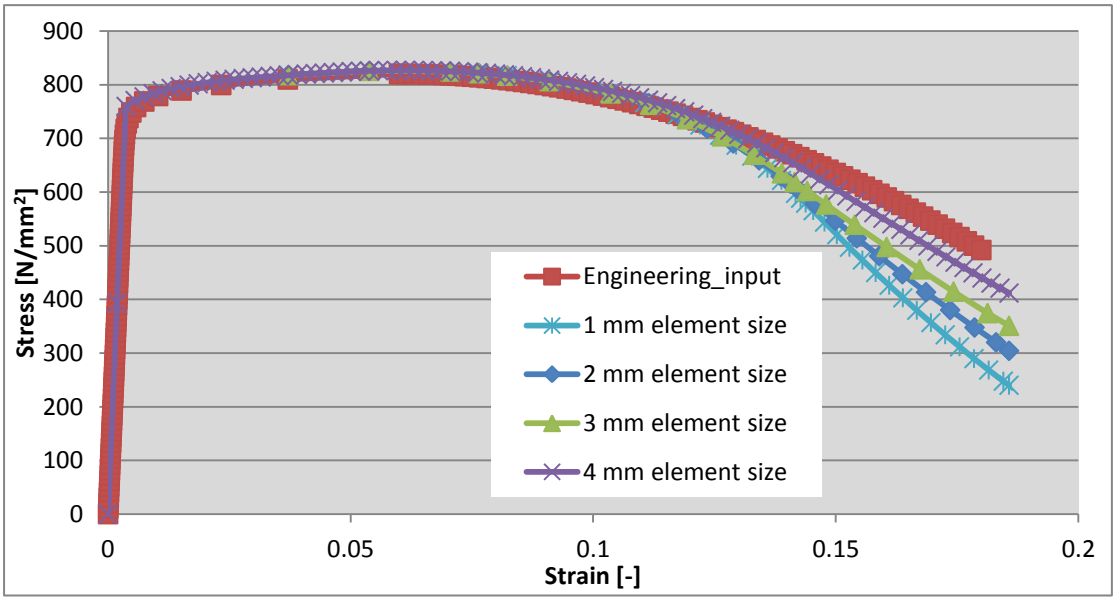

Figure 3.33: Stress strain comparison for different element sizes

3.2.5.2 Calibration

From Figure 3.33 it can be seen that the FEM results have small differences from engineering input data when the strain is very large. So in order to have a more accurate simulation result, a calibration of the true stress strain input for ANSYS is needed. Several reports such as [13] have dealt with the problem of modeling the correct behavior after necking. However, the values of true stress strain input data after necking are manually modified in this report. Several calibrations are done based on different element sizes (Figure 3.34). After this data calibration procedure, a more similar output curve could finally be established (Figure 3.35-Figure 3.37).

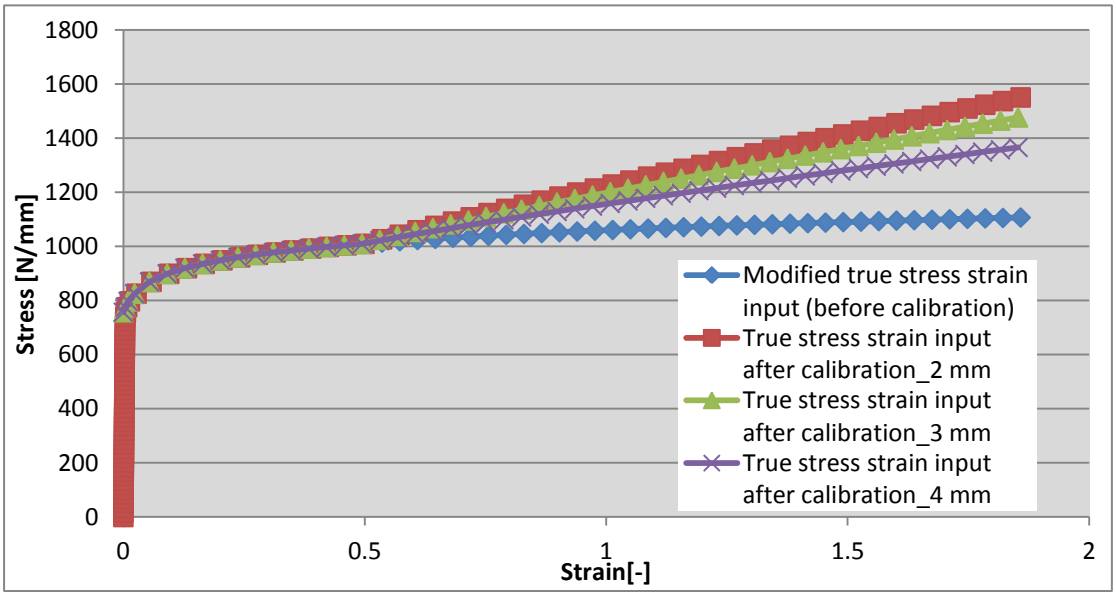

Figure 3.34: Comparison of true stress strain input

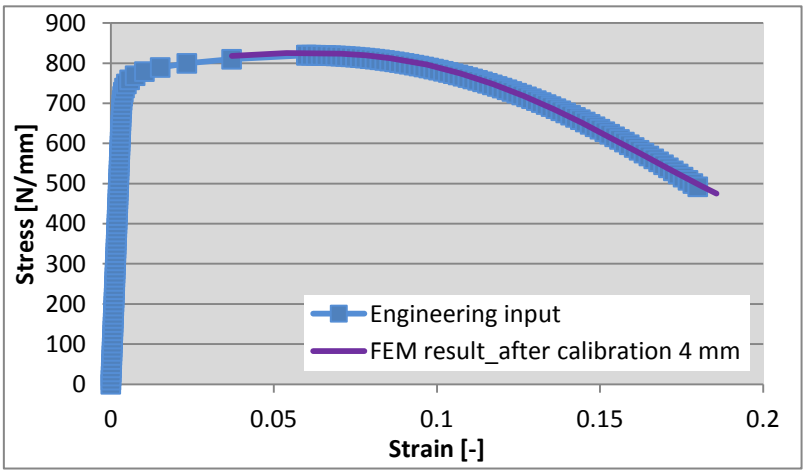

Figure 3.35: FEM result after calibration, mesh size: 4 mm

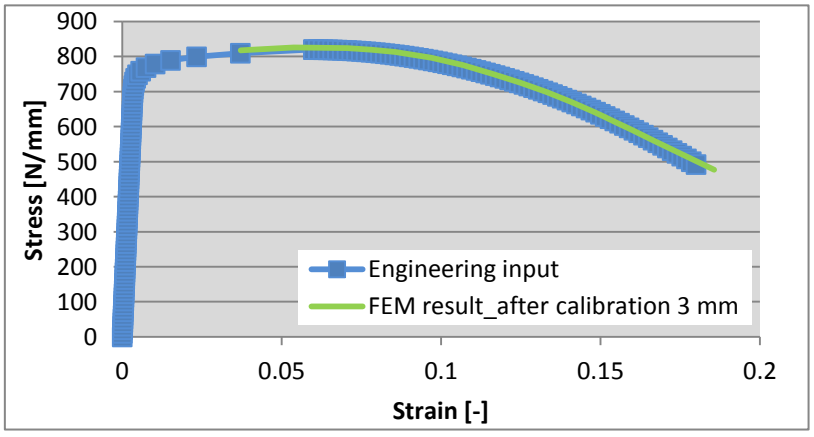

Figure 3.36: FEM result after calibration, mesh size: 3 mm

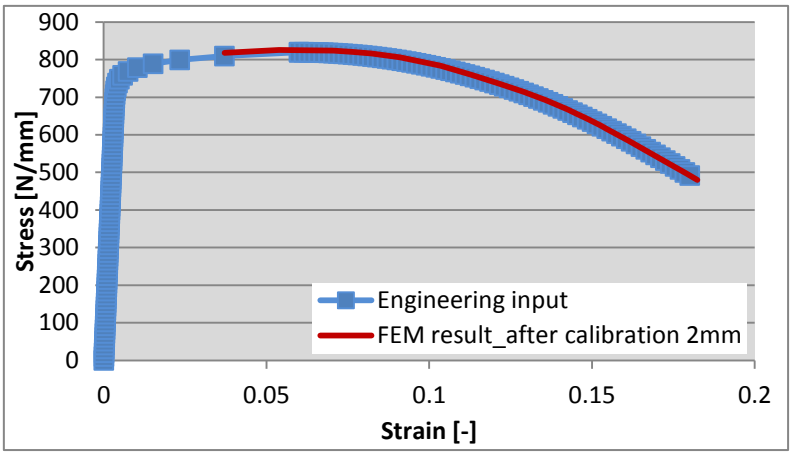

Figure 3.37: FEM result after calibration, mesh size: 2 mm

Theoretically, a specific element size should use the corresponding calibrated material input. However, for element sizes smaller than 2 mm, the calibrated true stress strain inputs only have very small differences, so for any element sizes smaller than 2 mm, the 2 mm input is adopted for subsequent numerical simulations.

Other material inputs can be found in Appendix B.

4. FE validations of connections

4.1 Connections type B

In this section, validations are carried out for five B-geometries. The B-geometry is an X-connection with a low stress concentration factor (SCF) and the simplified geometry is presented in Figure 4.1 [8]. This geometry has no geometrical discontinuity in the direction of the weld and therefore it can be approximated by 2D geometries (Figure 4.2 [8]), however, it has been proven that the 2D and 3D analytical results have relatively big differences when the strain became very large (Figure 3.18). So in this chapter only 3D analyses are carried out.

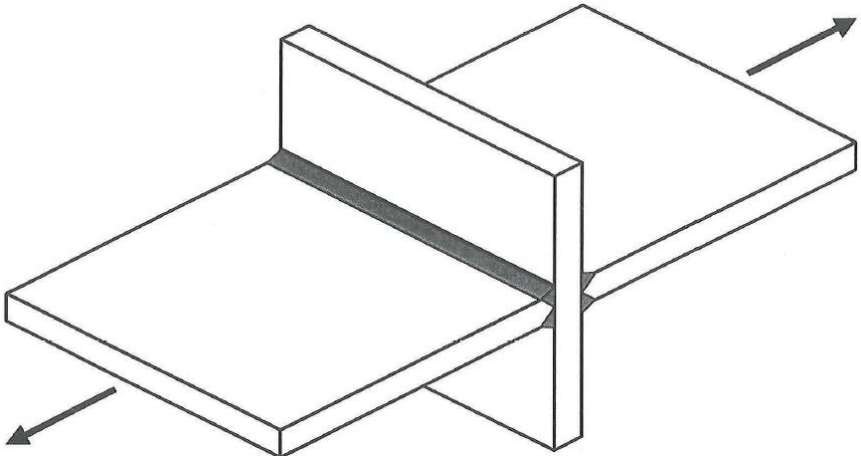

Figure 4.1: Specimen geometry B (with low SCF)

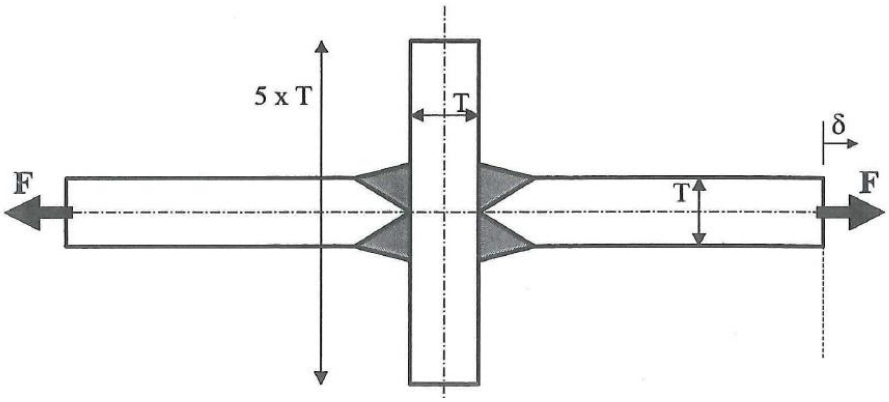

Figure 4.2: Side view of geometry B

In the next sections the FEM results are compared to the experimental results. Specimen 3B1 and 4B1 are the first validation made and therefore extensively investigated with different variables.

The comparison is mainly based on the load-displacement curve over the length of test gauges. For specimen 1B1 and 3B1 the measuring equipment did not function until the end of the test and an additional interpretation of the experimental results is necessary.

4.1.1 Specimen 3B1 (fail in plate)

4.1.1.1 Geometry

Specimen 3B1 is a 12 mm thick S690 undermatched weld specimen. The geometry is presented in Figure 4.3 [8]. This specimen consists of two horizontal plates and one vertical plate. The plates are connected by undermatched K-joint. In this case the K-joint is not fully penetrated and has a small (vertical) incomplete penetration.

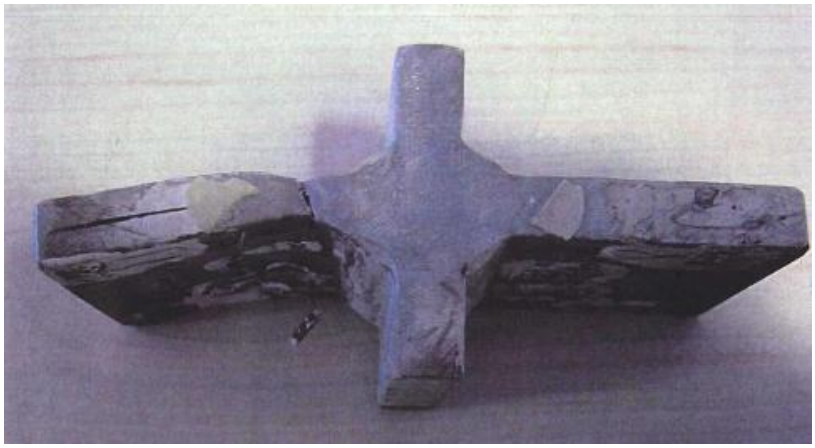

Figure 4.3: Specimen 3B1

The dimensions of the specimen are taken from report [8] (Figure 4.4). Figure 4.4 also includes the displacement measurement (LVDT's). The side view shows that upper right weld has the smallest dimensions, so only this quarter of the geometry is modeled due to double symmetry. A length of 74.5 mm, half of the measuring length of LVDT's 3 and 4 is used.

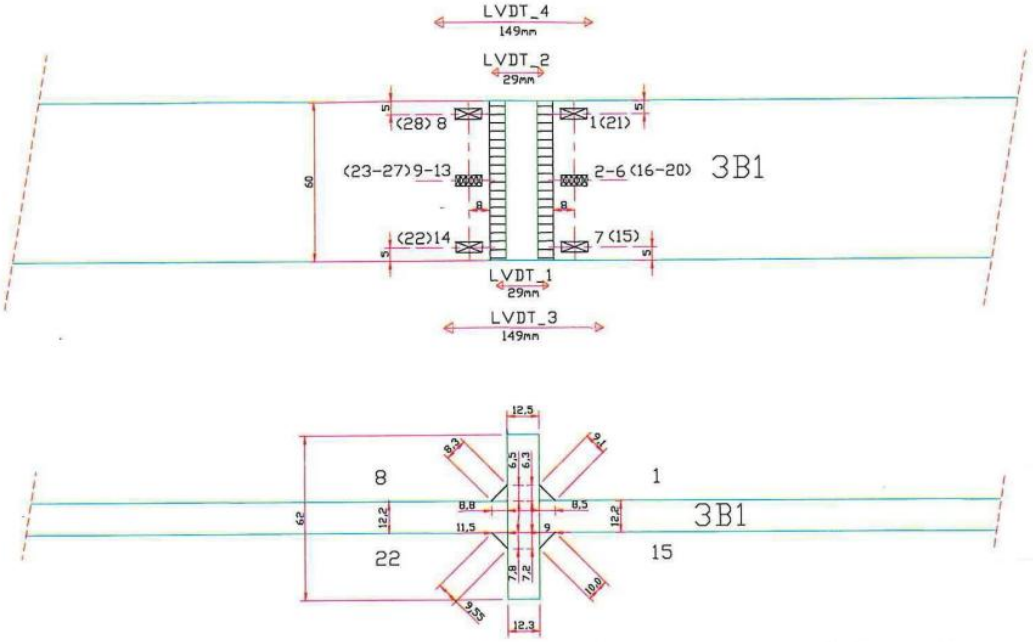

Figure 4.4: Measured geometry – top view (upper figure) and side vied (lower figure)

4.1.1.2 Modeling

Note that the geometry studied in FEM presents a simplification of the actual situation: it assumes a uniform and constant plate and weld over the whole specimen. The weld is simplified to a triangular geometry. The influence of the heat affect zone (HAZ), weld beads, surface irregularities and weld toe radii is not taken into consideration. However, the incomplete penetration is taken into account by assuming a vertical gap of 2 mm over the plate thickness (Figure 4.5).

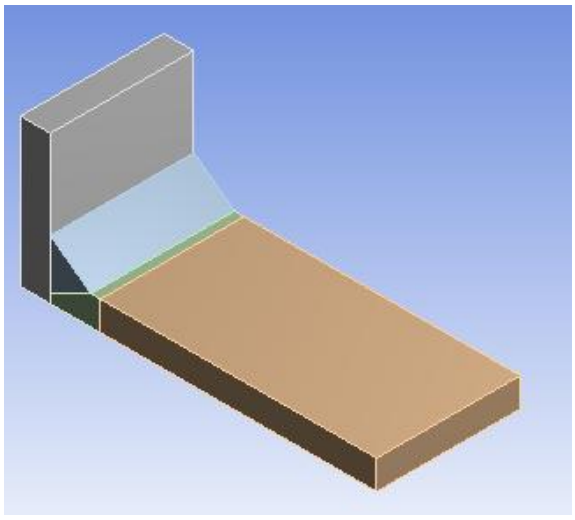

Figure 4.5: FE-geometry specimen 3B1-3D full

In order to test the influence of element size, several different meshes are used. Some examples of the mesh are presented in Figure 4.6 and Figure 4.7. SOLID 186 (20 nodes brick) element is used for all analyses.

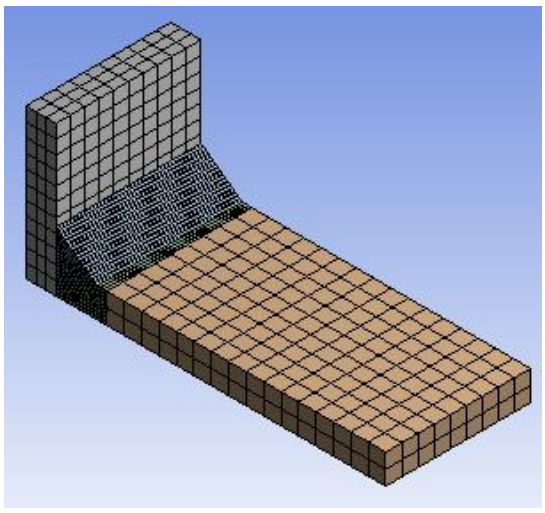

(a)

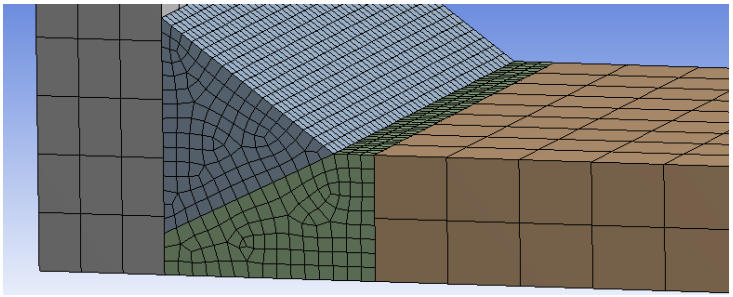

(b)

Figure 4.6: FE-mesh specimen 3B1_refined near weld
(a) general mesh, (b) weld interface detail, 0.7 mm element size

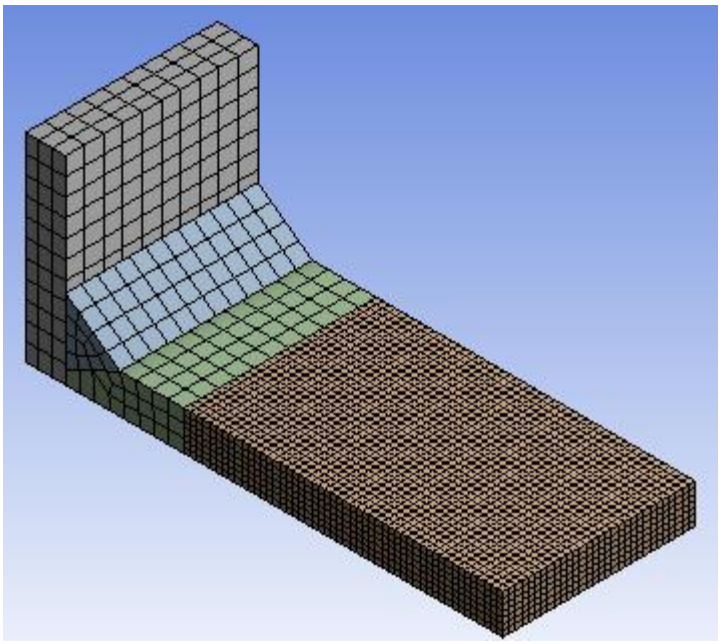

Figure 4.7: FE-mesh specimen 3B1_refined plate, 1 mm

Again, the boundary conditions only applied in the area of symmetry, a directional displacement is given as the external load (Figure 4.8). All the parts are connected by "bond connection" except the 2 mm vertical defect (between the gray and green parts in Figure 4.7).

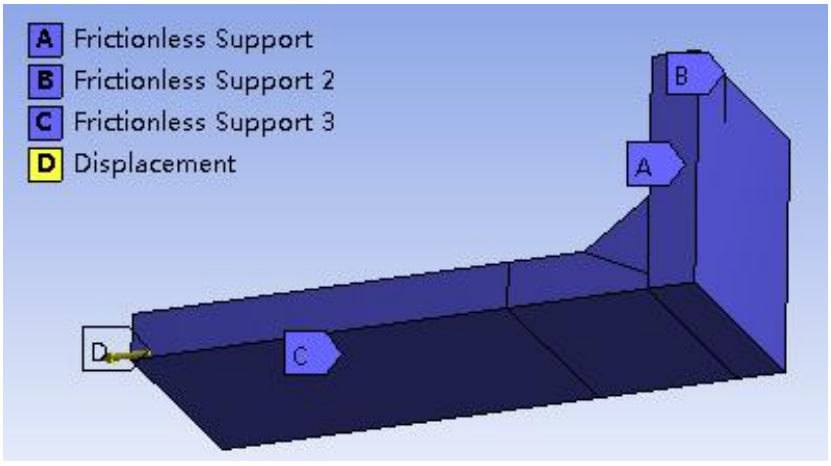

Figure 4.8: Boundary conditions

The resulting load-displacement curves are presented in Figure 4.9. Apart from the influence of different mesh at different parts of the specimen, different material inputs are also compared (besides of 'original input' all simulations are used calibrated input corresponds with element size). And the influence of the number of substeps is also checked.

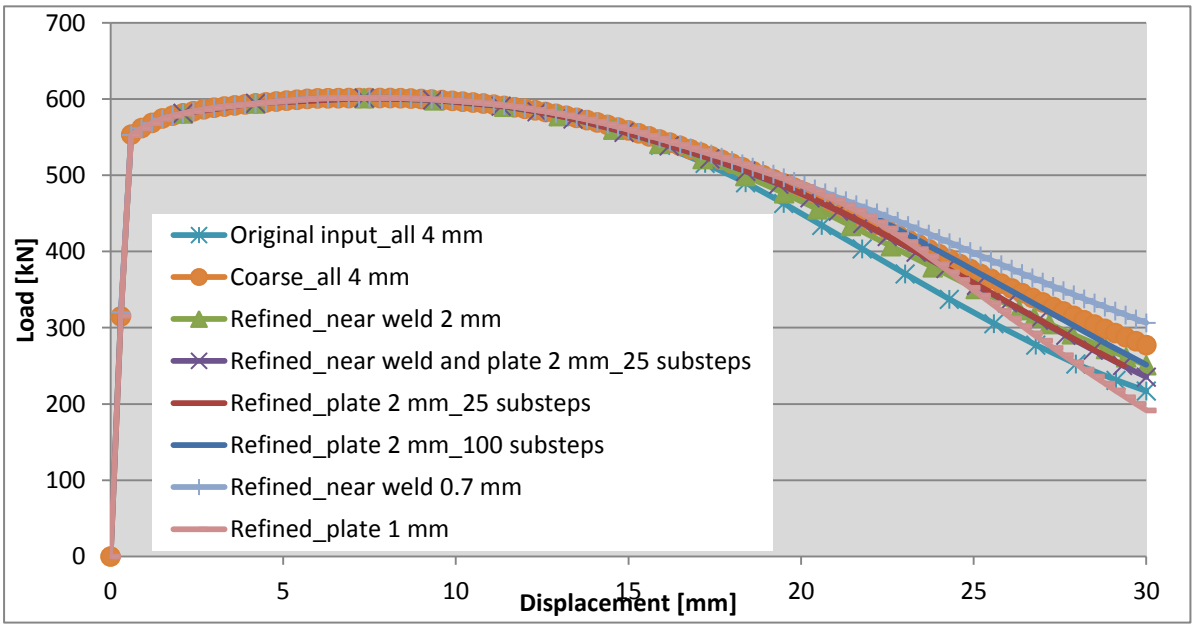

Figure 4.9: FE-analyses results of Specimen 3B1

Various observations can be made:

1) For all the analyses, the resulting curves are identical before necking and only have relatively small differences when the directional deformation is very large;
2) For different element sizes with corresponding calibrated material input, the results only have very small differences. However, with the original (before calibration) material input, the deference is relatively big, so the calibration can give a more accurate simulation result;
3) The number of substeps also has a slight influence on the simulation result;
4) Even smaller element sizes are tested for materials both near weld and plate (respectively 0.7 mm and 1 mm). However, all the simulation results show that the failure is at the plate, so the refinement at plate should give a more accurate result.

4.1.1.3 Interpretation of experimental results [8]

The method of interpretation of experimental results in this report is the same as [8]. The length of the model is taken equal to the displacement gauge LVDT's 3 and 4. The experimental load-displacement curves of these LVDT's are plotted in Figure 4.10. It also includes the 'corrected bench displacement', which is the displacement of the ends of test rig scaled with a factor 0.15 to compensate the difference in measuring length.

From Figure 4.10, several observations can be made. Firstly, it can be seen that the elastic branches are not identical, which indicates that a certain curvature over the width of the specimen. Secondly, the figure also shows that the LVDT's fell off the specimen before failure, so a correction procedure is needed if we want to have information at failure. Finally, the

corrected bench result does not present accurate results at large displacement because after the elastic phase, the plastic deformations occur locally near the necking point, most likely within the range of the LVDT's.

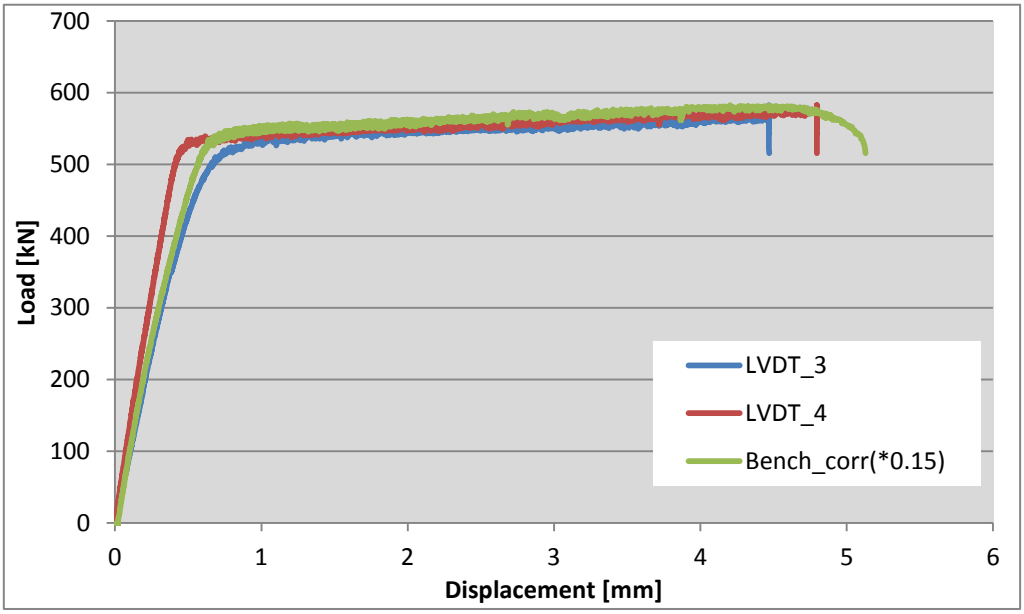

Figure 4.10: Experimental results

However, the exact moment when necking starts is not clear, so the experimental results are modified with the following lower bound and upper bound [8]:

Lower bound

1) Up to failure of LVDT3, the average results of LVDT's 3 and 4;
2) Until the maximum load Fu is reached, the displacement increase of the corrected bench;
3) At displacements beyond Fu, the displacement increase of the not-corrected bench.

Upper bound

1) Up to failure of LVDT3, the average results of LVDT's 3 and 4;
2) At displacements beyond failure of LVDT3, the displacement increase of the not-corrected bench.

The results are presented in Figure 4.11. It shows that between the upper and lower bound there is a very wide range, and the actual deformations beyond the failure of the LVDT'S are substantial.

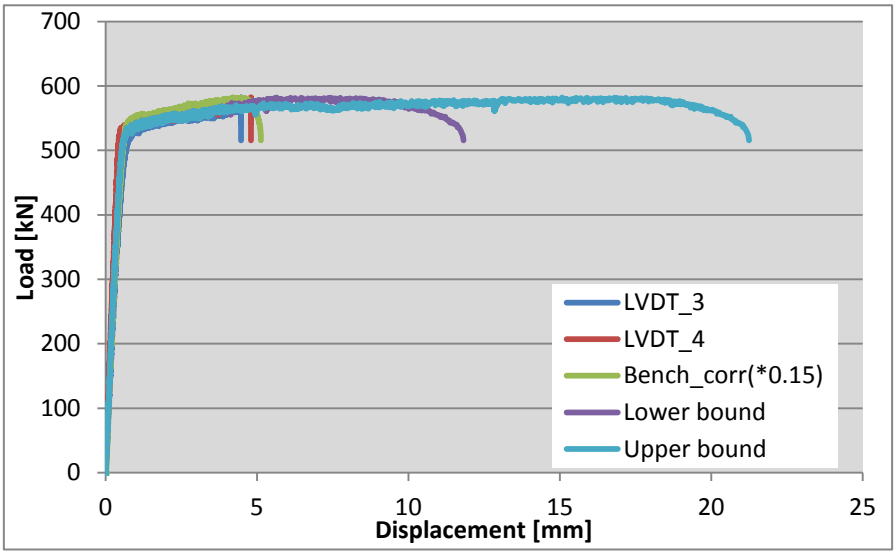

Figure 4.11: Determination of the upper and lower bounds of the experimental result

4.1.1.4 Comparison of experimental and FE-results

The FE-result compared to the experimental result is shown in Figure 4.12. In addition, the failure point based on Lemaitre's criterion is presented, using the value of ε_0=1.

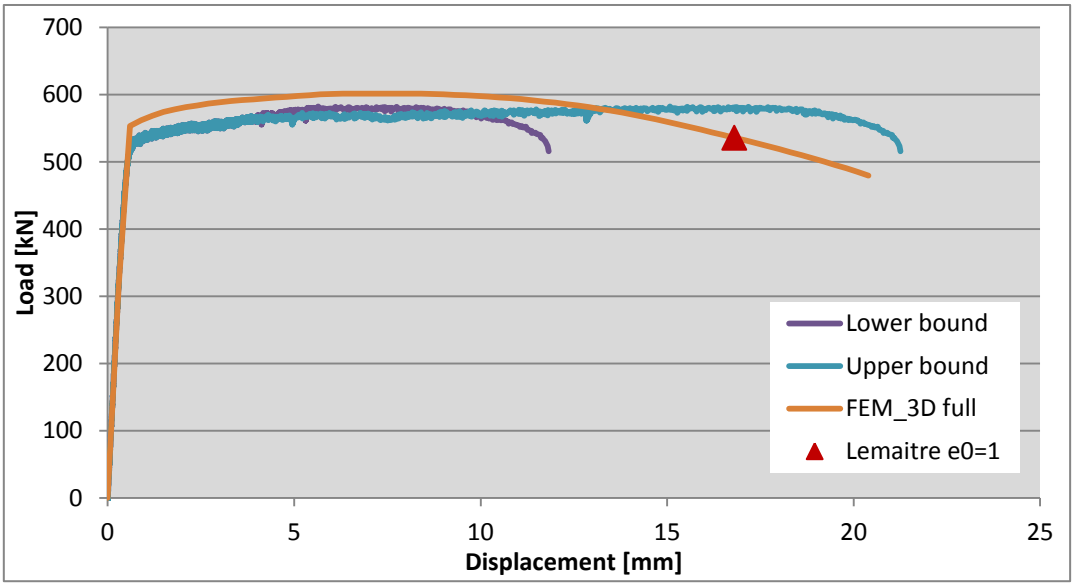

Figure 4.12: Comparison of experimental and numerical results

Several remarks can be made with respect to this figure:

1) In the elastic range the analyses agree with the experiment, the yield strength is slightly over predicted (3%). This difference might be attributed to the influence of HAZ;
2) The plastic capacity is also slightly overestimated by the FE-analysis (3%);
3) The FE-analysis failure result is positioned well within the range described by the upper and lower bounds after necking. The failure load can be predicted accurately;
4) The failure mode (plate failure) is predicted very well. According to FE-analysis, failure

starts at the center of the horizontal plate.

The influence of element sizes on Lemaitre's criterion is also checked (Figure 4.13 - Figure 4.15). It seems that with a smaller element size, the plastic strain near the necking point is more concentrated and has a larger maximum value. Meanwhile, the triaxiality also has a difference. So the Lemaitre's criterion might give different results when using different element sizes.

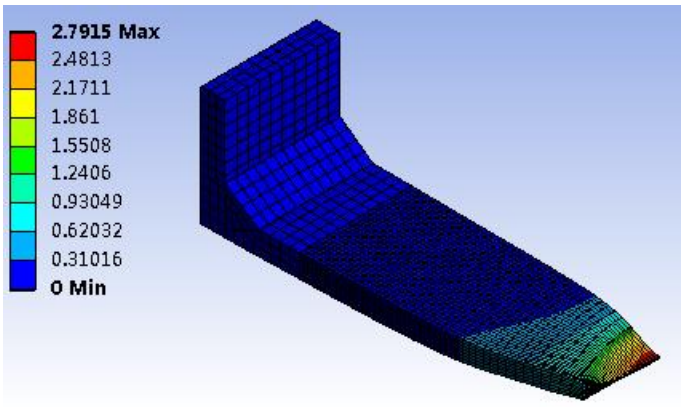

(a)

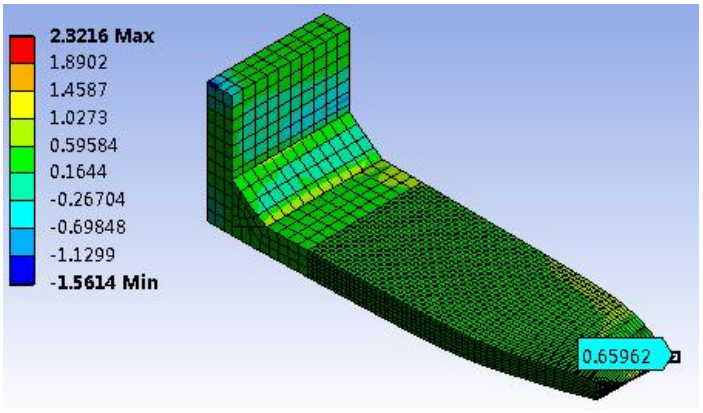

(b)

Figure 4.13: Results of 1 mm element size at a displacement of 30 mm (2*15)
(a) Equivalent plastic strain (b) triaxiality

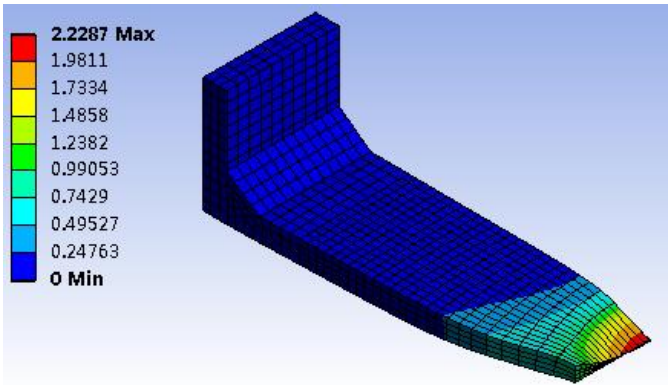

(a)

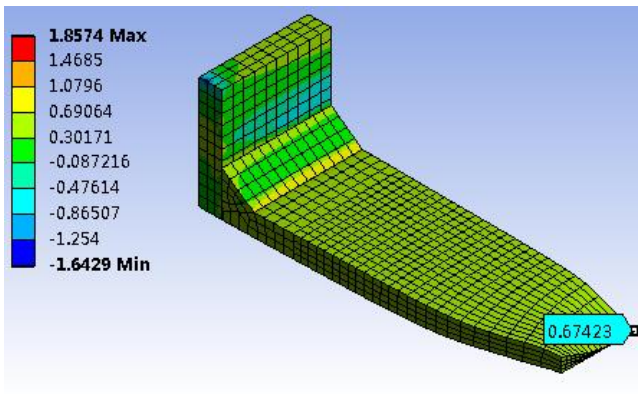

(b)

Figure 4.14: Results of 2 mm element size at a displacement of 30 mm (2*15)
(a) Equivalent plastic strain (b) triaxiality

Figure 4.15 checks the Lemaitre's criterion for two different element sizes. It can be seen that at later substeps two curves are actually different. However, the failure seems to occur at a very early stage, and the result shows that for both element sizes the failure happens in the 56th substep out of 100 total steps. So for Specimen 3B1 (failure at plate) the element size doesn't affect the Lemaitre's criterion result and the result is considered accurate.

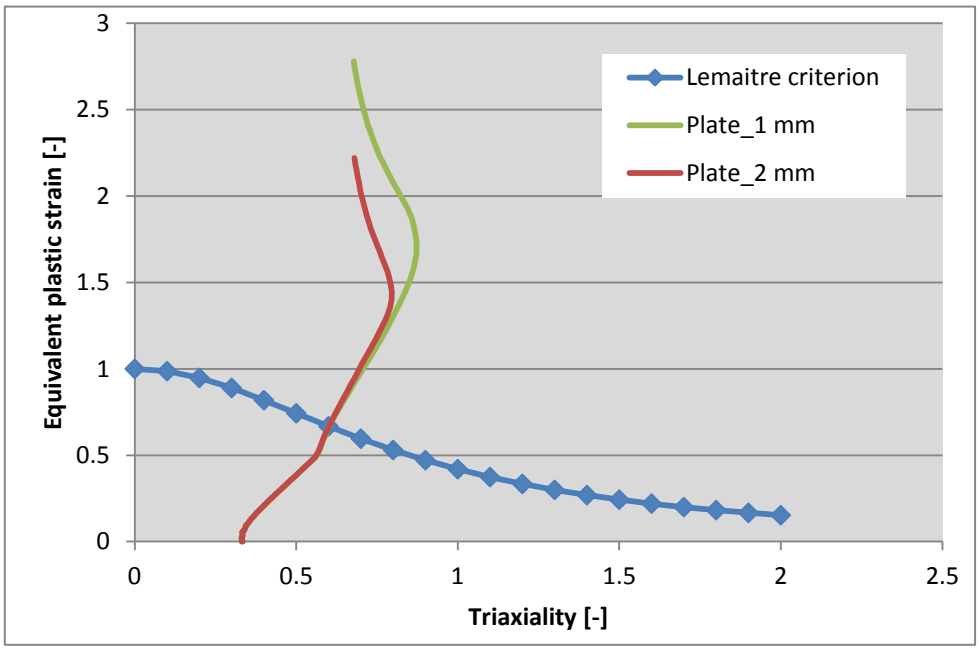

Figure 4.15: Lemaitre's criterion check

Figure 4.16 and Figure 4.17 show equivalent plastic strain at different substeps for the 3D full analysis.

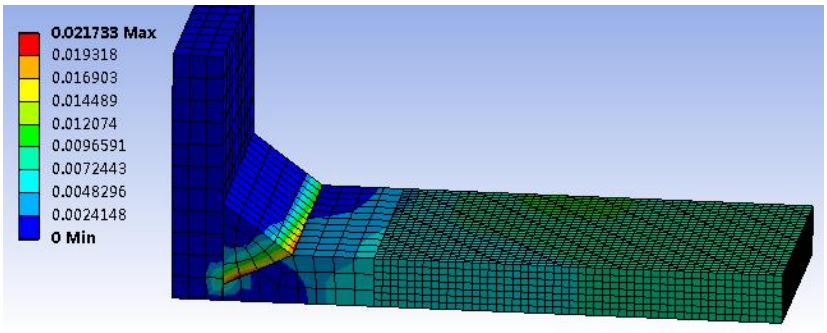

Figure 4.16: Equivalent plastic strain at a displacement of 1.5 mm (2*0.75, substep 5)

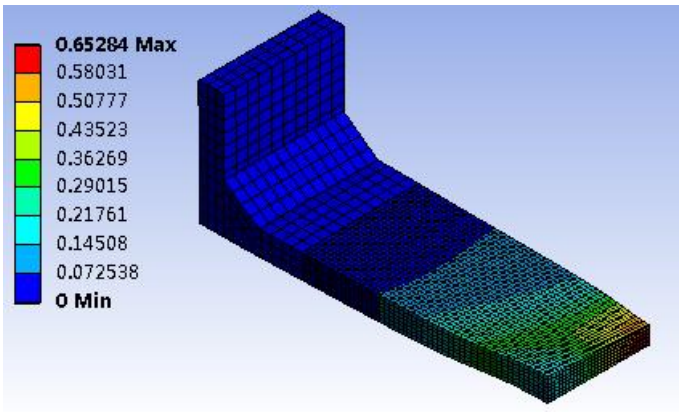

Figure 4.17: Equivalent plastic strain at failure (substep 56, 2*8.4=16.8 mm)

From the analysis it could be concluded that the initial plasticity occurs in the weld (Figure 4.16). This phenomenon can also be found with undermatched weld metal. However, the amount of plasticity remained limited. It seems that the dimensions of the weld have the overall strength exceeds that of the horizontal plate, even though it's undermatched. Thus, in the analysis the failure is due to necking of the plate and this is in accordance with the experimental result.

Based on the presented results, it is concluded that the FE-analyses provide comparable results to the experiment if the failure happens in the plate. They present relatively accurate load-displacement curves and the calculated deformation at failure is within the upper and lower bounds.

4.1.2 Specimen 4B1 (fail in weld)

4.1.2.1 FEM-analyses

Specimen 4B1 is a 10 mm thick S1100 undermatched specimen. The plates are connected by undermatched K-joint with incomplete penetration. The experimental result shows that the failure is at the weld (Figure 4.18, [8]).

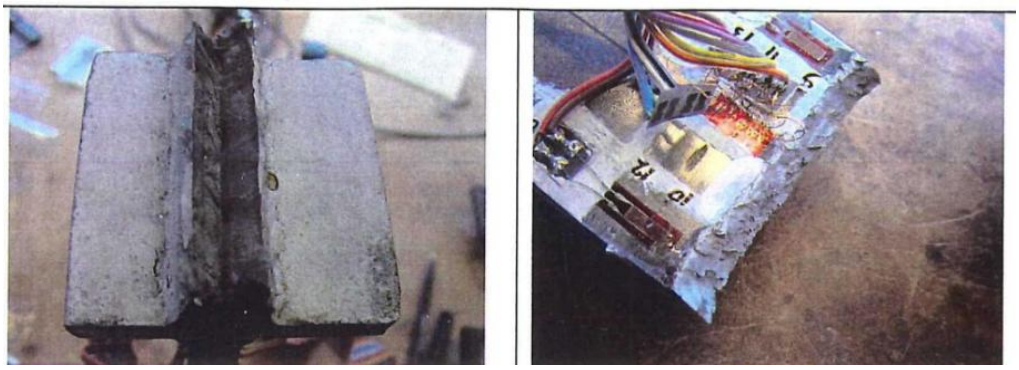

Figure 4.18: Failure of specimen 4B1

The measured dimensions are given in Figure 4.19. The side view shows that the lower left weld has the smallest dimensions.

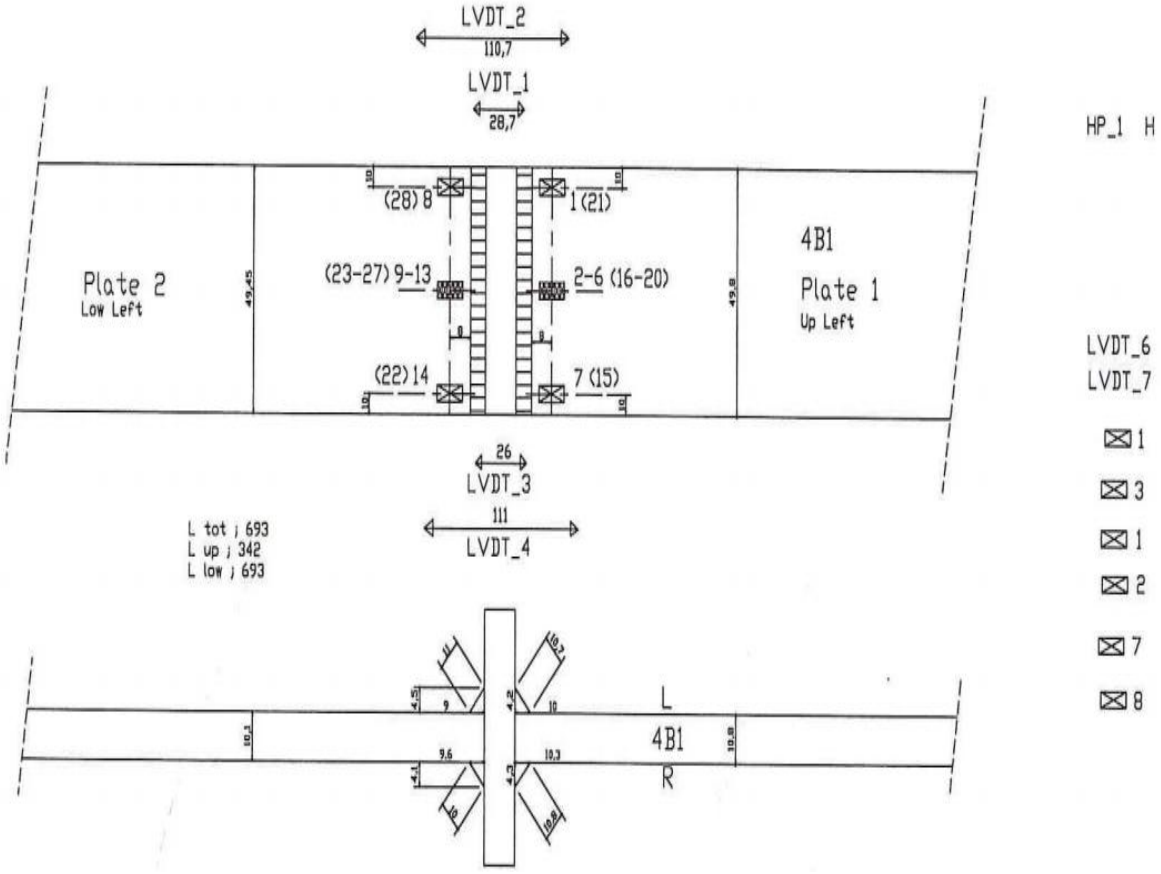

Figure 4.19: Measured dimensions specimen 4B1

The FEM geometry and the mesh are given in Figure 4.20 (refinement near weld, 0.5 mm).

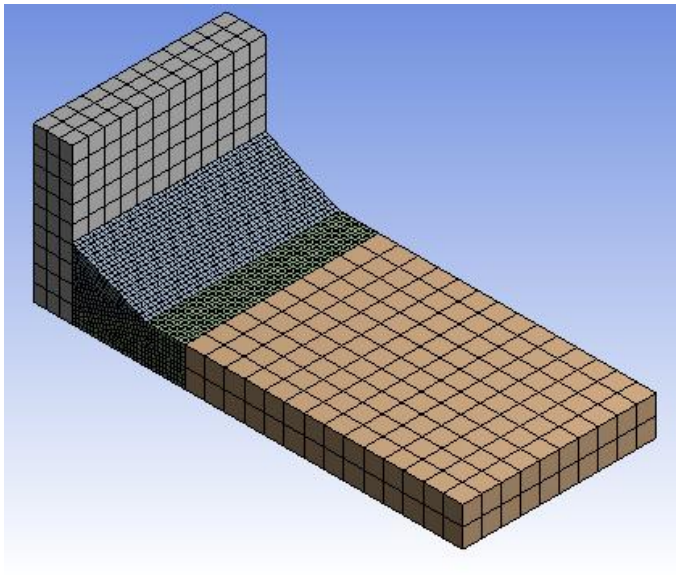

Figure 4.20: Geometry and mesh specimen 4B1, 0.5 mm element size

Figure 4.21 shows the equivalent plastic strain result at the end of FE-analyses (at a displacement of 6 mm) based on two different element sizes. From Figure 4.21 we can see that numerical simulation predicts the specimen fails in plate if the element size is relatively big (2 mm). However, with smaller element size (0.5 mm) near weld, FE-result shows that the specimen fails in weld, which is in accordance with the test result.

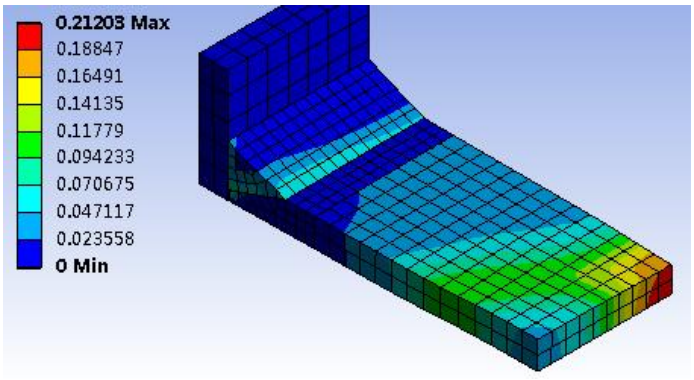

(a)

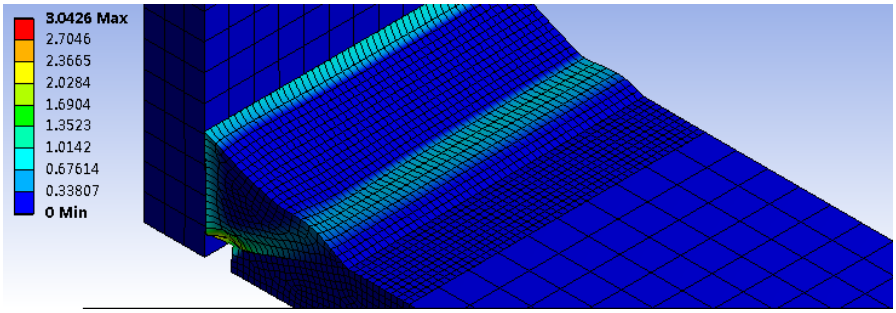

(b)

Figure 4.21: Equivalent plastic strain at the end of FE-analysis
(a) 2 mm element size, (b) 0.5 mm element size

More analyses were done based on several different element sizes (Figure 4.22). Note that the analyses of specimen 3B1 show that if the specimen fails in plate, the element size won't have an obvious influence on the simulation results, so no refinement at plate is made.

The results show that with element size bigger than 1 mm, the specimen will fail in plate; with element size smaller than 0.7 mm, the specimen will fail in weld.

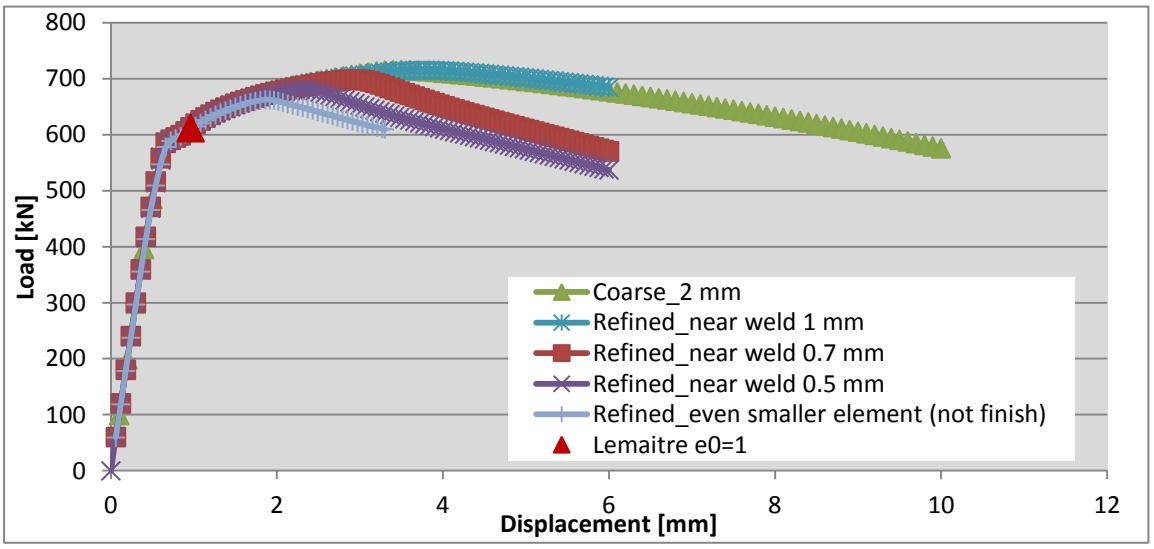

Figure 4.22: FE-analyses results of Specimen 4B1

From Figure 4.22 it seems that using different element sizes will give different load-displacement FE-results. However, this is because of the given displacement in the simulation is very large compared to actual deformation capacity of the specimen. Actually both the experimental and the FE-analyses (using Lemaitre's criterion, based on simulation result with 0.5 mm element size) results show that the failure happens at a very small displacement, when all the simulation results are still identical. So the element size is considered having very little influence on the load-displacement curve.

Lemaitre's criterion

No problems were encountered in the experiment with the LVDT's. So the numerical results can be compared directly with the average of the two LVDT's.

From Section 4.1.1 it is known that the element size might affect the result of Lemaitre's criterion. From Figure 4.23 we can see that the equivalent plastic strain results have a very big difference when using different element sizes at the same displacement. It is obvious that with smaller element size, the equivalent plastic strain is more concentrated and has a much higher value.

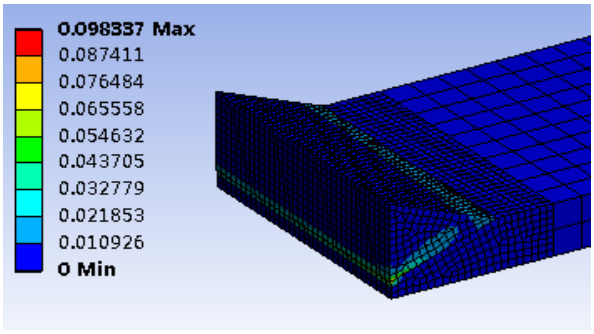

(a)

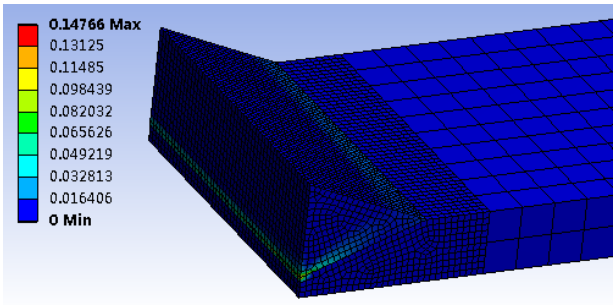

(b)

Figure 4.23: Equivalent plastic strain at a displacement of 0.96 mm (2*0.48)
(a) 0.7 mm element size, (b) 0.5 mm element size

So the influence of element size on Lemaitre's criterion is checked again using two similar element sizes (0.5 mm and 0.7 mm) and the results are shown in Figure 4.24. From Figure 4.24 it can be observed that unlike specimen 3B1, for specimen 4B1 the difference happens in a very early stage. The result shows that for 0.5 mm element size the failure happens in the 16th substep out of 100 total steps (displacement: 0.96 mm), while for 0.7 mm element size the failure happens at the 22th substep (displacement: 1.32 mm) (Figure 4.25). And for both analyses, the failure occurs at the weld root at (near) the middle of specimen width.

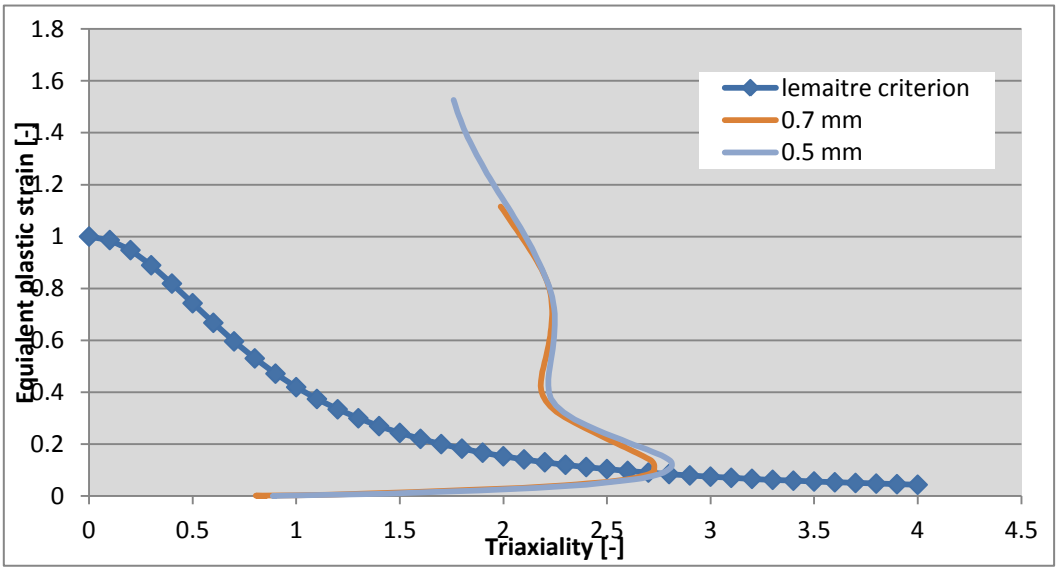

Figure 4.24: Lemaitre's criterion check

Figure 4.25 shows the comparison of experimental and numerical results, the Lemaitre's criterion is also shown based on two checked element sizes.

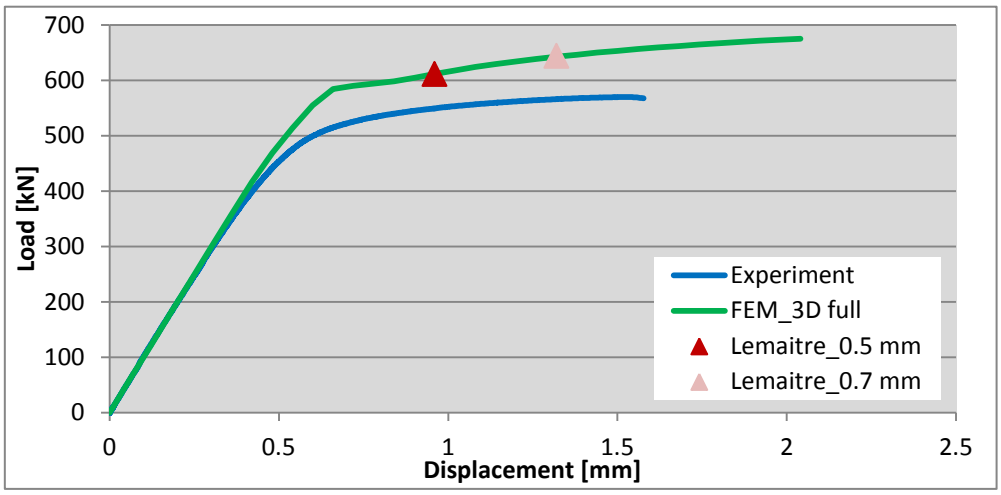

Figure 4.25: Comparison of experimental and numerical results

Several remarks can be made with respect to this figure:

1) In the elastic range the analyses agree with the experiment, the yield strength is over predicted;

2) The plastic capacity is overestimated (less than 8 %) by the FE-analysis. However, the simulative and the experimental results have similar hardening trend in plastic stage;

3) Failure deformation according to the Lemaitre's criterion is highly influenced by the element size used in the simulation;

4) The deformation capacity is underestimated by FE-analyses and smaller element size will give a more conservative result;

5) The failure mode (weld failure) is predicted very well if the element size near weld is small enough. According to FE-analyses, failure starts at (near) the middle of the weld root.

Based on the presented results, it can be concluded that the FE-analyses provide comparable load-displacement results to the experiment if the failure happens in the weld. However, for deformation capacity, the error between the numerical simulation (based on Lemaitre's criterion) and experimental results is big.

For specimens fail in weld, because of the complexity near weld, a refinement is necessary. It is unfortunately that due to the limitation of the calculation device, 0.5 mm is the smallest element size that can be used in the simulations. For more accurate simulation results, a smaller element size is necessary.

4.1.3 Specimen 1B1

Specimen 1B1 is a 12 mm thick S690 overmatched specimen. The failed specimen is presented in Figure 4.26, [8].

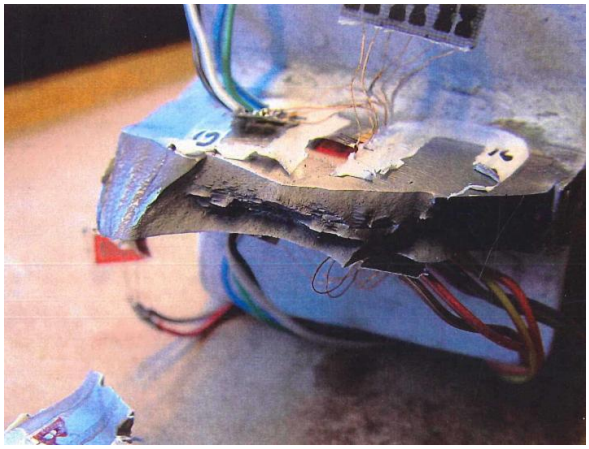

Figure 4.26: Specimen 1B1

The measured dimensions of the specimen are presented in Figure 4.27 ([8]). The dimensions in the side view show that upper right weld has the smallest dimensions.

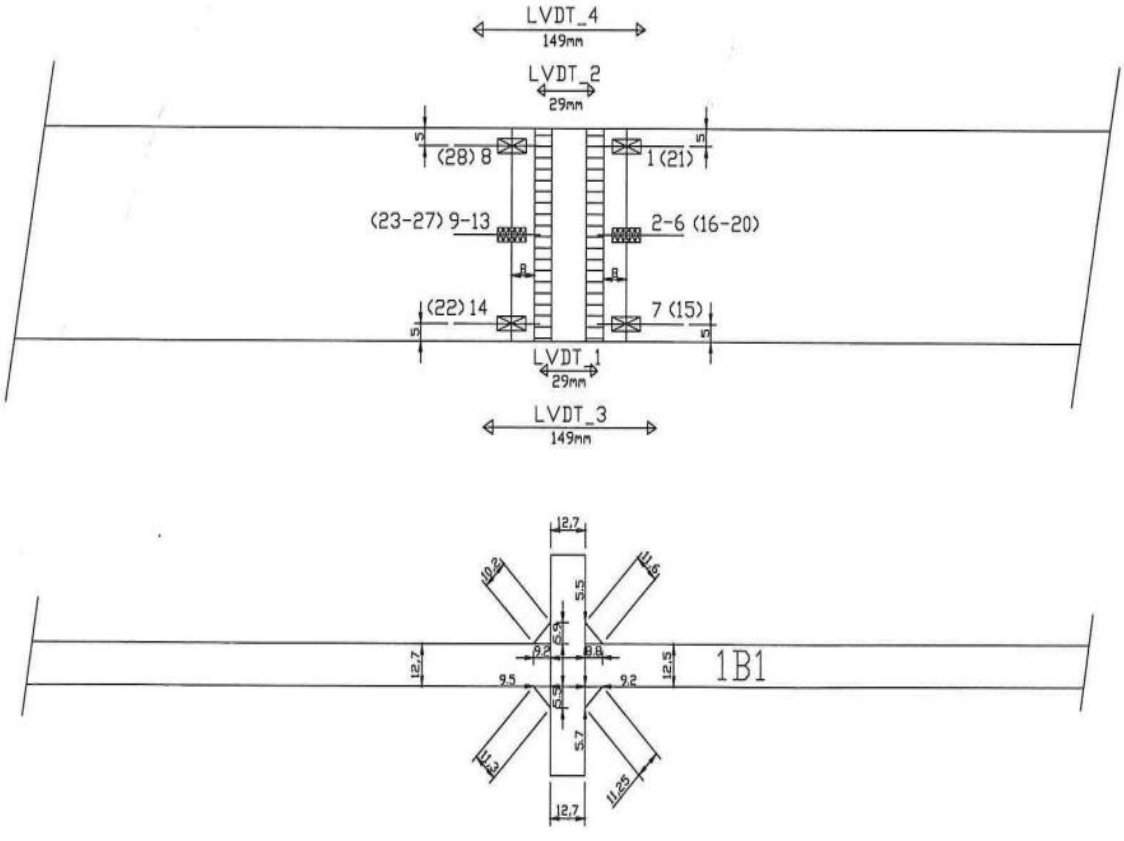

Figure 4.27: Measured dimensions of specimen 1B1

The geometry and the mesh are comparable to specimen 3B1 (Figure 4.28).

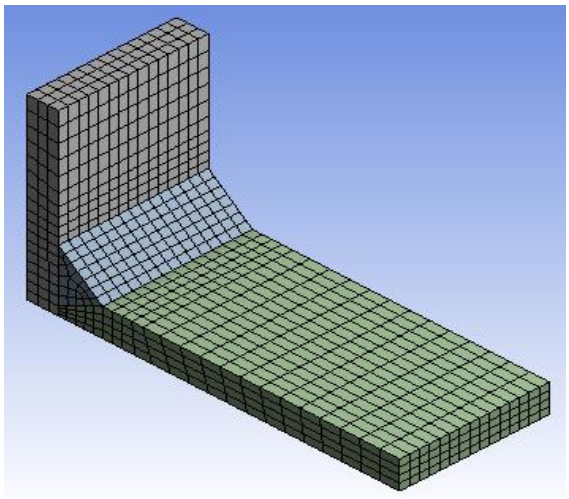

Figure 4.28: Geometry and mesh specimen 2B4, 2 mm element size

The element size effect is briefly checked and the results are given in Figure 4.29. It seems that the element size won't affect the load-displacement curve. And the following analysis is based on the results of 2 mm element size near weld.

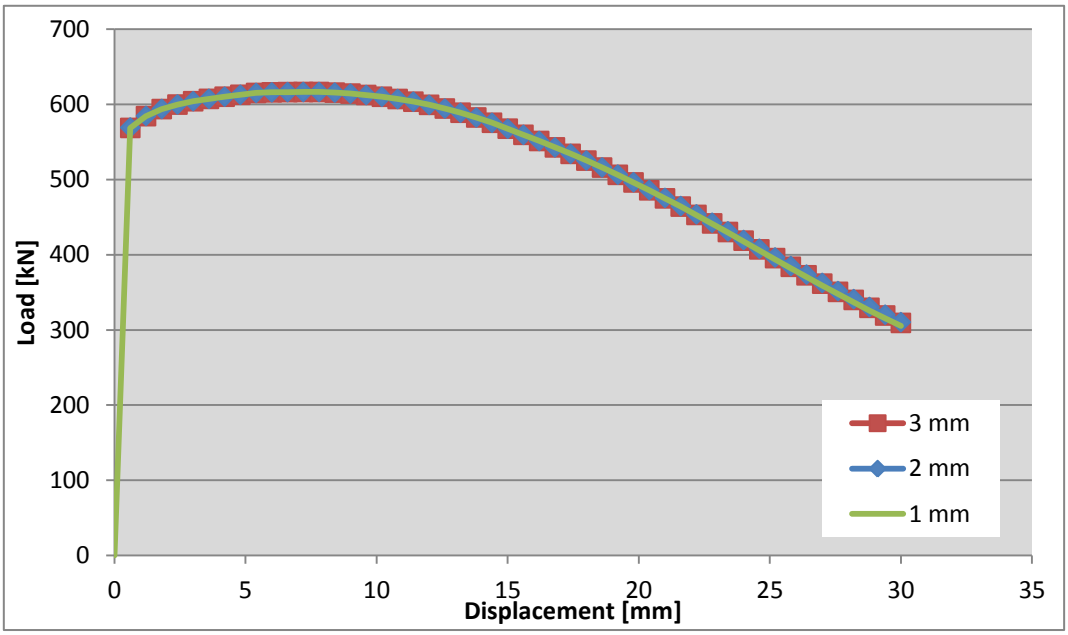

Figure 4.29: FE-analyses results of Specimen 1B1

As the LVDT's fell of the specimen, the same interpretation procedure as for 3B1 is carried out. The experimental load-displacement curves, including the lower and upper bounds are given in Figure 4.30, using the corrected data different from the report [4].

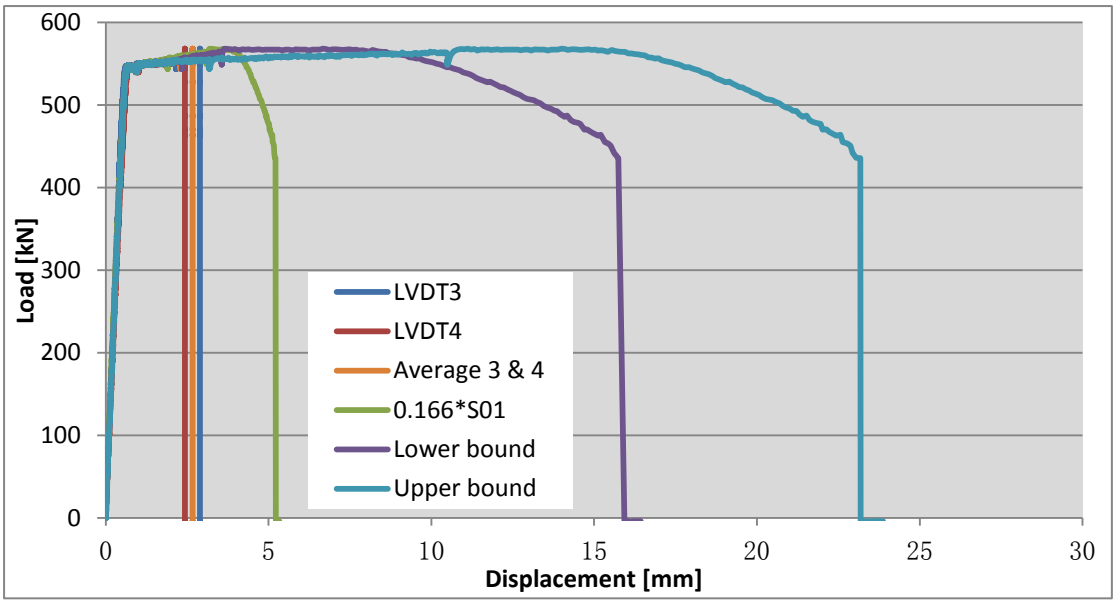

Figure 4.30: Determination of upper and lower bound of the experiment results

The comparison of the FEM analyses with the experimental results is given in Figure 4.31.

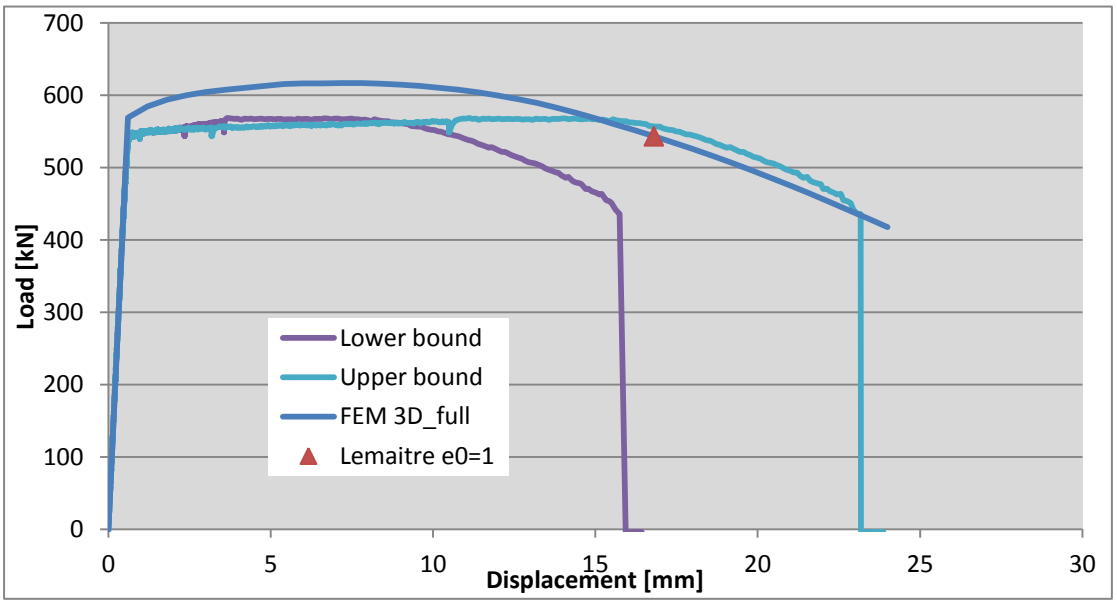

Figure 4.31: Comparison of experimental and numerical results for specimen 1B1

The comparison between FEM and experimental result shows that:

1) In the elastic range the analysis agrees with the experiment;

2) The maximum load is over predicted by 8 % in the analysis;

3) The deformation capacity in the FEM analysis is between the upper and lower bounds.

The distribution of the plastic strain at the end of the FEM analysis is given in Figure 4.32. The distribution of plastic strain at the end of the FEM analysis (at a displacement of 30 mm) shows that the overmatched welded connection is not critical and failure can be expected in the plate. This is confirmed by the experiment.

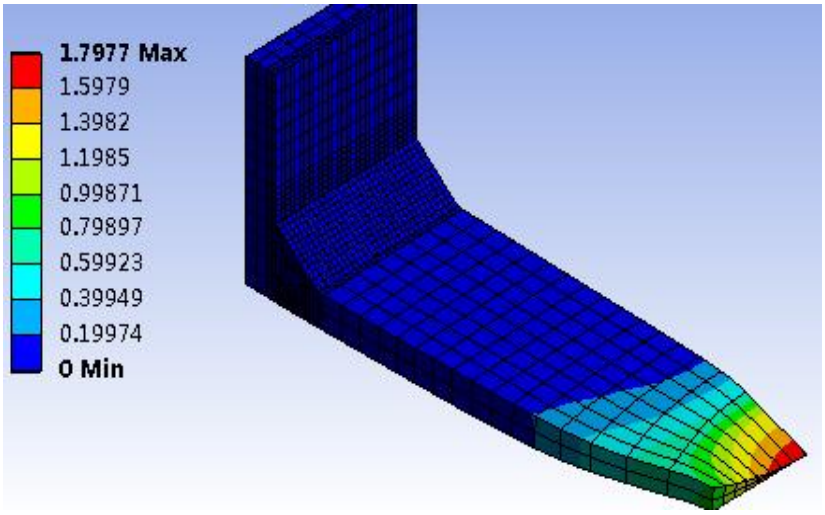

Figure 4.32: Distribution of plastic strain in specimen (end of FEM analysis)

4.1.4 Specimen 2B4

Specimen 2B4 is a 40 mm thick S690 overmatched specimen (Figure 4.33, [8]). The plates are connected by means of an overmatched full penetration K-joint.

Figure 4.33: Specimen 2B4

The measured dimensions are given in Figure 4.34 [8]. The dimensions in the side view show that the upper left weld has the smallest dimensions.

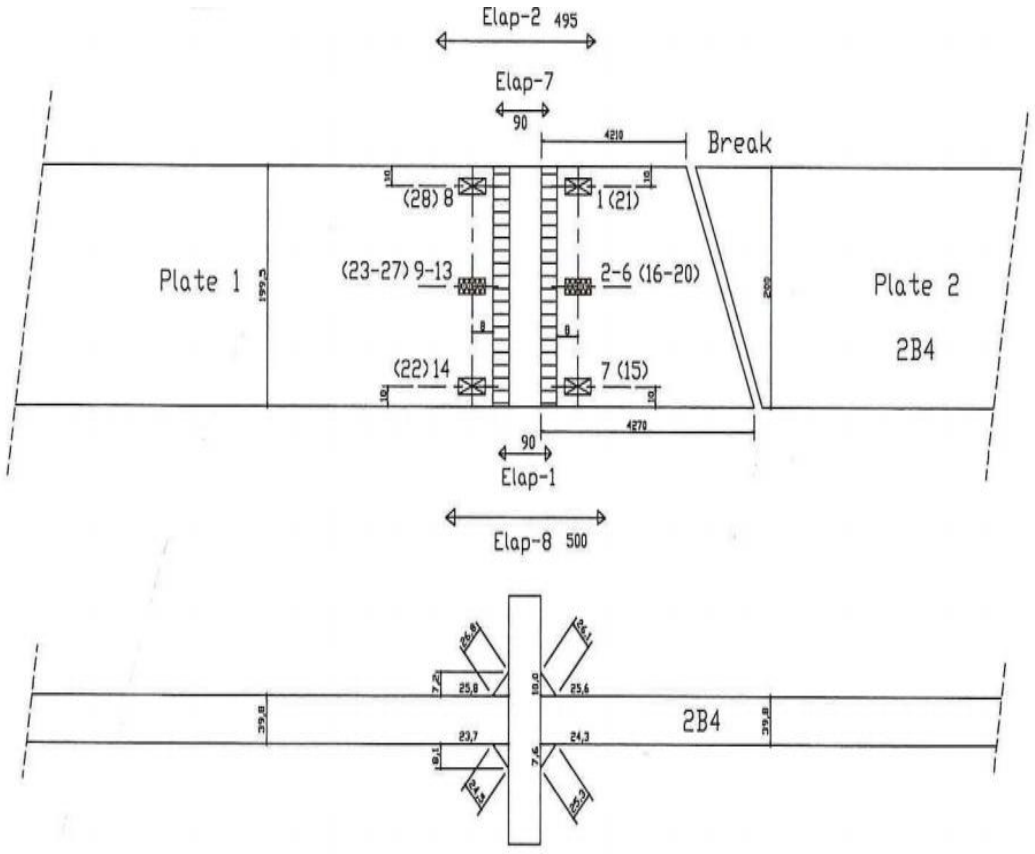

Figure 4.34: Measured dimensions specimen 2B4

For specimens with 40 mm plate thickness, it is modeled with a root opening of 5 mm (Figure 4.35).

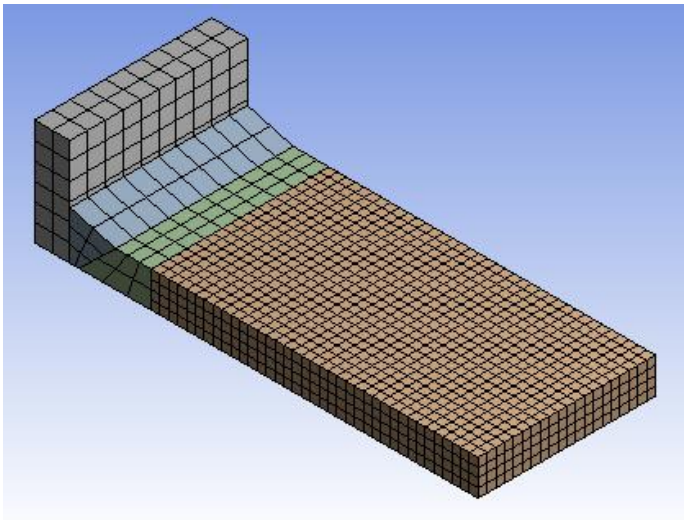

Figure 4.35: Geometry and mesh specimen 2B4, 5 mm element size at plate

The element size effect is checked and the results are given in Figure 4.36, the refinement at plate is not necessary based on the result of specimen 3B1. However, the 5 mm element size for plate material is used for the following analysis.

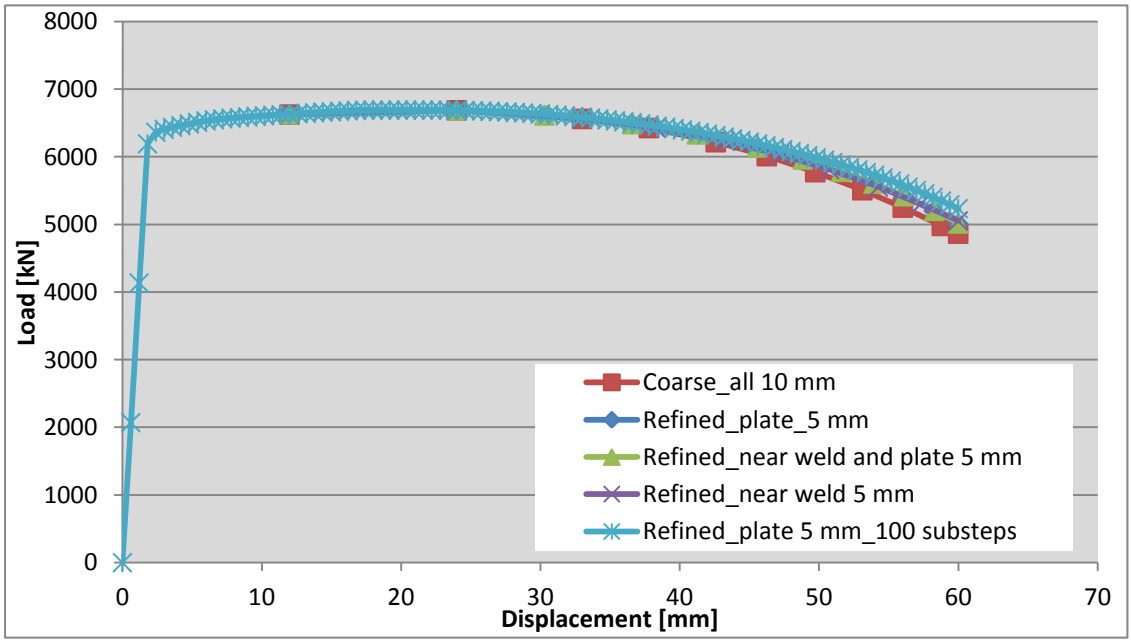

Figure 4.36: FE-analyses results of Specimen 2B4

No problems were encountered in the experiment with the LVDT's. So, the numerical results can be compared directly with the average of the two LVDT's (Figure 4.37).

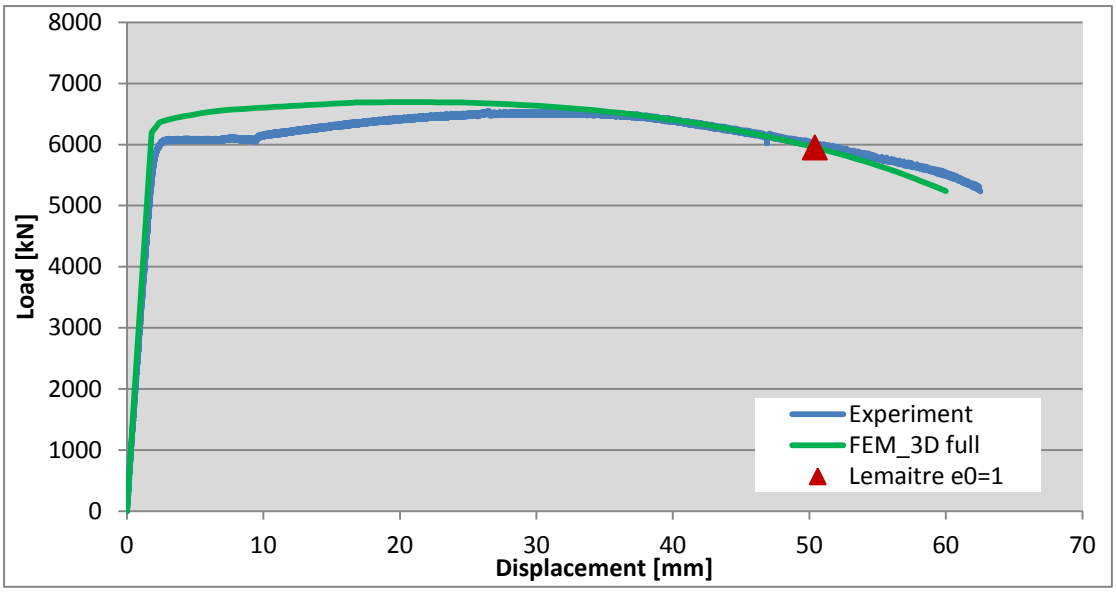

Figure 4.37: Comparison of experimental and numerical results for specimen 2B4

The comparison between FEM and experimental results showed that:

1) In the elastic range the analysis agrees with the experiment;

2) The maximum load is slightly over predicted (1 %) in the analysis;

3) The deformation capacity is underestimated by the Lemaitre's criterion.

The distribution of the equivalent plastic strain at the end of the FE-analyses (at a displacement of 60 mm) is given in Figure 4.38. It shows that the overmatched welded connection is not critical and failure can be expected in the plate. This is confirmed by the experiment.

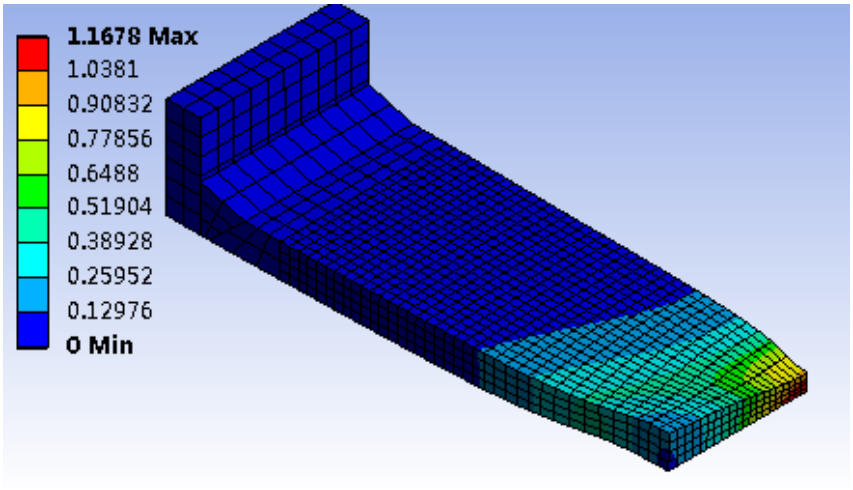

Figure 4.38: Over view of plastic strain at a displacement of 60 mm (2*30)

4.1.5 Specimen 5B1

Specimen 5B1 is a 40 mm thick S1100 undermatched specimen (Figure 4.39, [8]). The dimensions in the side view (Figure 4.40, [8]) show that lower left weld has the smallest dimensions.

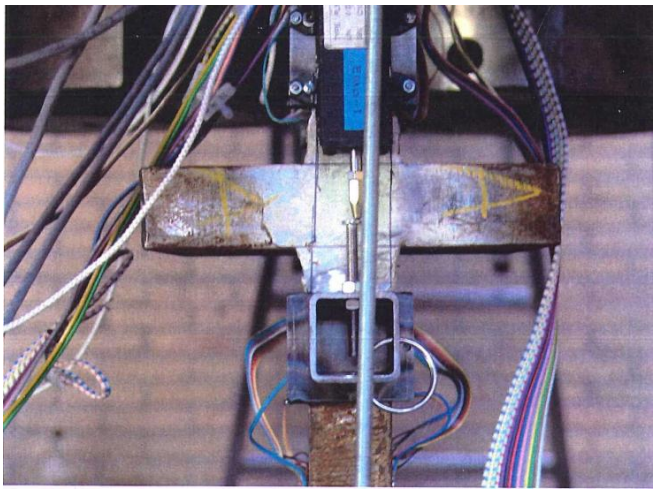

Figure 4.39: Specimen 5B1

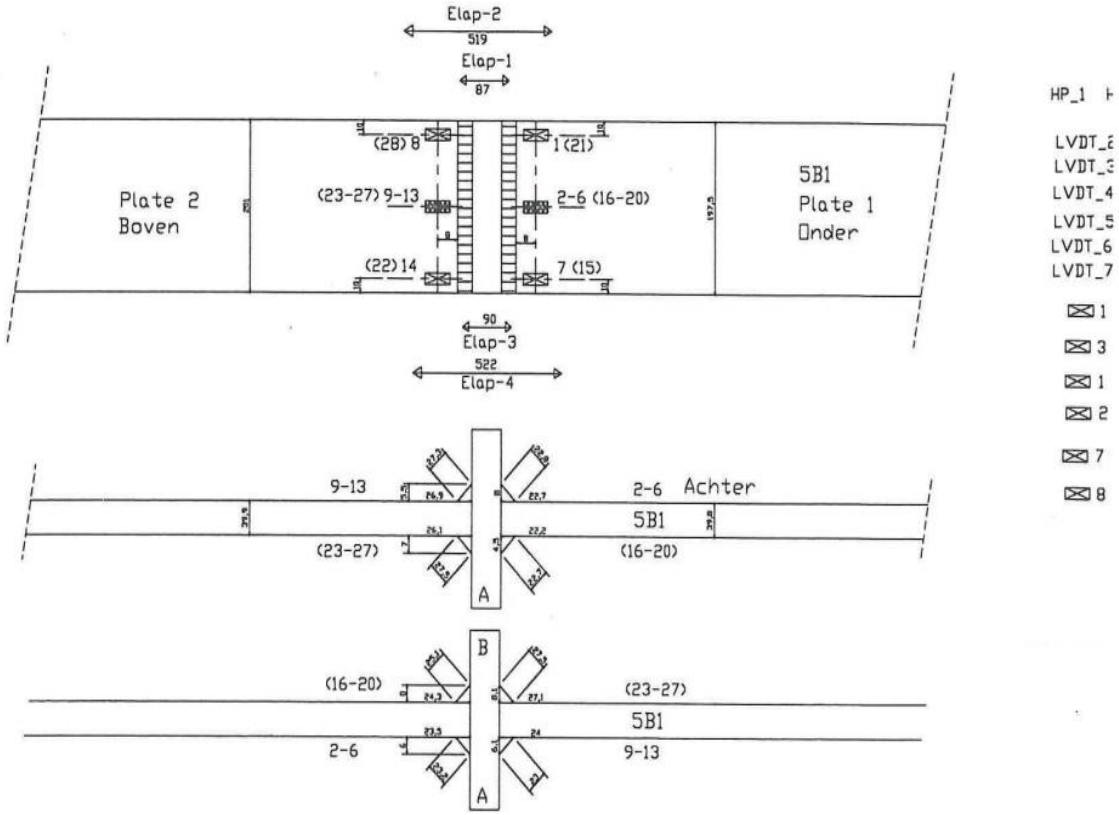

Figure 4.40: Measured geometry specimen 5B1

The geometry and the mesh are comparable to specimen 2B4 (Figure 4.41). The specimen did not fail in the experiment because the load capacity was too high for the test rig.

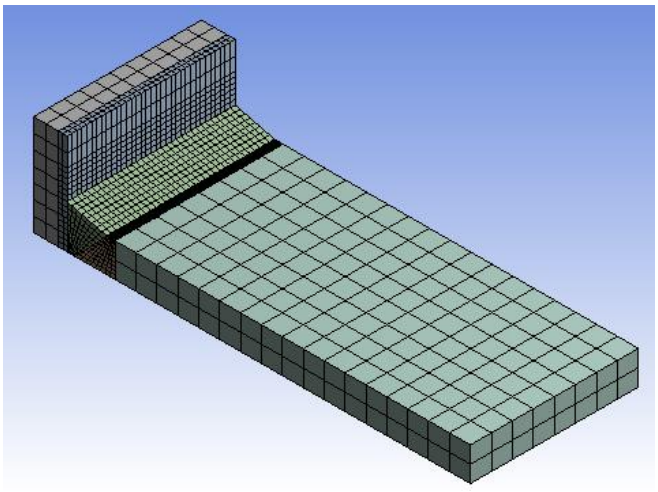

Figure 4.41: Geometry and mesh specimen 5B1, refined near weld, 3 mm

From the analyses of specimen 4B1 we know that for specimen fails at weld (undermatched weld connection), a refinement is necessary. However, the calculation device can't finish the simulation with the element size smaller than 3 mm because of "Insufficient memory was available for the solver engine to obtain a solution", the simulation will stop at the middle of calculation and only partial of the results are available (Figure 4.42). So the following analysis has to be taken with the smallest possible element size (3 mm).

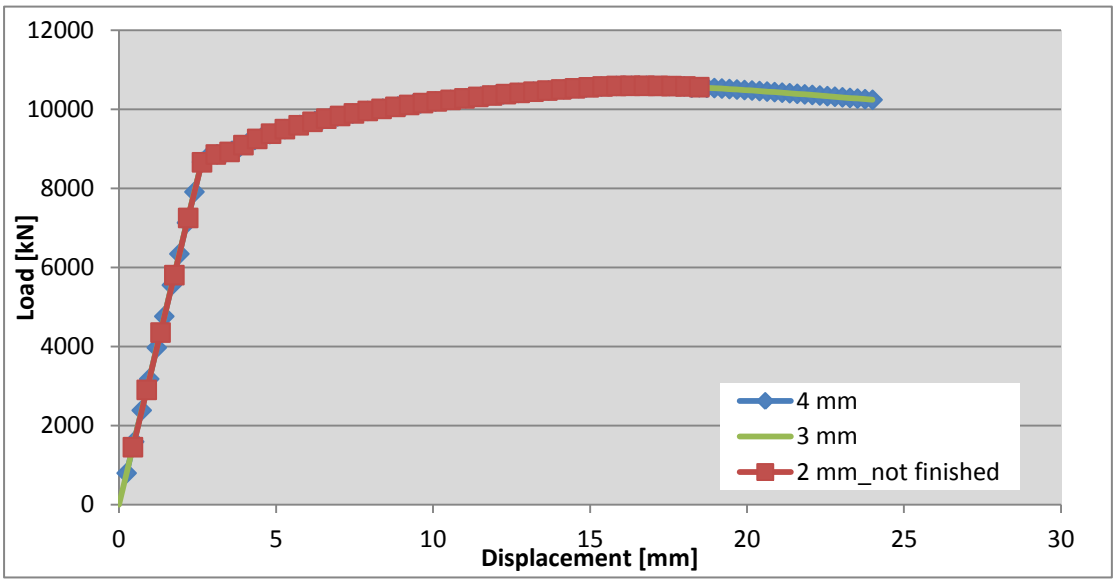

Figure 4.42: FE-analyses results of Specimen 5B1

The comparison of the numerical and experimental results is given in Figure 4.43. It seems that in the elastic range the analysis result has a slightly higher stiffness than the experiment. Because of the limitation of the element size, the deformation capacity seems quite inaccurate (fails in plate at a very large displacement), based on the analyses of specimen 4B1, the specimen could fail in weld if the element size is small enough.

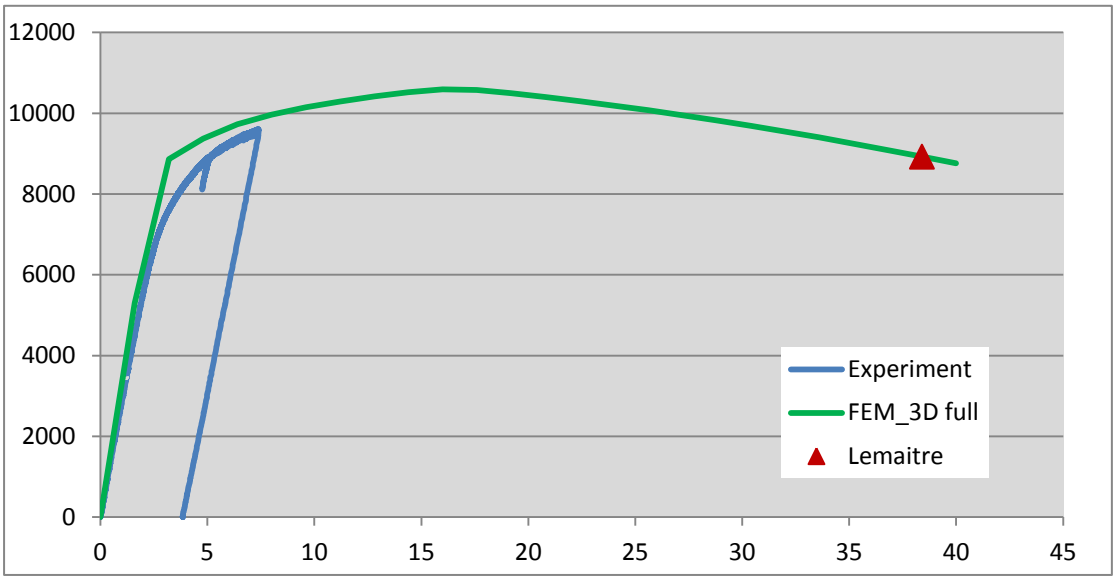

Figure 4.43: Comparison of experimental and numerical results for specimen 5B1

The distribution of the equivalent plastic strain at a displacement of 3.6 mm (2*1.8) is given in Figure 4.44.

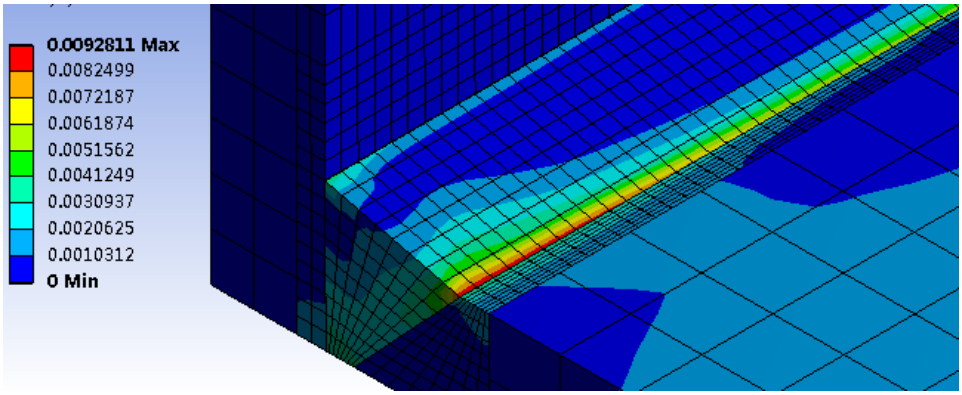

Figure 4.44: Equivalent plastic strain at a displacement of 3.6 mm

4.2 Connections type C

In this section, validations are carried out for five C-geometries. The C-geometry is an X-connection with a high stress concentration factor (SCF) and the simplified geometry is presented in Figure 4.45. This geometry can not be approximated by 2D geometries, so 3D geometries are used for analyses.

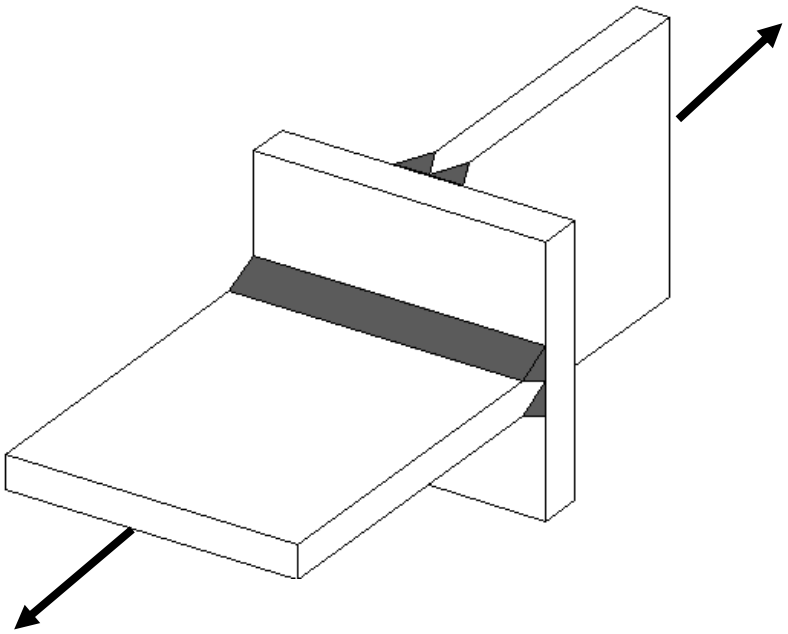

Figure 4.45: Specimen geometry C (with high SCF)

In the next sections the FEM results are compared to the experimental results. The simulation procedures are similar to connection B.

The comparison is mainly based on the load-displacement curve over the length of test gauges. For specimen 1C1 the measuring equipment did not function until the end of the test and an additional interpretation of the experimental results is also made.

4.2.1 Specimen 1C1

Specimen 1C1 is a 12 mm thick S690 undermatched specimen (Figure 4.46, [8]). The measured dimensions (Figure 4.47) show the smallest weld dimensions (9.05 mm).

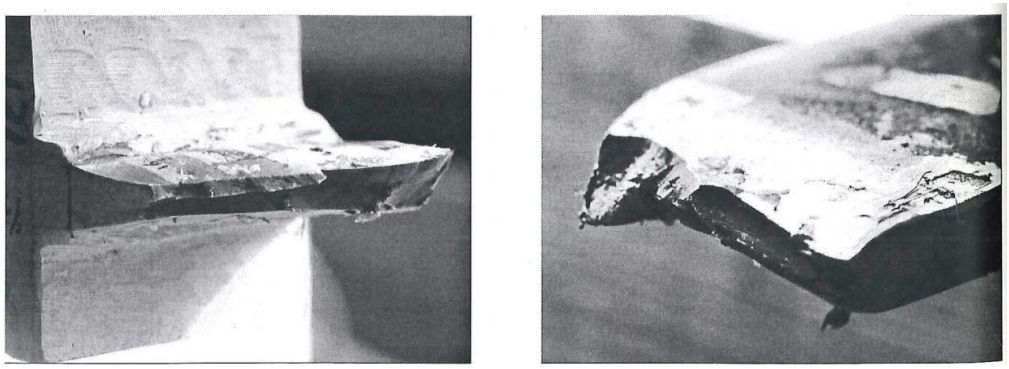

Figure 4.46: Specimen 1C1

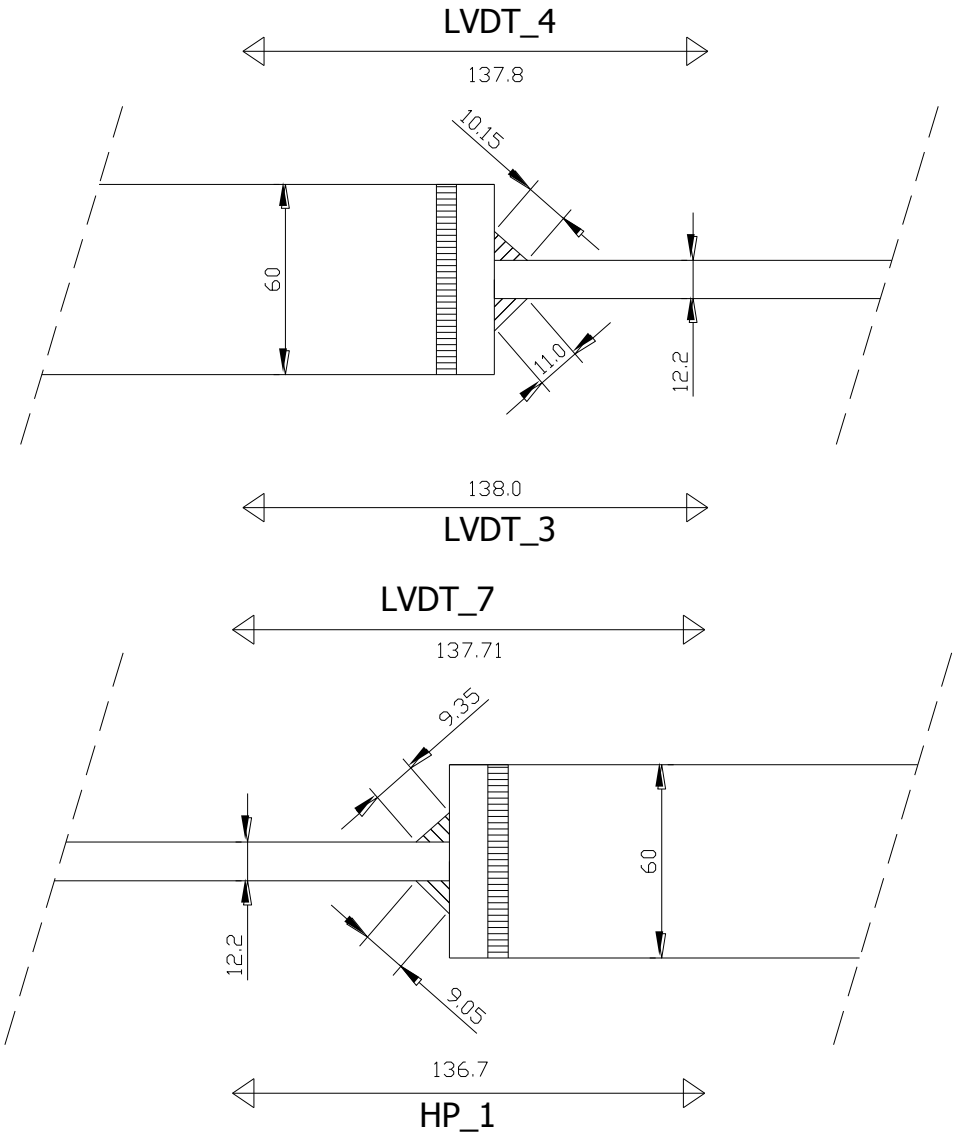

Figure 4.47: Measured dimensions specimen 1C1

The geometry and the mesh are given in Figure 4.48. Both the left and right parts are modeled with the same (smallest) weld size. Previous section has already proven that if the failure happens in plate, the element size at plate doesn't really matter, so the refinement is made only near the weld.

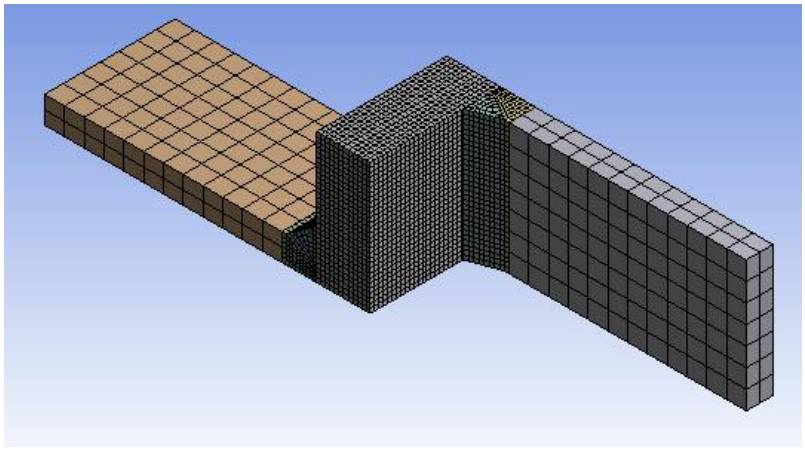

Figure 4.48: Geometry and mesh specimen 1C1, refined near weld, 1 mm

The influence of element size is checked and compared in Figure 4.49. The 1 mm element size near weld is used for the following analysis.

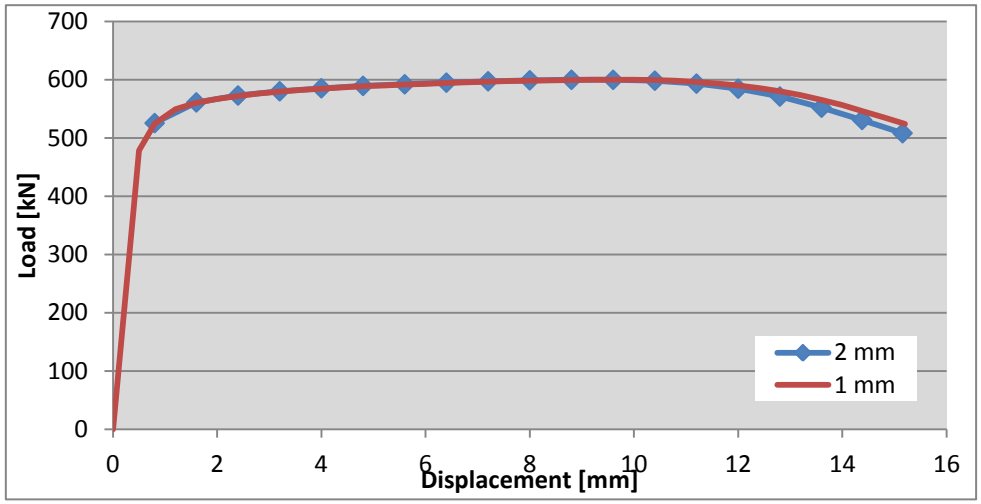

Figure 4.49: FE-analyses results of Specimen 1B1

The FE-analyses show that for this specimen, the failure happens in the plate (Figure 4.57), which is in accordance with the test result.

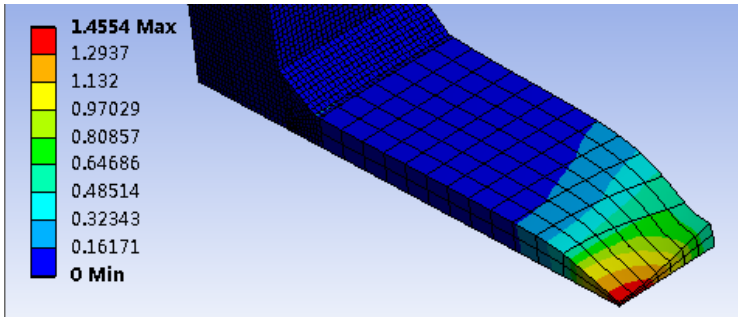

Figure 4.50: Equivalent plastic strain at the displacement of 14 mm

As the LVDT's fell of the specimen, the same interpretation procedure as for 3B1 is carried out. The experimental load-displacement curves, including the lower and upper bounds are given in Figure 4.51. Because of gauge LVDT4 and HP1 provide questionable data, only LVDT3 and LVDT7 results are used.

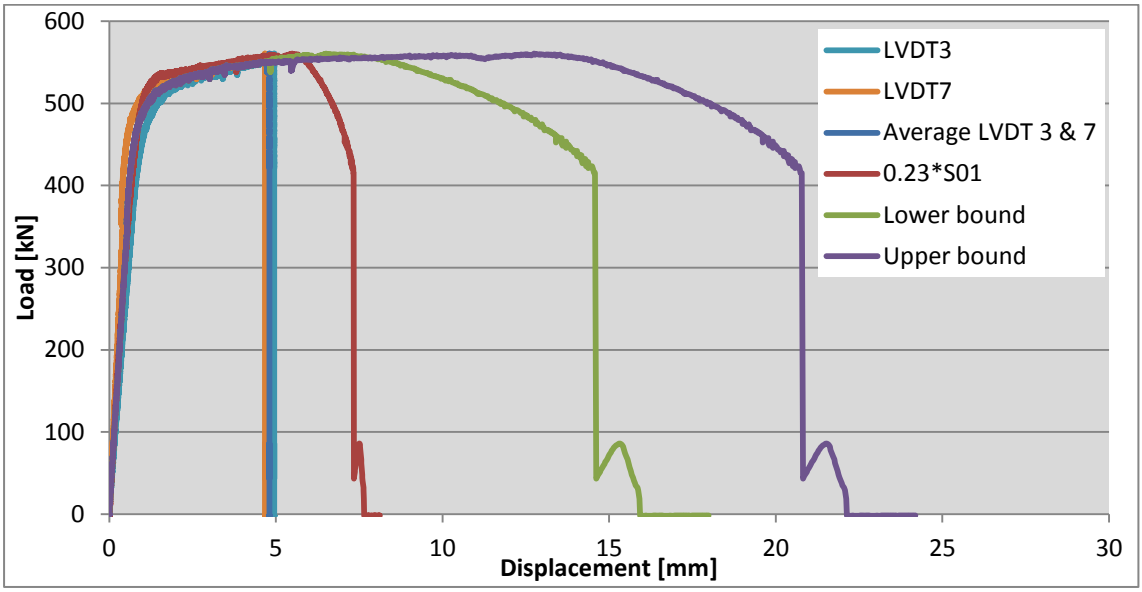

Figure 4.51: Determine of upper and lower bound of the experimental results

The comparison of the numerical and experimental results is given in Figure 4.52. It seems that in the elastic range the analysis result has a slightly higher stiffness than the experimental result. The maximum load is over predicted by 7 % in the FE-analysis. The deformation capacity in the FE-analysis is between the upper and lower bounds.

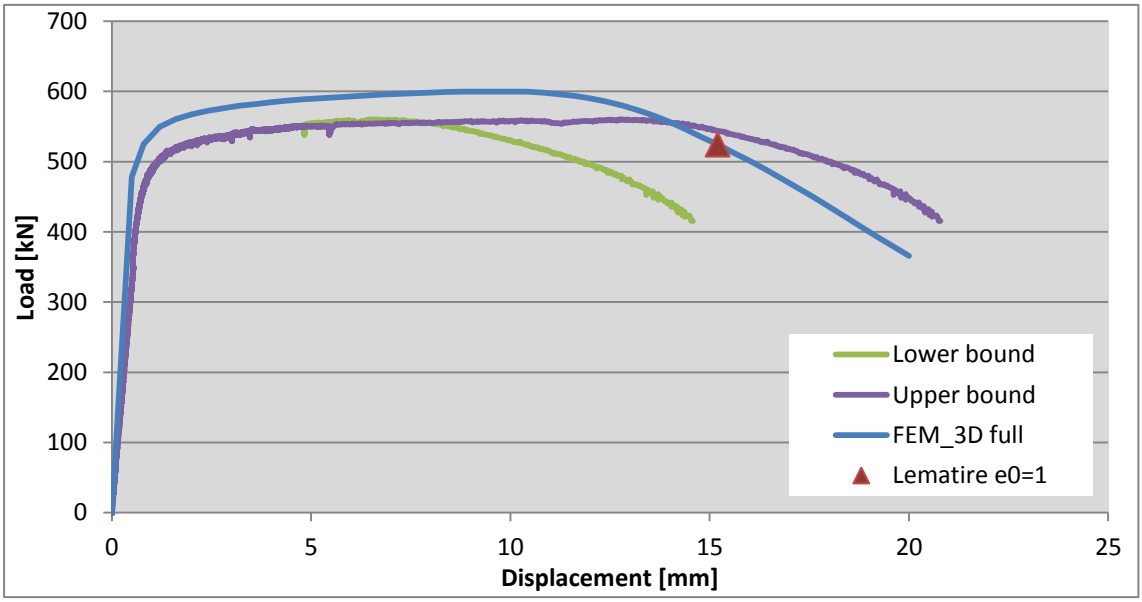

Figure 4.52: Comparison of experimental and numerical results for specimen 1C1

4.2.2 Specimen 2C1

Specimen 2C1 is a 40 mm thick S690 overmatched specimen (Figure 4.53, [8]). The measured dimensions (Figure 4.54) show the smallest weld dimensions (25.8 mm).

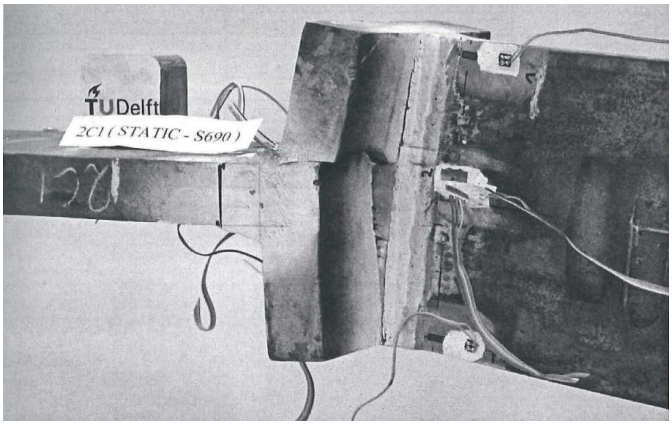

Figure 4.53: Specimen 2C1

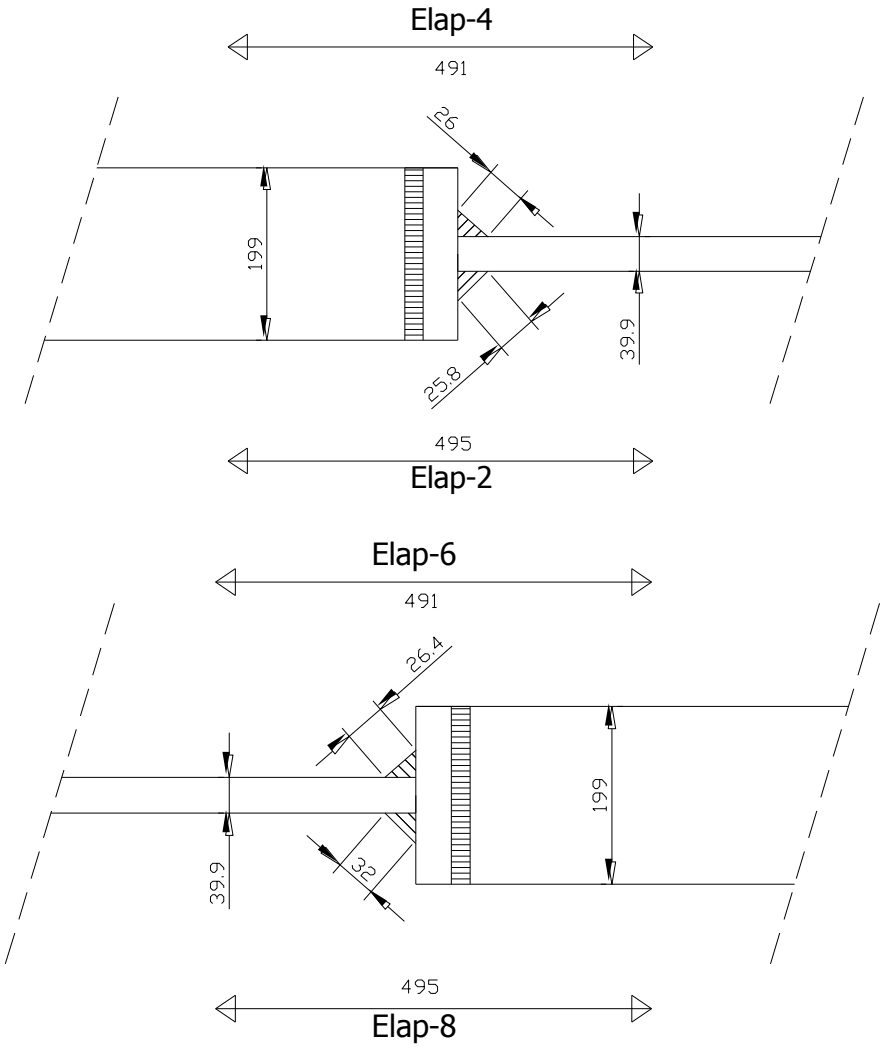

Figure 4.54: Measured dimensions specimen 2C1

The geometry and the mesh are comparable to specimen 2B4, both the left and right parts are modeled with the same (smallest) weld size, the refinement is made near the weld (Figure 4.55).

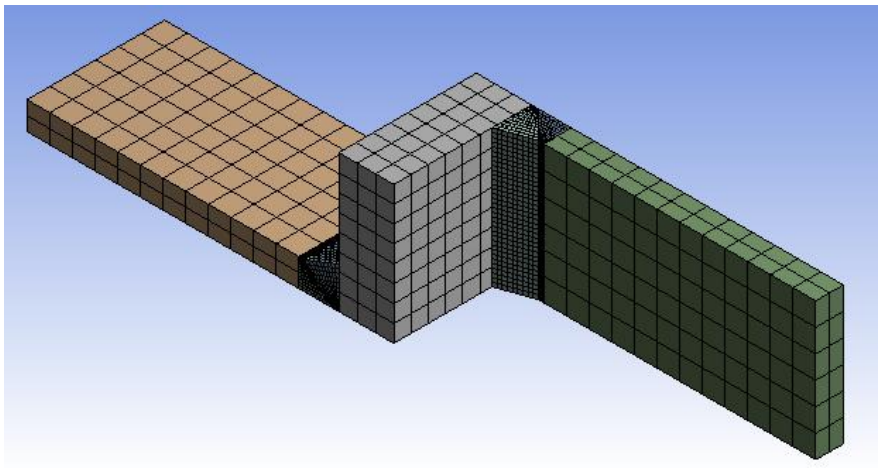

Figure 4.55: Geometry and mesh specimen 2C1, refined near weld, 3 mm

The influence of element size is checked and compared in Figure 4.56. The 3 mm element size near weld is used for the following analysis.

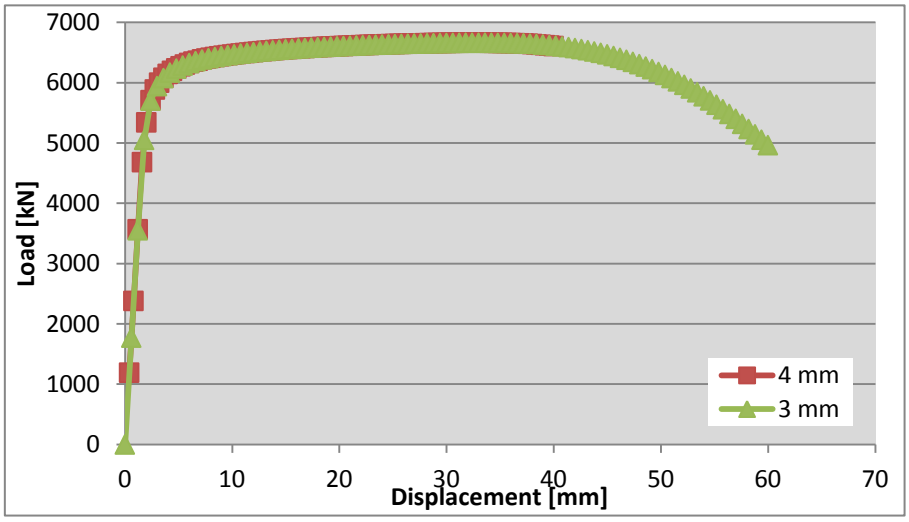

Figure 4.56: FE-analyses results of Specimen 2B1

The FE-analyses show that for this specimen, the failure happens in the plate (Figure 4.57).

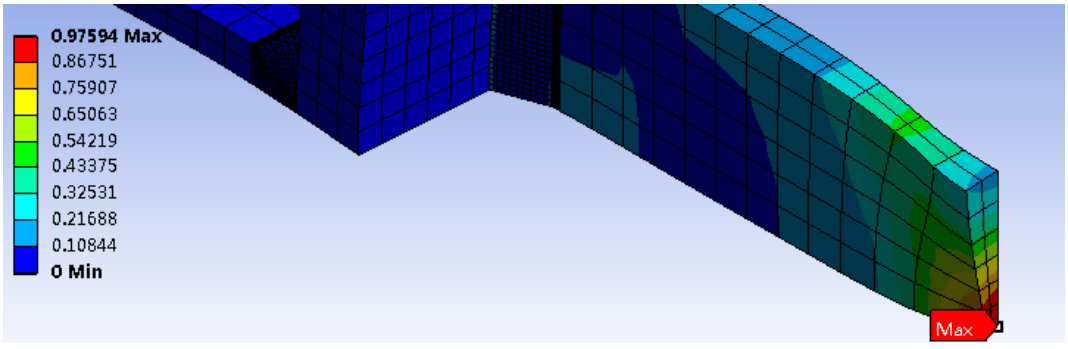

Figure 4.57: Equivalent plastic strain at the end of FE-analysis (3 mm element size)

The comparison of the numerical and experimental results is given in Figure 4.58. It seems that in the elastic range the analysis agrees with the experiment. And the maximum load is over predicted by the FE-analysis (less than 12%).

However, the ultimate deformation capacity has a dramatic difference with the experimental result. Based on the analyses of specimen 3B1, we know that for specimens fail in plate, the estimated deformation shouldn't have such a big error. From Figure 4.53 we know that in the test the specimen fails in the connection plate and adjacent weld. This phenomenon has never been found from the other specimens. So the difference between experimental and analytical results is possibly because of the test specimen has some defects and fails in an unexpected position.

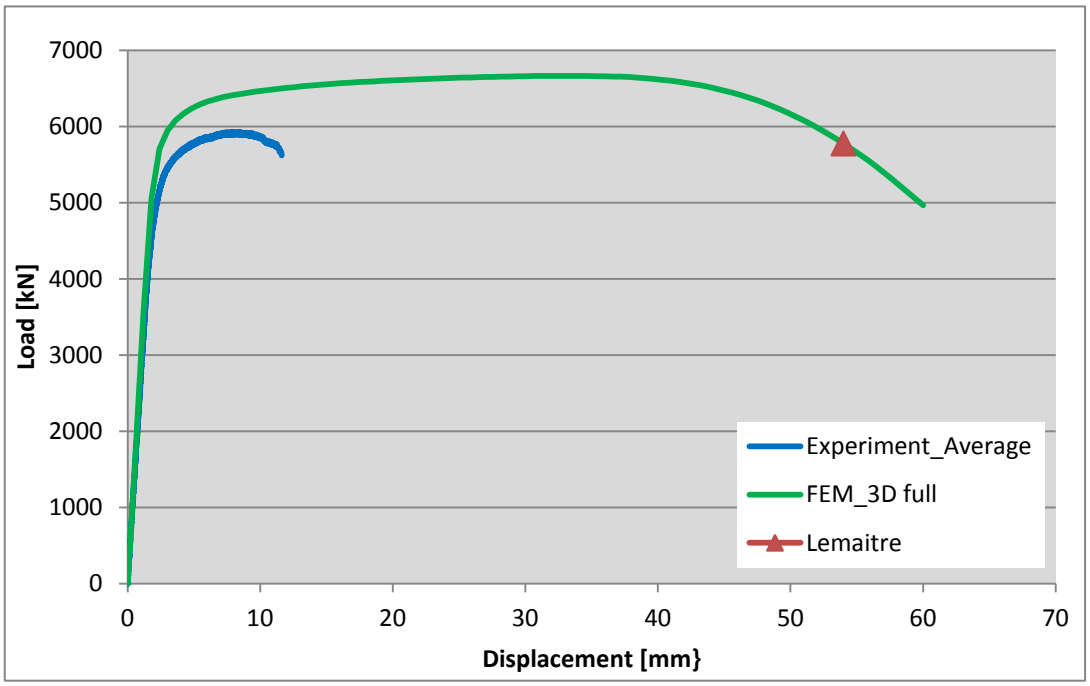

Figure 4.58: Comparison of experimental and numerical results for specimen 2C1

4.2.3 Specimen 3C1

Specimen 3C1 is a 12 mm thick S690 undermatched specimen (Figure 4.59). The measured dimensions (Figure 4.54) show the smallest weld dimensions (9.45 mm).

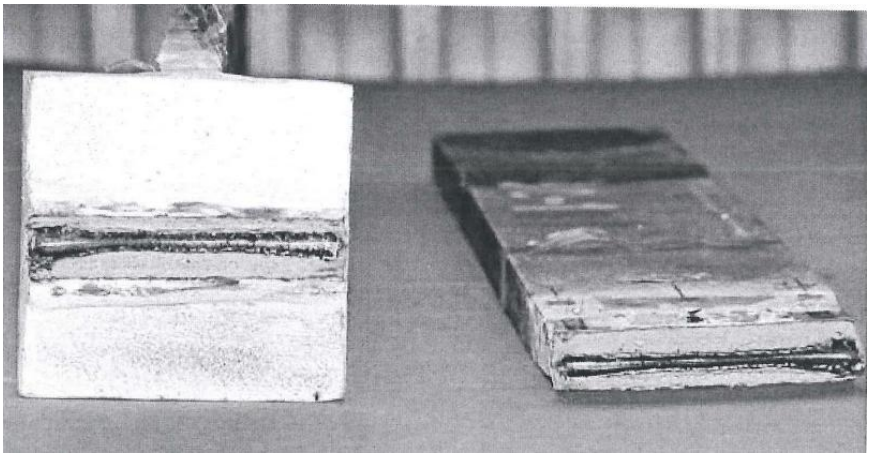

Figure 4.59: Specimen 3C1

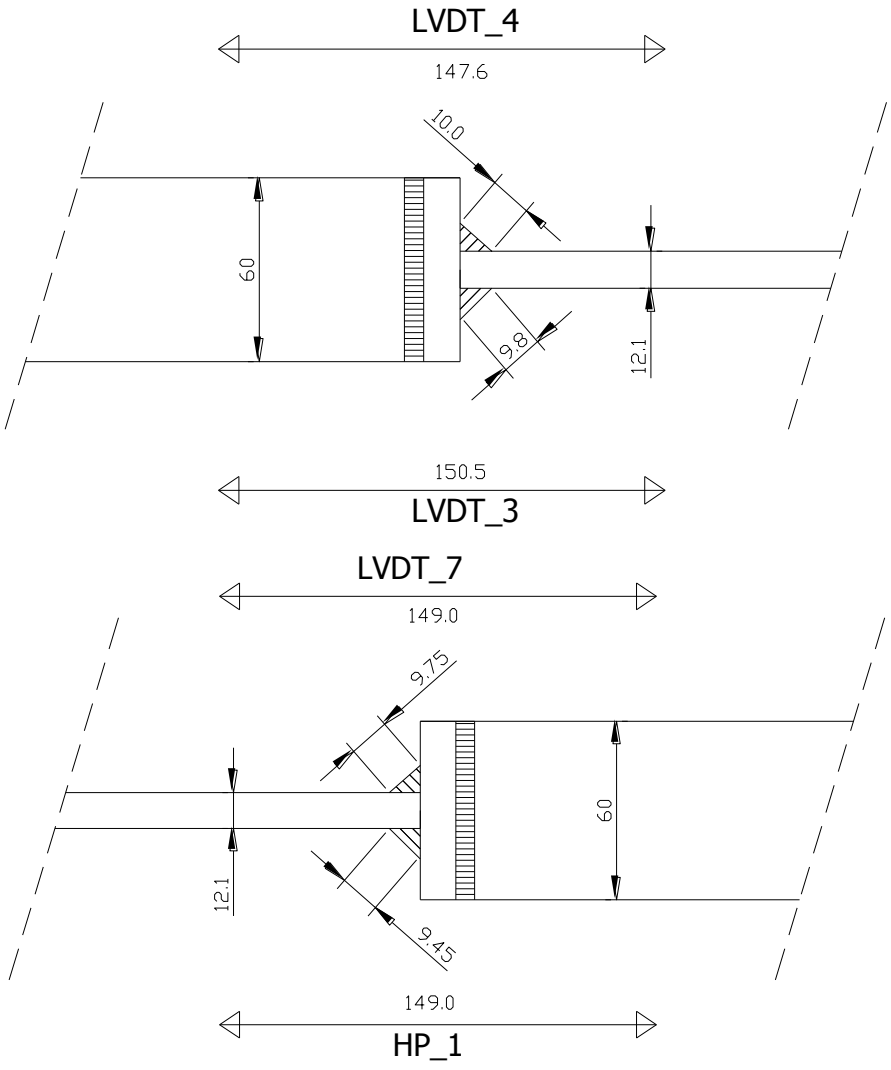

Figure 4.60: Measured dimensions specimen 3C1

The geometry and the mesh are shown in Figure 4.61, both the left and right parts are modeled with the same (smallest) weld size, the refinement is made near weld.

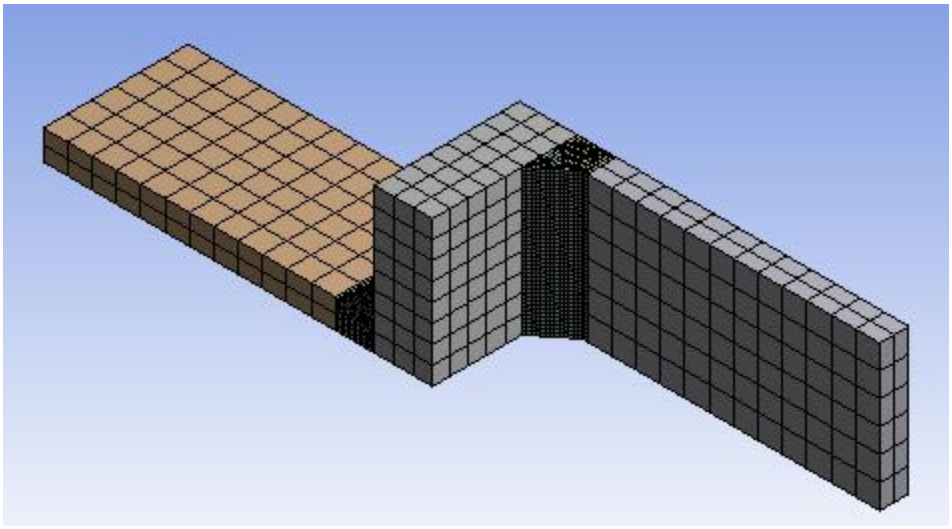

Figure 4.61: Geometry and mesh specimen 3C1, refined near weld, 0.7 mm

The influence of element size is checked and compared in Figure 4.62. The 0.7 mm element size near weld is used for the following analysis.

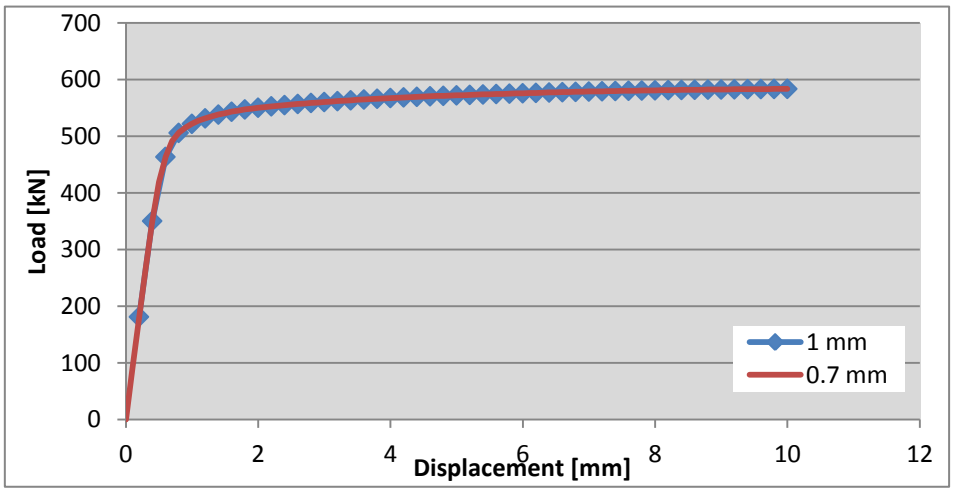

Figure 4.62: FE-analyses results of Specimen 3B1

The FE-analyses show that for this specimen, the failure happens in the weld (Figure 4.63), which is in accordance with the experimental result.

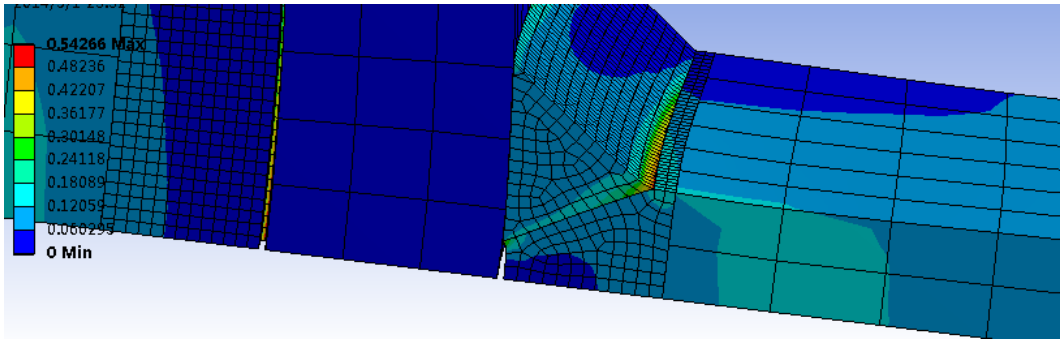

Figure 4.63: Equivalent plastic strain at the end of FE-analysis (0.7 mm element size)

The comparison of the numerical and experimental results is given in Figure 4.64. It seems that in the elastic range the analysis agrees with the experiment. And the maximum load is slightly over predicted by the FE-analysis (2%).

The ultimate deformation capacity is also seems comparable to the experimental result. However, based on the analyses of specimen 4B1, we know that for specimens fail in plate, the estimated deformation using Lemaitre's criterion is related to element size. So for more accurate simulation results, a smaller element size is recommended.

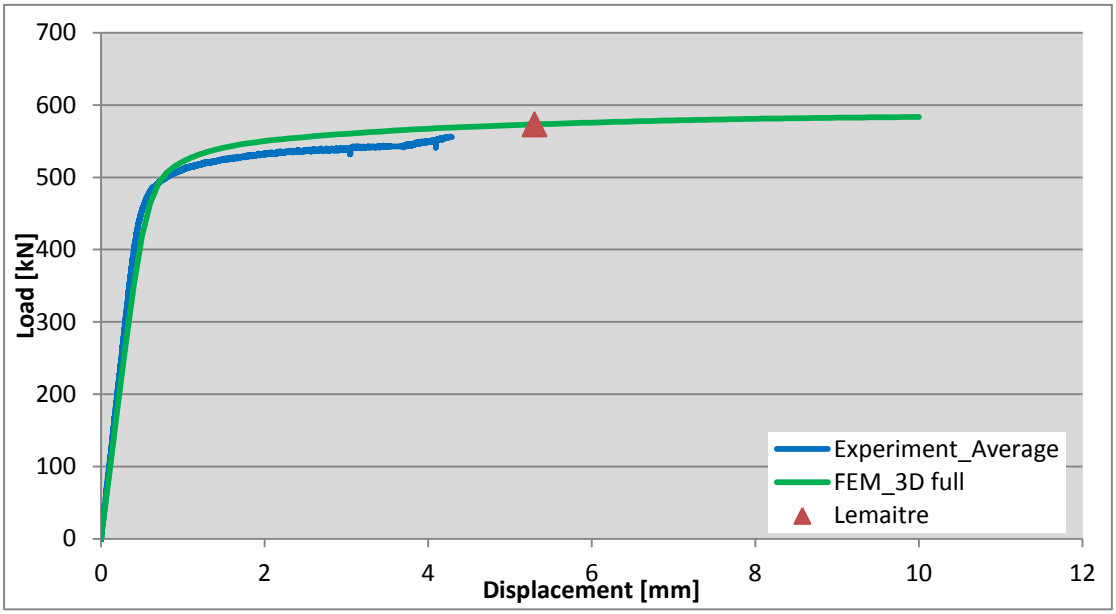

Figure 4.64: Comparison of experimental and numerical results for specimen 3C1

The stress concentration can be visualized in Figure 4.65, but the stress is more concentrated in weld.

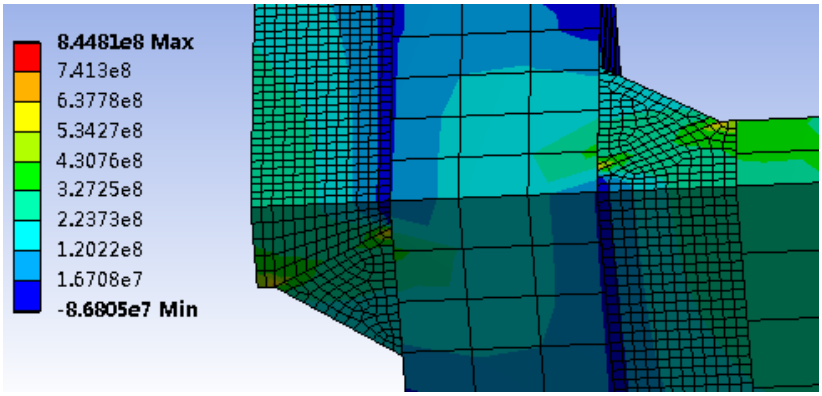

Figure 4.65: Stress concentration (normal stress at a displacement of 0.2 mm)

4.2.4 Specimen 4C1

Specimen 4C1 is a 10 mm thick S1100 undermatched specimen (Figure 4.66). The measured dimensions (Figure 4.67) show the smallest weld dimensions (6 mm x 6 mm).

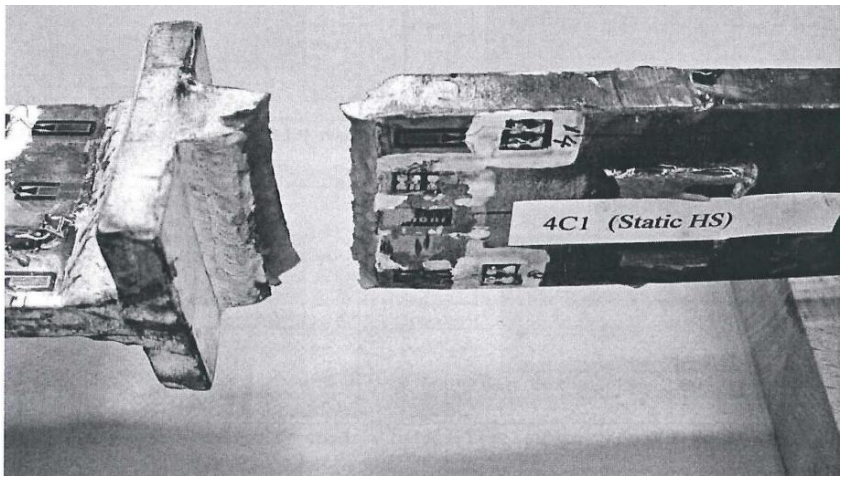

Figure 4.66: Specimen 4C1

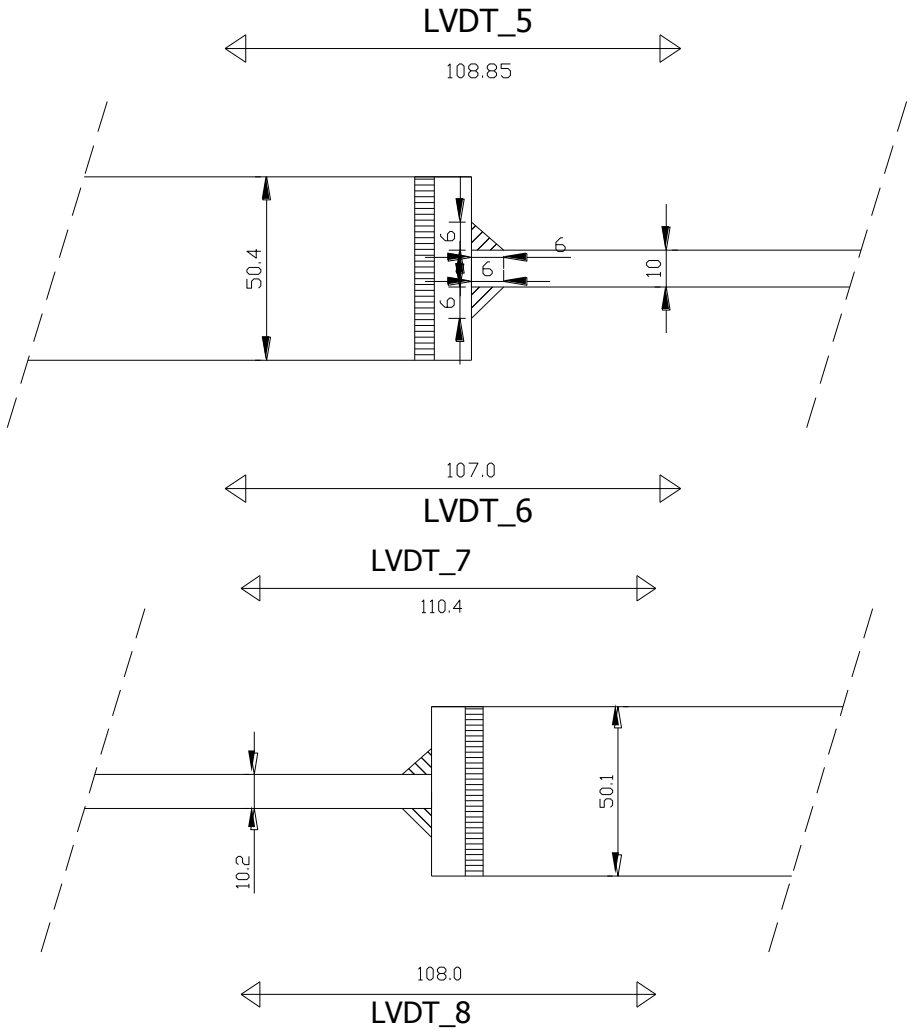

Figure 4.67: Measured dimensions specimen 4C1

The geometry and the mesh are shown in Figure 4.68, both the left and right parts are modeled with the same (smallest) weld size, the refinement is made near weld.

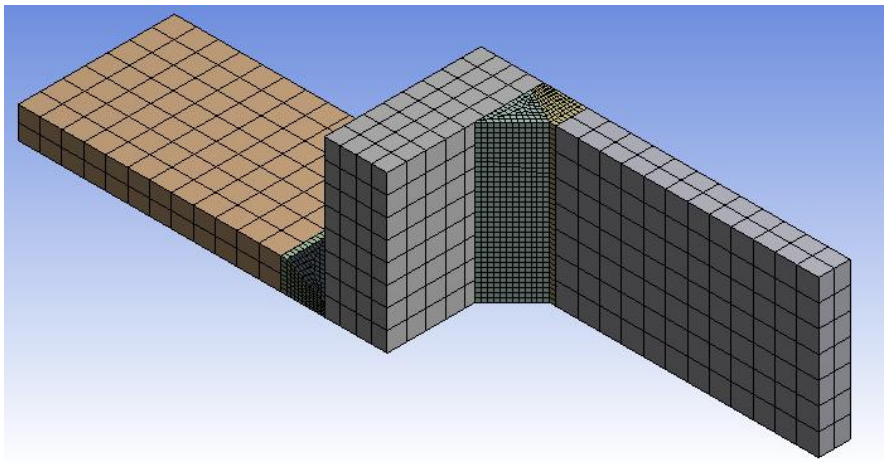

Figure 4.68: Geometry and mesh specimen 4C1, refined near weld, 0.7 mm

The influence of element size is checked and compared in Figure 4.69. The 0.7 mm element size near weld is used for the following analysis.

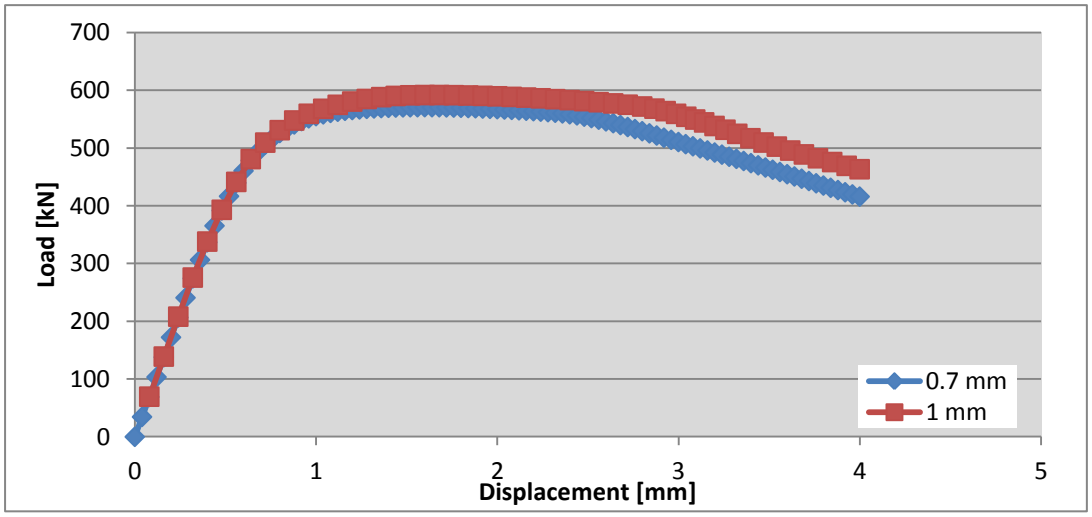

Figure 4.69: FE-analyses results of Specimen 4B1

The FE-analyses show that for this specimen, the failure happens in the weld (Figure 4.70), which is in accordance with the experimental result.

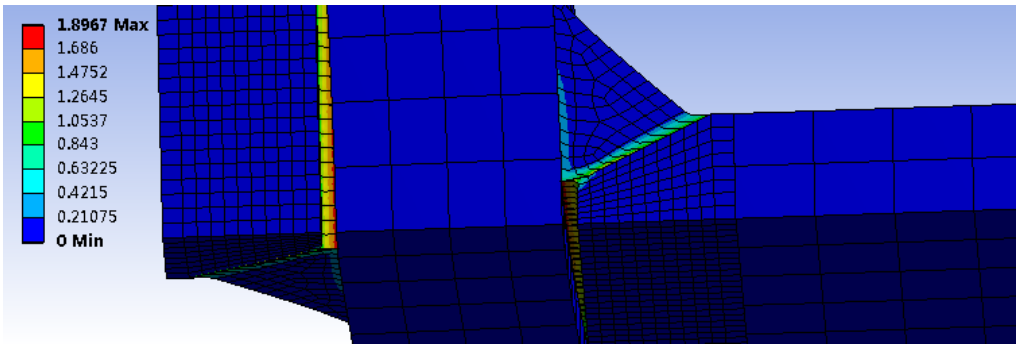

Figure 4.70: Equivalent plastic strain at a displacement of 2 mm (0.7 mm element size)

The comparison of the numerical and experimental results is given in Figure 4.71. It seems that in the elastic range the analysis has a higher stiffness than the experiment.

The ultimate deformation capacity is under estimated by the FE-analysis. Based on the Lemaitre's criterion, the specimen fails at a very early stage and because of that, the maximum load is also under estimated (around 9%). However, this FEM result is related to the element size and considered not very accurate.

For more accurate simulation results, a smaller element size is recommended.

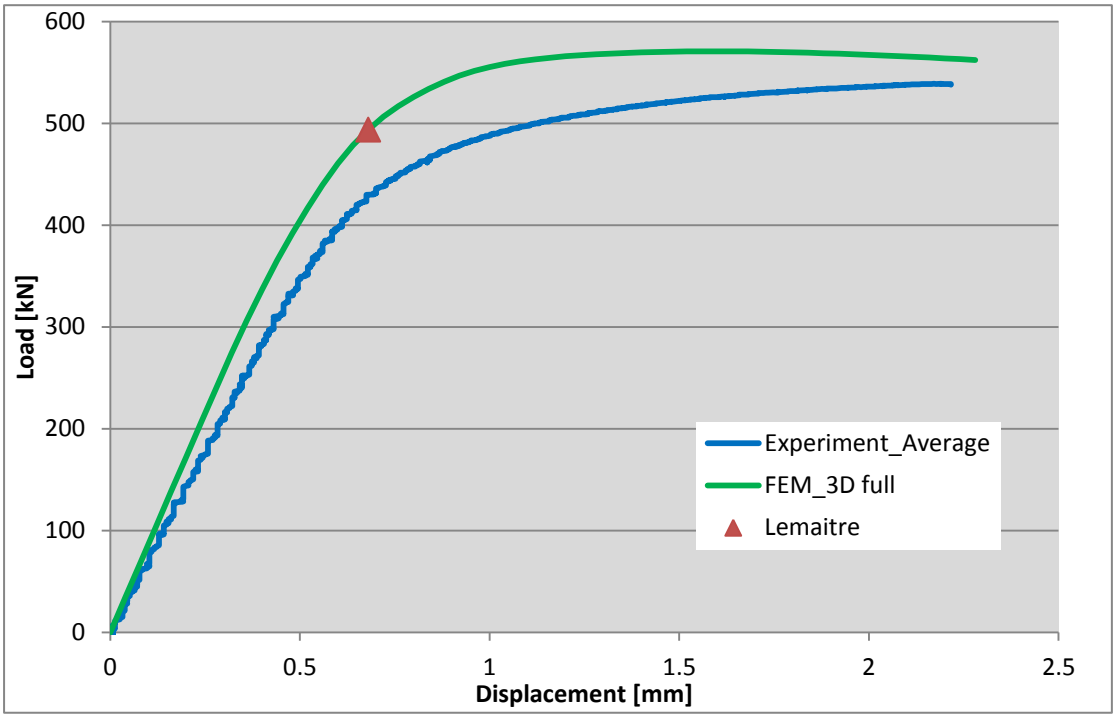

Figure 4.71: Comparison of experimental and numerical results for specimen 4C1

4.2.5 Specimen 5C1

Specimen 5C1 is a 40 mm thick S1100 undermatched specimen (Figure 4.72). The measured dimensions (Figure 4.73) show the smallest weld dimensions (25.8 mm).

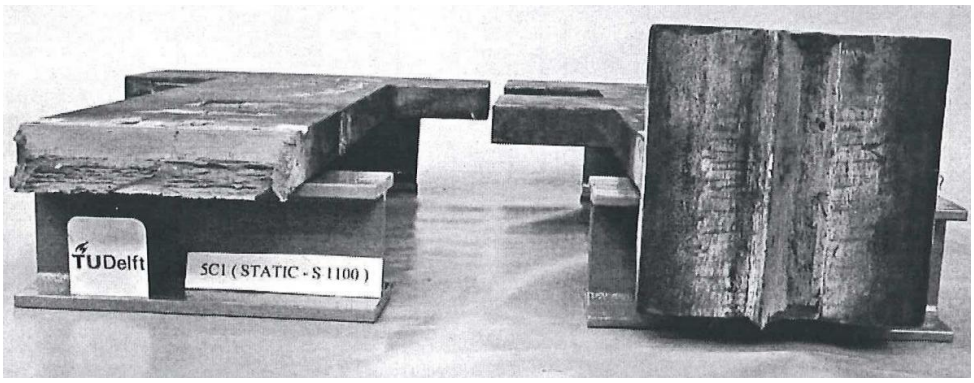

Figure 4.72: Specimen 5C1

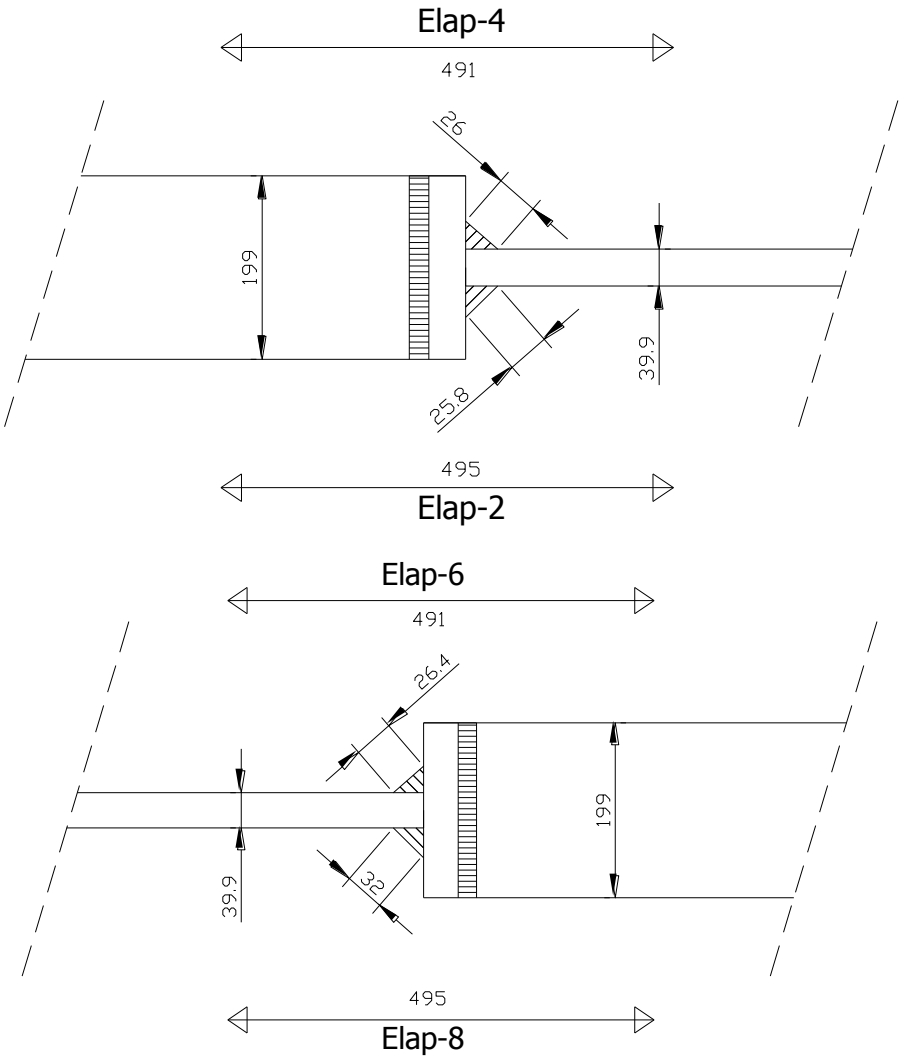

Figure 4.73: Measured dimensions specimen 5C1

The geometry and the mesh are shown in Figure 4.74, both the left and right parts are modeled with the same (smallest) weld size, the refinement is made near weld.

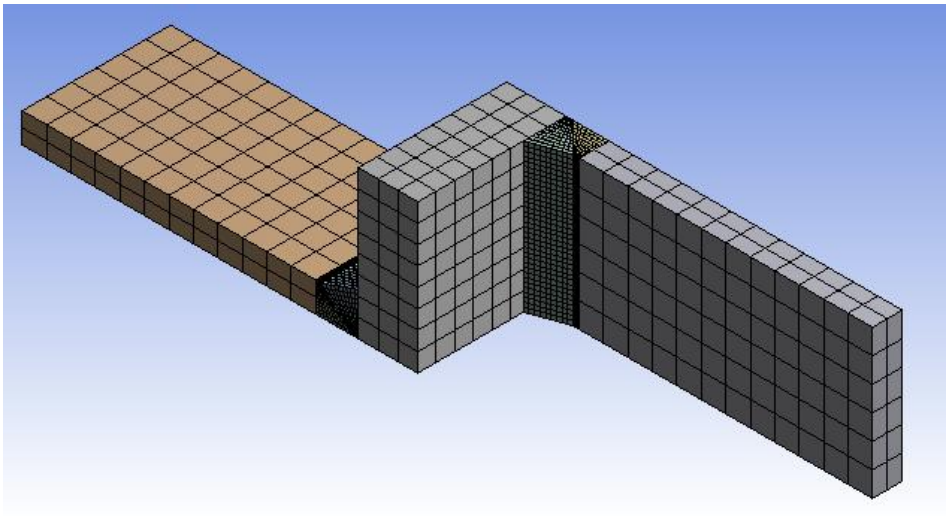

Figure 4.74: Geometry and mesh specimen 5C1, refined near weld, 3 mm

The influence of element size is checked and compared in Figure 4.75. The 3 mm element size near weld is used for the following analysis.

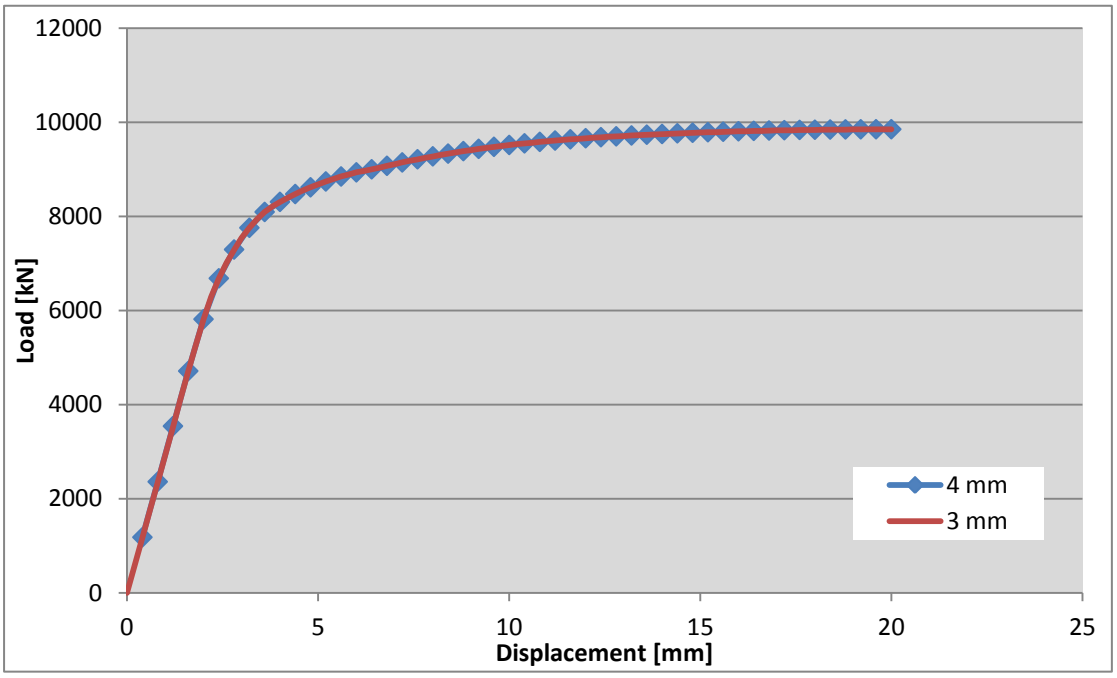

Figure 4.75: FE-analyses results of Specimen 5B1

The comparison of the numerical and experimental results is given in Figure 4.76. It seems that in the elastic range the analysis result has a slightly higher stiffness than the experimental result. Similar to specimen 5B1, due to the limitation of the element size, the deformation capacity seems quite inaccurate (fails in plate at a quite large displacement), again, it is considered that the specimen should fail in weld if the element size is small enough.

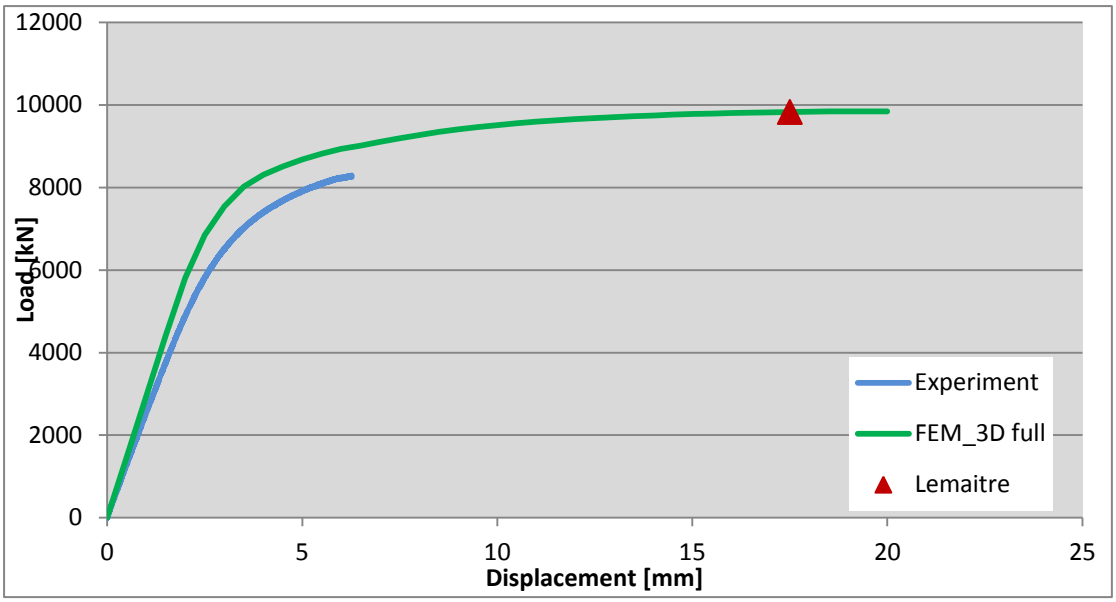

Figure 4.76: Comparison of experimental and numerical results for specimen 5B1

The distribution of the equivalent plastic strain at a displacement of 3 mm is given in Figure 4.77.

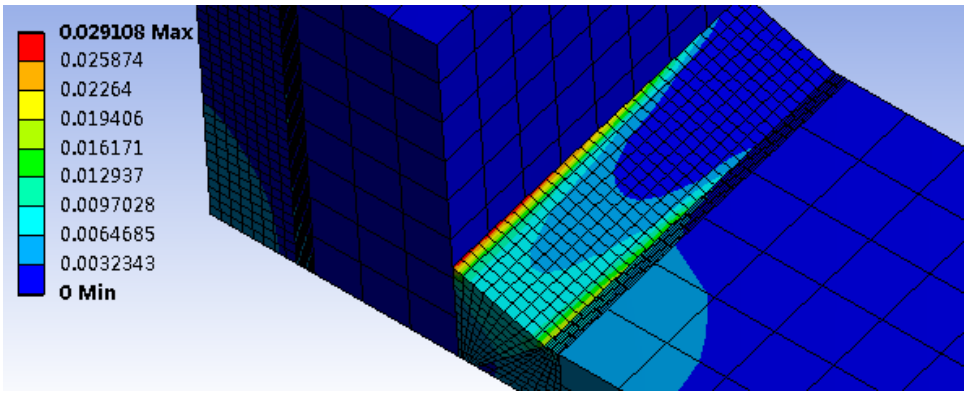

Figure 4.77: Equivalent plastic strain at a displacement of 3 mm

4.3 FEM result comparisons

Comparisons are made between B and C connections based on FE-analyses results to see the influence of the stress concentration.

4.3.1 Connection 1

Connection 1 is an S690 12 mm overmatched weld. Both B and C connections fail in plate. From Figure 4.78 several conclusions can be made:

1) In the elastic range two connections are identical;
2) The FE-analyses results show that the two connections have similar load-displacement curves;
3) C (high SCF) connection has a slightly lower yield strength and ultimate strength than B (low SCF) connection;
4) Failure according to Lemaitre's criterion gives comparable deformation capacity for two connections.

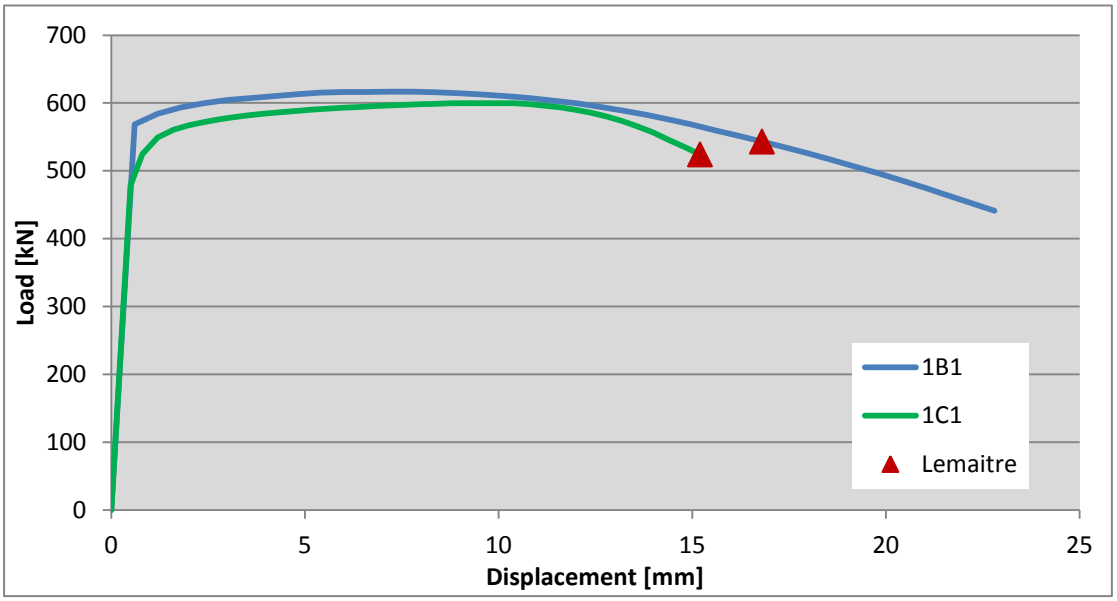

Figure 4.78: Comparison connection 1

4.3.2 Connection 2

Connection 2 is an S690 40 mm overmatched weld. Both B and C connections fail in plate. From Figure 4.79 several conclusions can be made:

1) In the elastic range two connections are identical;
2) The FE-analyses results show that the two connections have similar load-displacement curves;
3) C (high SCF) connection has a slightly lower yield strength and almost the same ultimate strength with B (low SCF) connection;
4) Failure according to Lemaitre's criterion gives comparable deformation capacity for two connections.

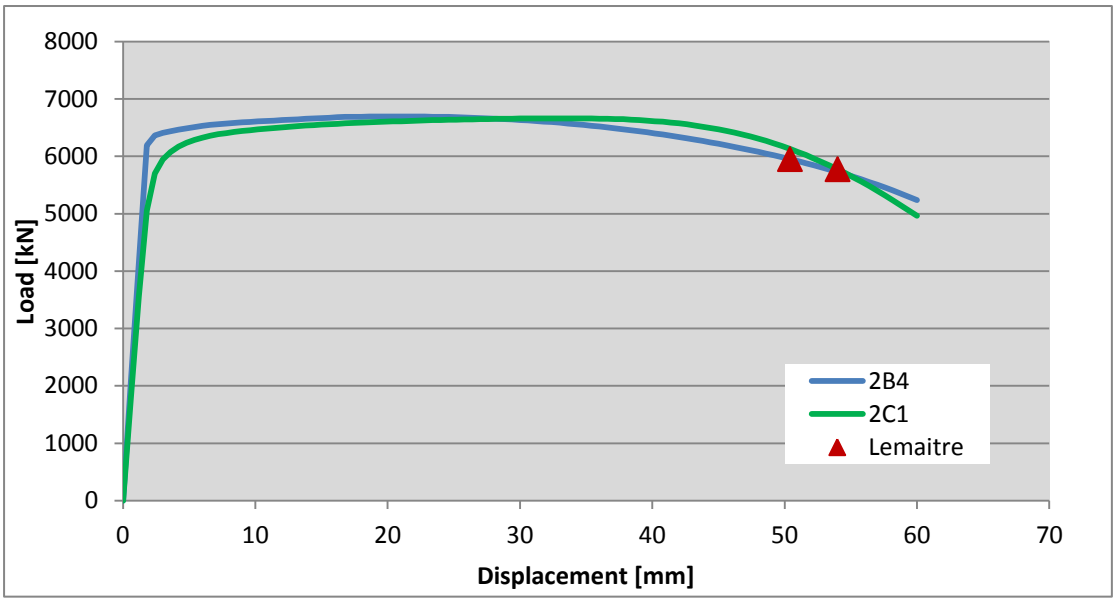

Figure 4.79: Comparison connection 2

4.3.3 Connection 3

Connection 3 is an S690 12 mm undermatched weld. B connection fails in plate and C connection fails in weld. From Figure 4.80 several conclusions can be made:

1) In the elastic range two connections are identical;

2) The FE-analyses results show that the two connections have similar load-displacement curves before failure;

3) C (high SCF) connection has a slightly lower yield strength and ultimate strength than B (low SCF) connection;

4) The SCF affects the failure mode in this case. Failure according to Lemaitre's criterion gives a very big difference. For specimen 3C1 which fails in weld, the deformation capacity is dramatically lower (around 70%, the element size might cause some calculation error) than the specimen fails in plate (3B1).

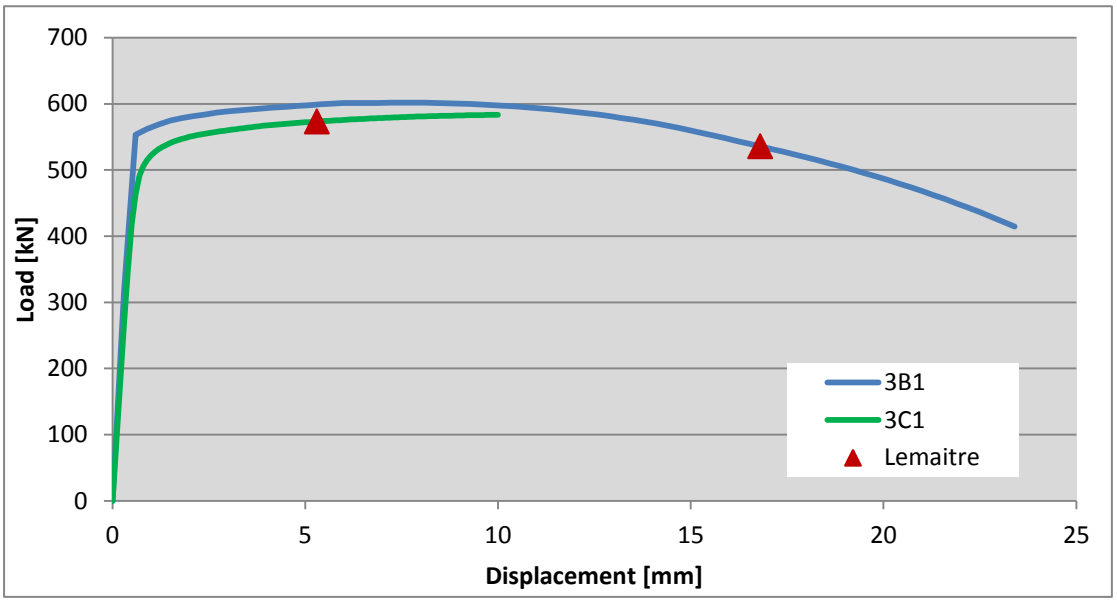

Figure 4.80: Comparison connection 3

4.3.4 Connection 4

Connection 4 is an S1100 10 mm undermatched weld. Both B and C connections fail in weld. From Figure 4.81 several conclusions can be made:

1) In the elastic range two connections are not identical, C connection has a smaller stiffness than B connection. This might because of the difference of the given weld dimensions;

2) The FE-analyses results show that the two connections have comparable load-displacement curves;

3) C (high SCF) connection has a lower yield strength and ultimate strength than B (low SCF) connection;

4) Failure according to Lemaitre's criterion has a difference. However, both specimens fail in weld, so both results are not accurate. To know an exact difference, a smaller element size is necessary.

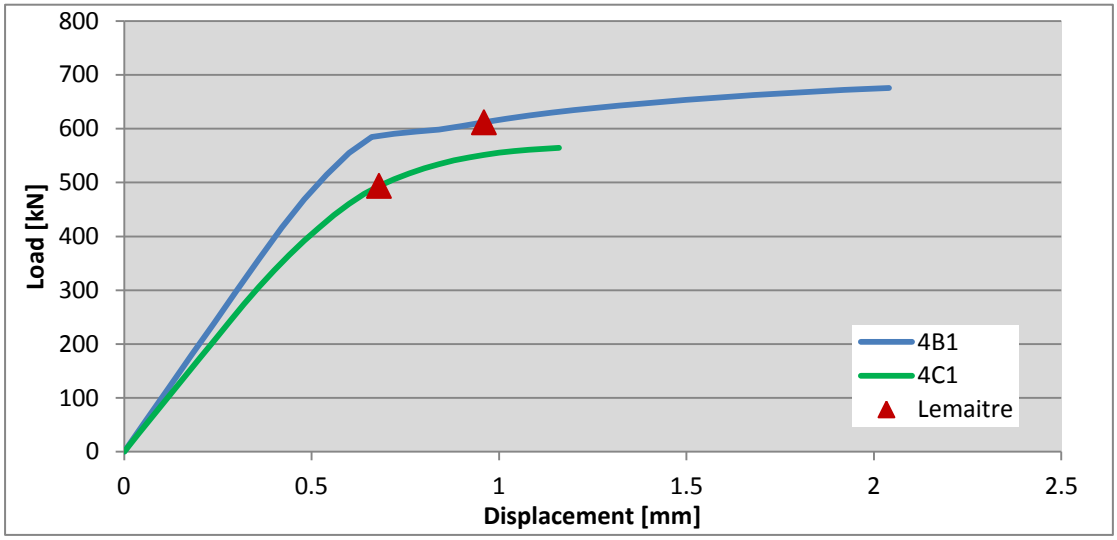

Figure 4.81: Comparison connection 4

4.3.5 Connection 5

Connection 5 is an S1100 40 mm undermatched weld. Due to the limitation of the element size, the failure deformation according to Lemaitre's criterion seems quite inaccurate, so it's not given here. From Figure 4.82 several conclusions can be made:

1) In the elastic range two connections are identical;

2) The FE-analyses results show that the two connections have similar load-displacement curves;

3) C (high SCF) connection has a slightly lower yield strength and ultimate strength than B (low SCF) connection.

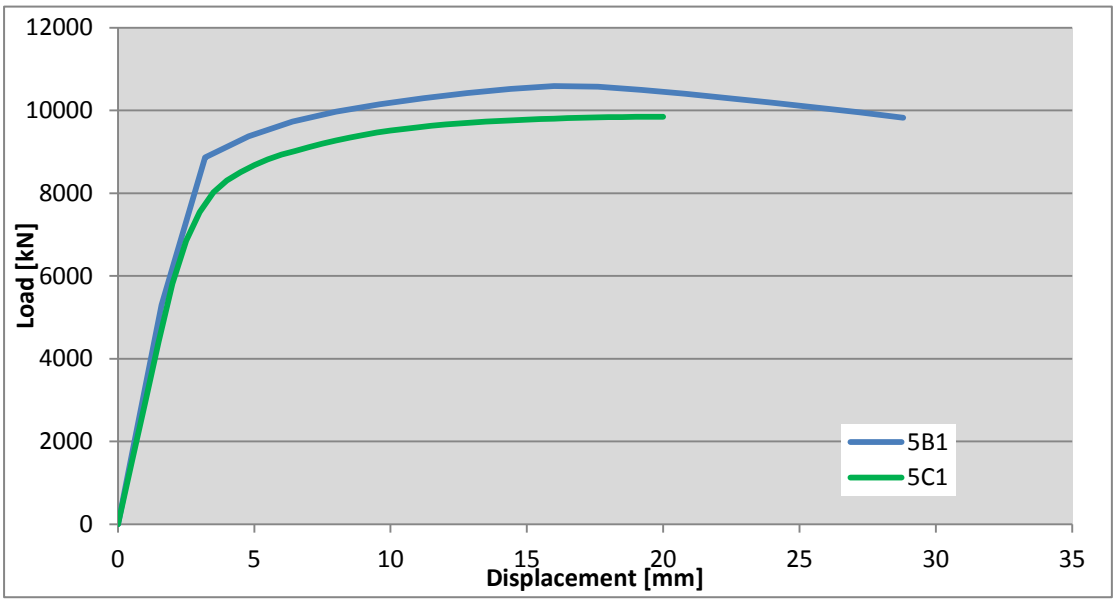

Figure 4.82: Comparison connection 5

5. Conclusions and recommendations

5.1 Conclusions

5.1.1 Validation of material input

- The material input can be numerically determined based on three real material properties (R_e, R_m and ε_u);
- The structural behavior is dependent on geometry and element size. The geometries used in simulations should be exactly the same as the ones in tests;
- Compared to 2D analyses, 3D analyses can give a more accurate result;
- Calibration of the true stress strain input will give an accurate simulation result. The true stress-strain input depends on the element size;

5.1.2 Validation of specimen tests

- The load-displacement FE-results are comparable to experimental results, the general trend is predicted very well. If specimen fails in plate, the failure load can be predicted accurately with the help of Lemaitre's criterion;
- In general the FEM model over predicted the ultimate strength (except specimen 4C1);
- In general the overmatched specimen will fail in plate and undermatched specimen will fail in weld. However, the undermatched specimen 3B1 fails in plate due to large weld reinforcement;
- For specimens that fail in plate the Lemaitre's criterion is less sensitive to element size, the deformation capacity based on the criterion can be accurately calculated;
- If the specimen fails in weld, the result of Lemaitre's criterion is highly related to the element size. Due to the limited computer performance, the element size is not small enough in this report. The deformation capacity can not be accurately predicted;

5.1.3 FEM result comparisons

- In general the specimens with high SCF have a slightly lower strength than specimens with low SCF;
- If both specimen B and specimen C fail in plate, the SCF seems only have a very limited influence on strength and deformation capacity;
- If the SCF affects the failure mode, then the deformation capacity will be dramatically affected. Specimen fails in weld will have a much lower deformation capacity than specimen fails in plate;
- For specimens that fail in weld, a smaller element size is needed to have an accurate result on deformation capacity.

5.2 Recommendations

- A more specific material data is needed to generate a more accurate material input;
- More accurate experimental results without error will be helpful to reduce the uncertainty of the validation results;
- The specimens' imperfections and flaws which occur during fabrication should be taken into account in the FE-analyses;
- HAZ, weld beads, surface irregularities and weld toe radii should also be taken into consideration;
- A smaller element size for specimens fail in weld is necessary;
- A detailed experimental and theoretical study with small scale specimens to validate or improve the failure criterion of Lemaitre is recommended;
- A parameter study on type B and C geometries with a more pronounced SCF for the C specimens by reducing the plate thickness is recommended (a brief study is given in Appendix C);
- Continue this investigation by validation connection type A.

References

[1] Lemaitre, J. (1985). A continuous damage mechanics model for ductile fracture. In *Journal of Engineering Materials and Technology*, *107, 83*.

[2] Dijkstra, O. D., & Kolstein, M. H. (2006). Numerical modeling of under matched welded high strength steel connections. In *Steel-a New and Traditional Material for Building: Proceedings of the International Conference in Metal Structures, Poiana Brasov, Romania, September 20-22, 2006* (p. 119). Taylor & Francis.

[3] Kolstein, M. H., Bijlaard, F. S. K., & Dijkstra, O. D. (2006). Integrity of welded joints made of steel grades S690 and S1100. In *Steel-a New and Traditional Material for Building: Proceedings of the International Conference in Metal Structures, Poiana Brasov, Romania, September 20-22, 2006* (p. 183). Taylor & Francis.

[4] Kolstein, M.H. (2005). Integrity of high strength steel structures, Part 1: Experiments'. In *Stevin report 6-05-6.* Delft Stevin University of Technology, The Netherlands.

[5] Kolstein, M.H., Dijkstra, O.D. (2005). Integrity of high strength steel structures, Part 2: Analysis of the experiments'. In *Stevin report 6-05-7.* Delft Stevin University of Technology, The Netherlands.

[6] Integrity of high strength steel structures – Deformation capacity. In *TNO report 2005-BCS-R0367.*

[7] Integrity of high strength steel structures – pilot FEM analyses. In *TNO report 2004-BC-R0054.*

[8] Integrity of high strength steel structures – Validation FEM analyses. In *TNO report 2005-BCS-R0446.*

[9] Integrity of high strength steel structures – Analytical model for welded connection. In *TNO report 2005-BCS-R0366.*

[10] Integrity of high strength steel structures – Parameter studies for welded X-Connections using 2D FEM analyses. In *TNO report 2005-BCS-R0368.*

[11] Pakiding, L. (2007). Design criteria for high strength steel joints. Master report report. Delft University of Technology, the Netherlands.

[12] Fabricius, A. (2009). Experimental and numerical analysis of the deformation capacity of high strength steel. Master report report. Delft University of Technology, the Netherlands.

[13] Joun, M., Eom, J.G., & Lee, M.C. (2008). A new method for acquiring true stress-strain curves over a large range of strains using a tensile test and finite element method. In *Mechanics of Materials, 2008, 40(7): 586-593.*

Appendices

A. Hardening rule [11]

Hardening rule is a phenomenon where yield stress increases with further plastic straining. There are several types of hardening rules which had been proposed in order to define the modification of the yield surface during plastic deformation. For example, isotropic hardening, kinematic hardening and mixed hardening which is the combination of both hardening. In the following section only the first two will be explained.

A.1 Isotropic hardening

This hardening rule assumed that the initial yield surface expands uniformly without distortion and translation as plastic flow occurs. The size of the yield surface is governed by the plastic strain history. Figure A.1 shows the representation of this hardening rule.

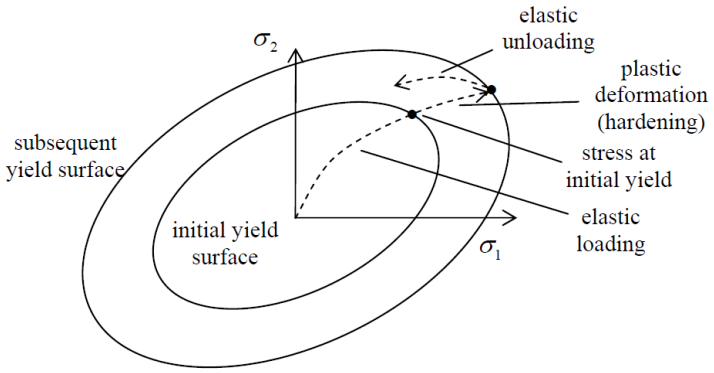

Figure A.1: Isotropic hardening

A.2 Kinematic hardening

The kinematic hardening assumes that the yield surface translate in the stress space during plastic deformation as a rigid body which means the size, shape and orientation of the surface is the same as before plastic deformation occurs and it is shown in Figure A.2. This hardening rule takes into account the Bauschinger effect which is not considered in isotropic hardening rule.

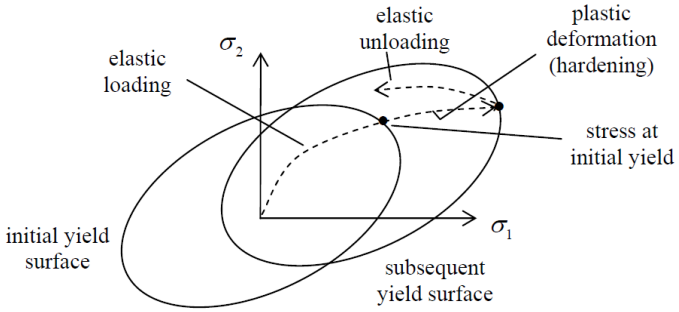

Figure A.2: Kinematic hardening

B. Material input

B.1 S690 40 mm plate

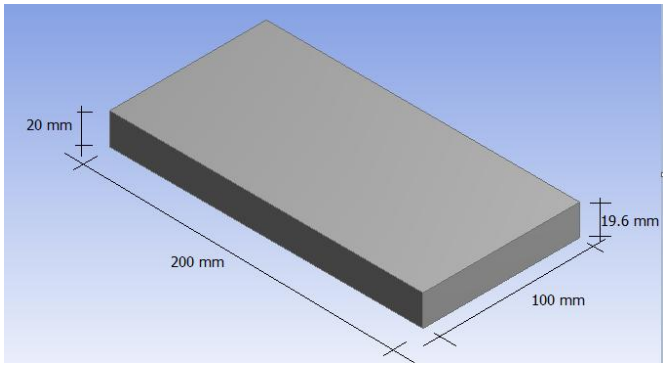

Figure B.1: Simulation geometry for 40 mm thickness plate

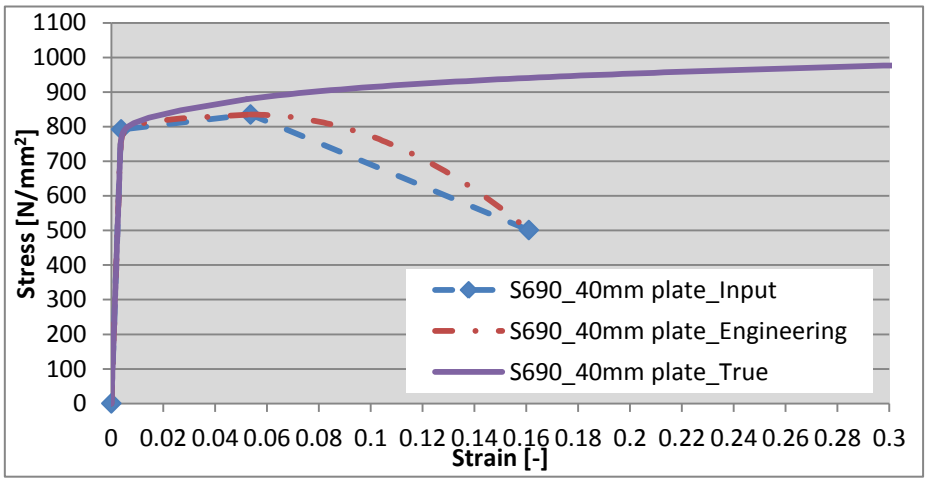

Figure B.2: Modified stress strain curves, S690 40 mm plate

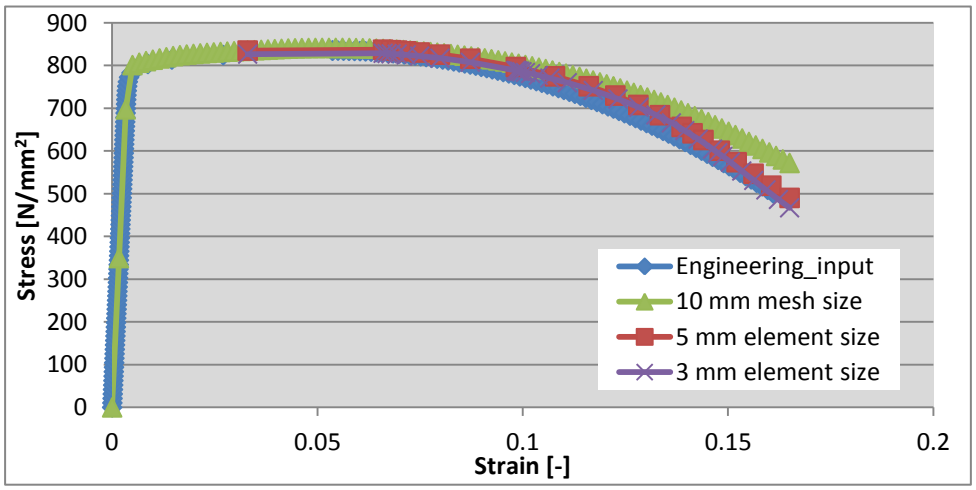

Figure B.3: Element size tests, S690 40 mm plate

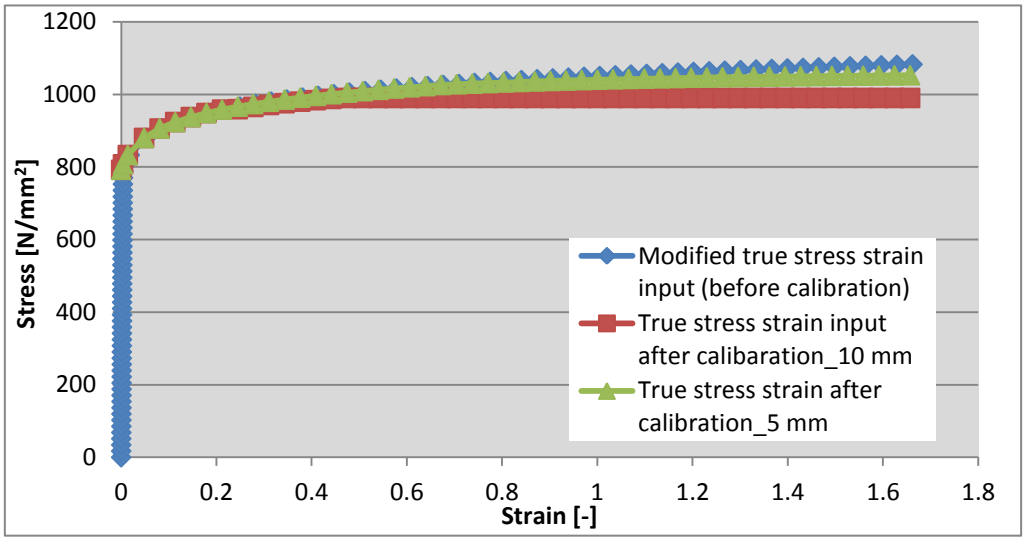

Figure B.4: Comparison of true stress strain input after calibration, S690 40mm plate

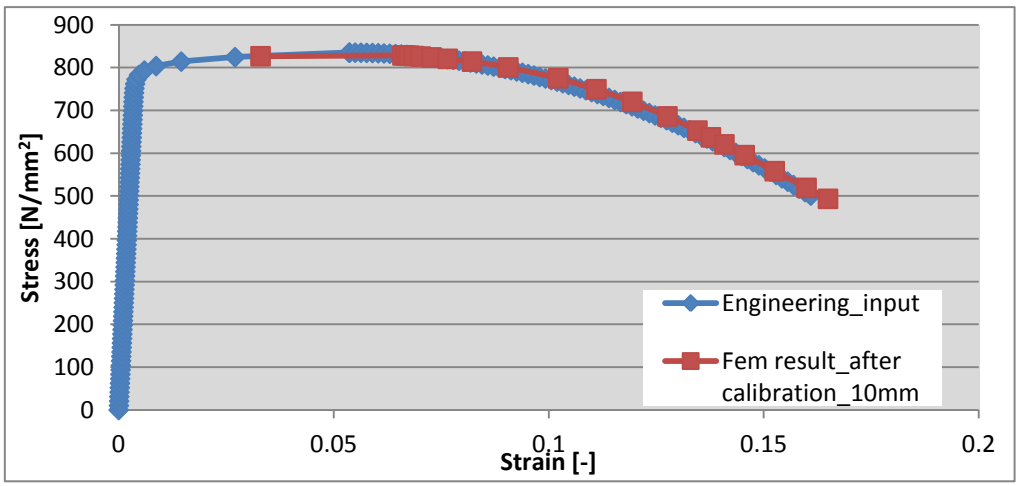

Figure B.5: FEM result after calibration, S690 40 mm plate, mesh size: 10 mm

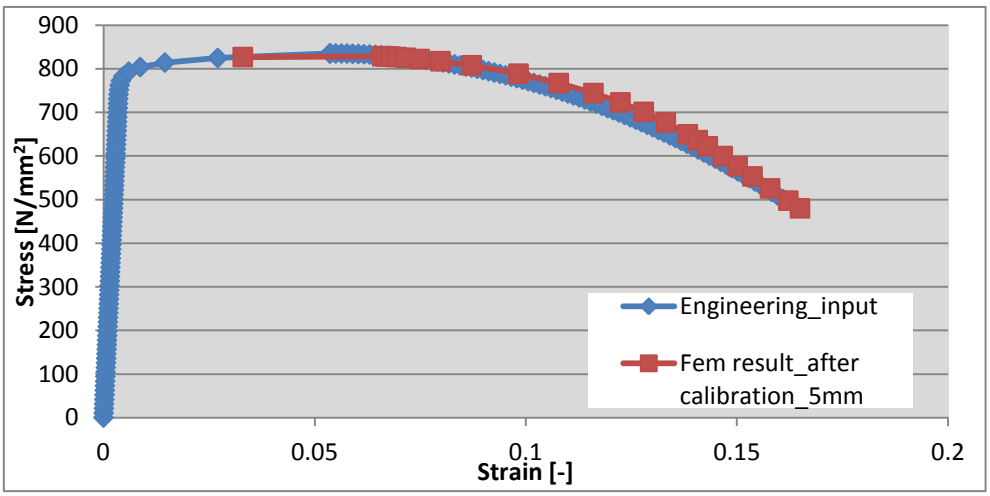

Figure B.6: FEM result after calibration, S690 40 mm plate, mesh size: 10 mm

For any element size smaller than 5 mm, the 5 mm input is adapted for subsequent numerical simulations.

B.2 S1100 10 mm plate

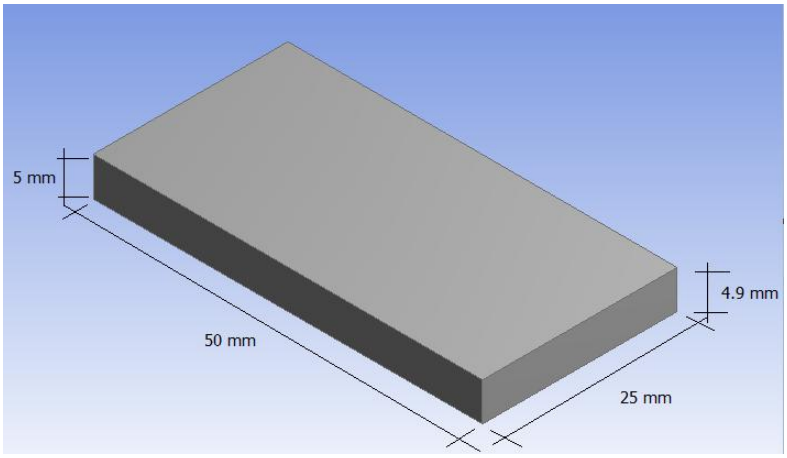

Figure B.7: Simulation geometry for 10 mm thickness plate

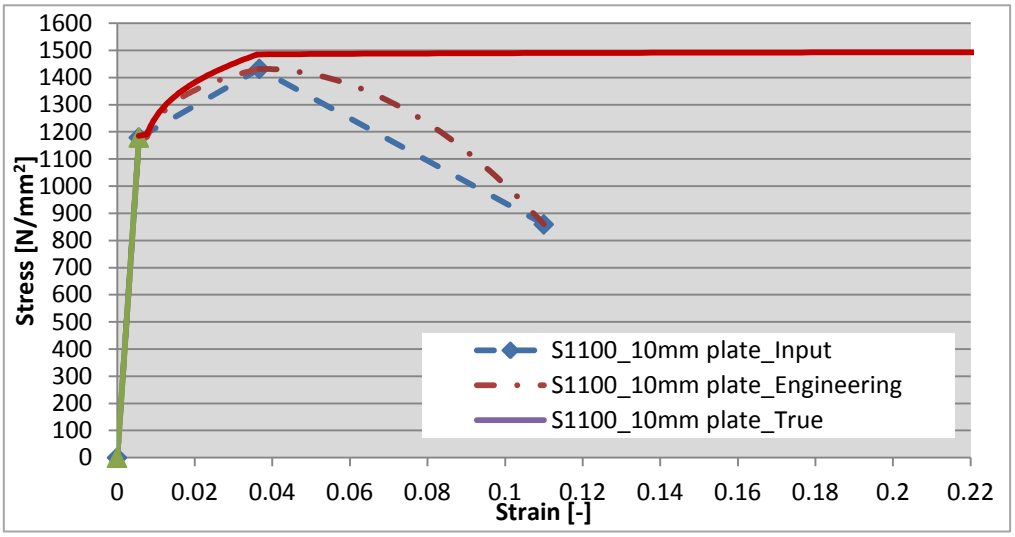

Figure B.8: Modified stress strain curves, S1100 10 mm plate

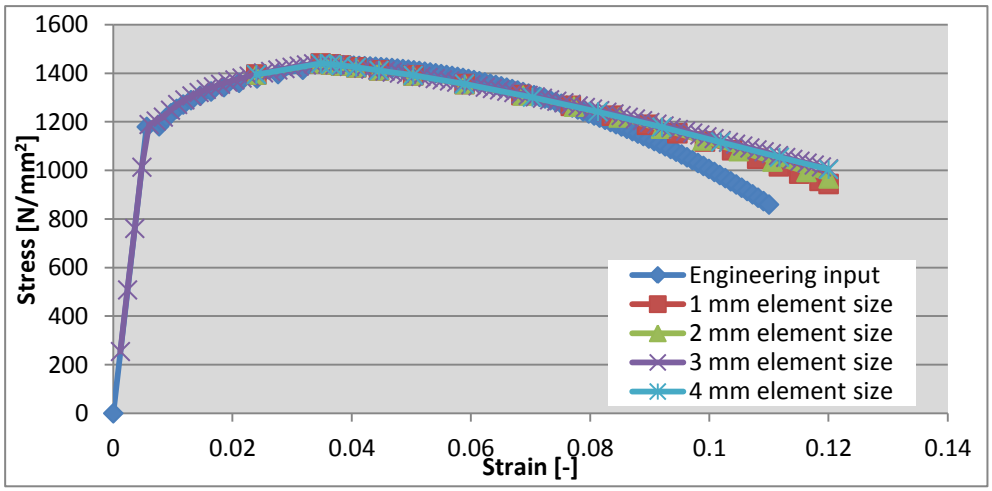

Figure B.9: Element size tests, S1100 10 mm plate

ANSYS doesn't allow a downward input for plastic hardening part of the material, so this material can't be calibrated, the modified true stress strain curve will be used for this material.

B.3 S1100 40 mm plate

The geometry is the same as S690 40 mm plate.

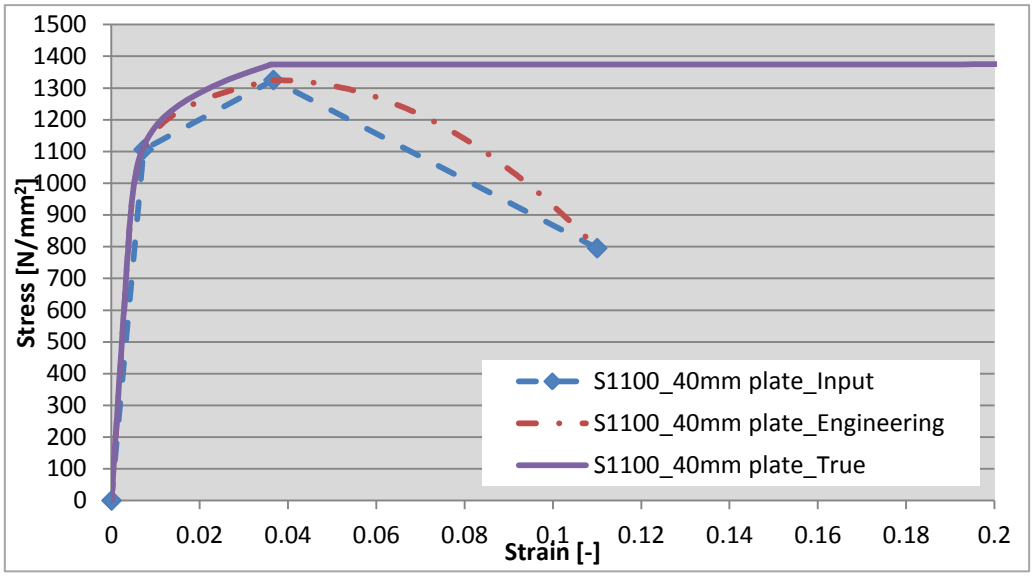

Figure B.10: Modified stress strain curves, S1100 40 mm plate

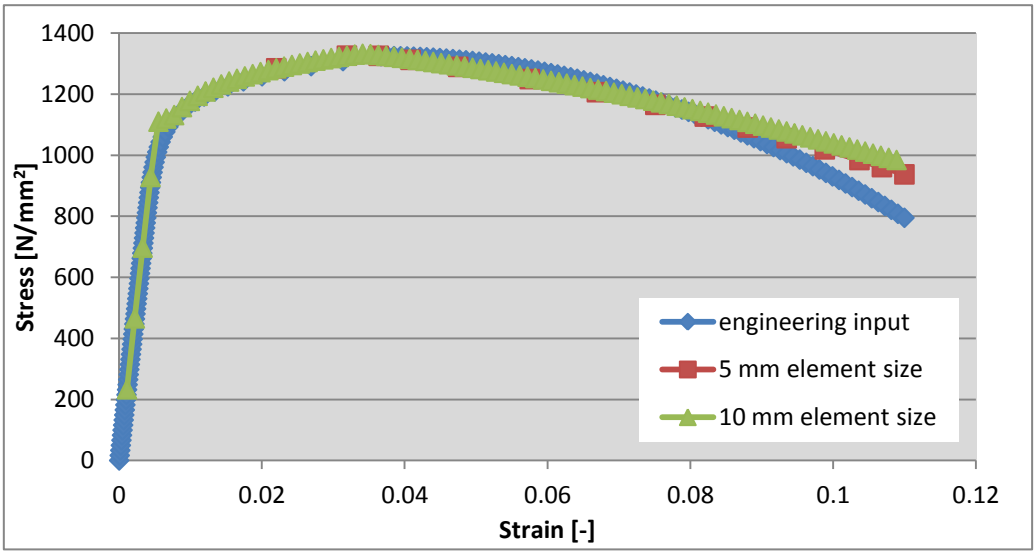

Figure B.11: Element size tests, S1100 40 mm plate

ANSYS doesn't allow a downward input for plastic hardening part of the material, so this material can't be calibrated, the modified true stress strain curve will be used for this material.

B.4 S690 12 mm undermatched weld

All the weld geometries are considered the same as corresponding plate sizes.

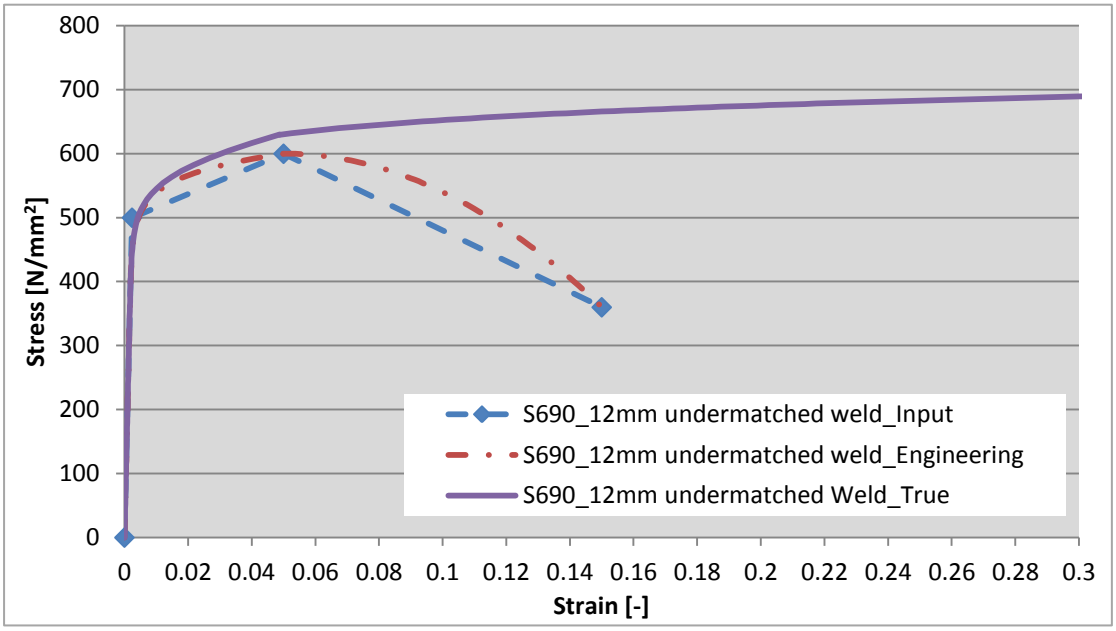

Figure B.12: Modified stress strain curves, S690 12 mm undermatched weld

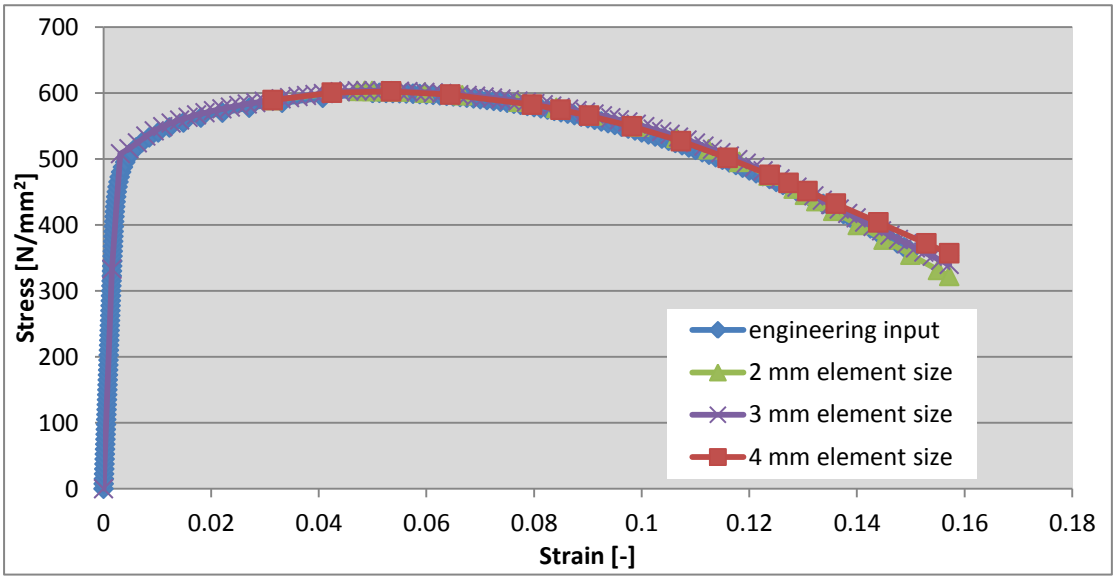

Figure B.13: Element size tests, S690 12 mm undermatched weld

From the element size tests, it seems that a calibration is not necessary, so the modified true stress strain curve will be used for this material.

B.5 S690 12 mm overmatched weld

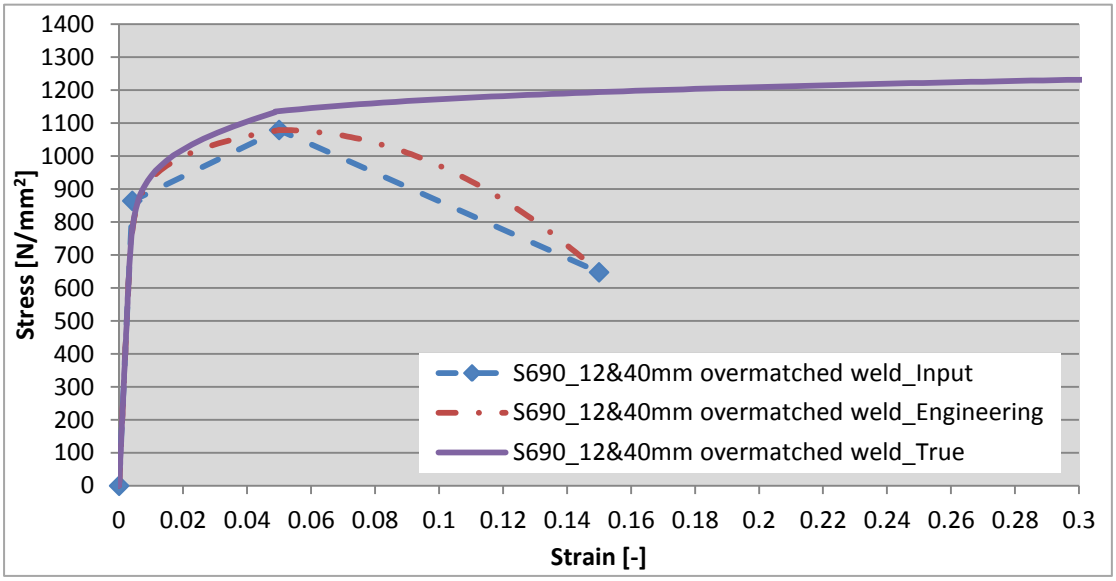

Figure B.14: Modified stress strain curves, S690 12 mm overmatched weld

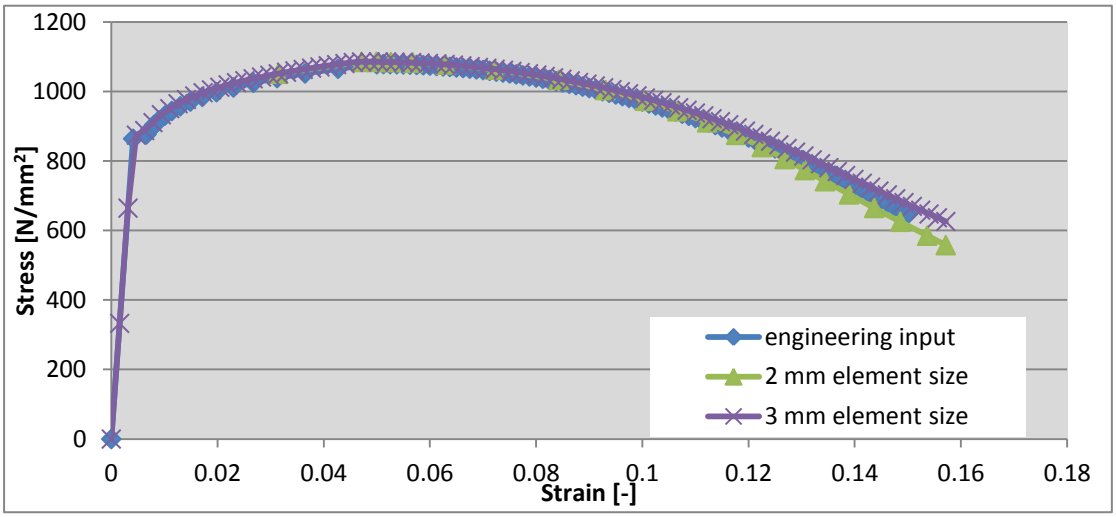

Figure B.15: Element size tests, S690 12 mm overmatched weld

From the element size tests, it seems that a calibration is not necessary, so the modified true stress strain curve will be used for this material.

B.6 S690 40 mm overmatched weld

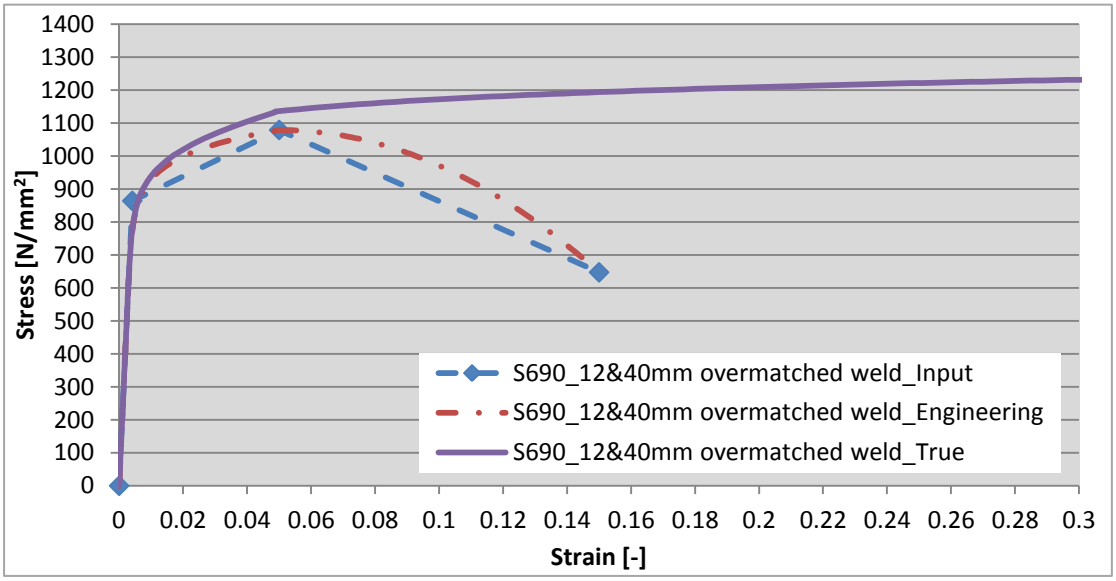

Figure B.16: Modified stress strain curves, S690 40 mm overmatched weld

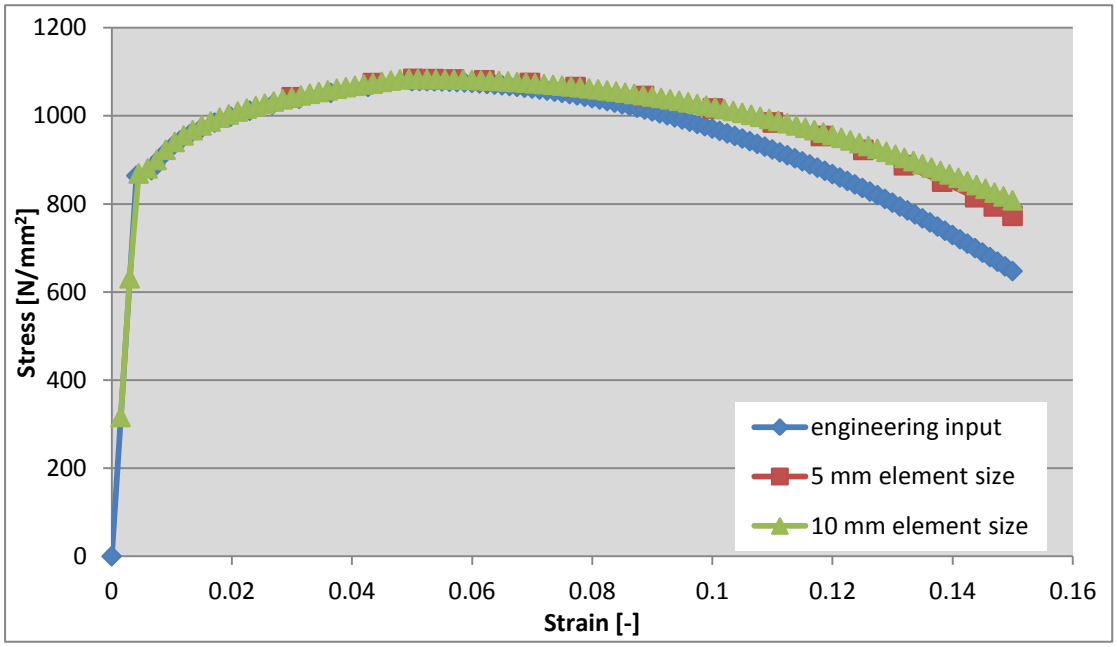

Figure B.17: Element size tests, S690 40 mm overmatched weld

From the element size tests, it seems that for both 5 mm and 10 mm element sizes, only one calibration is enough.

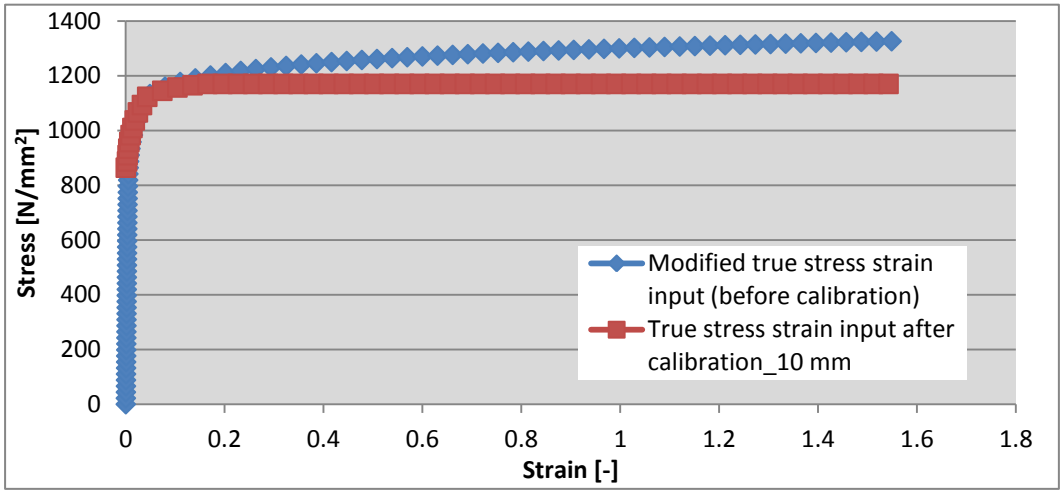

Figure B.18: Comparison of true stress strain input after calibration, S690 40 mm overmatched weld

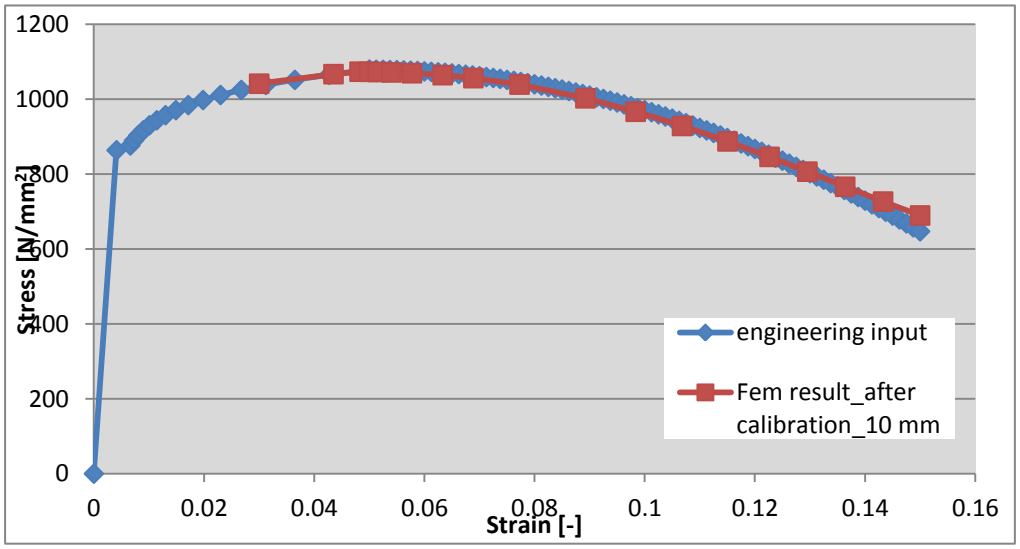

Figure B.19: FEM result after calibration, S690 40 mm overmatched weld, mesh size: 10 mm

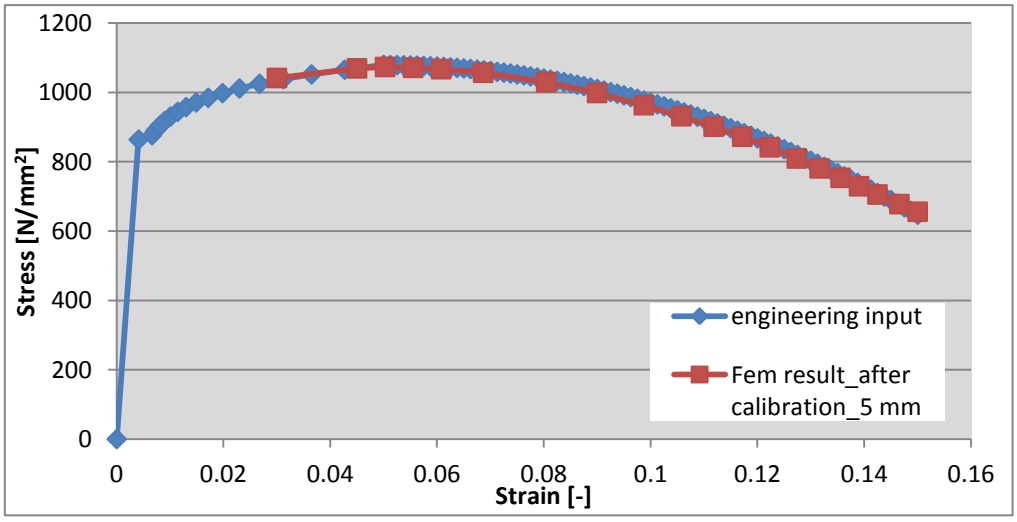

Figure B.20: FEM result after calibration, S690 40 mm overmatched weld, mesh size: 5 mm

For any element sizes smaller than 10 mm, the 10 mm input is adapted for subsequent numerical simulations.

B.7 S1100 10 mm undermatched weld

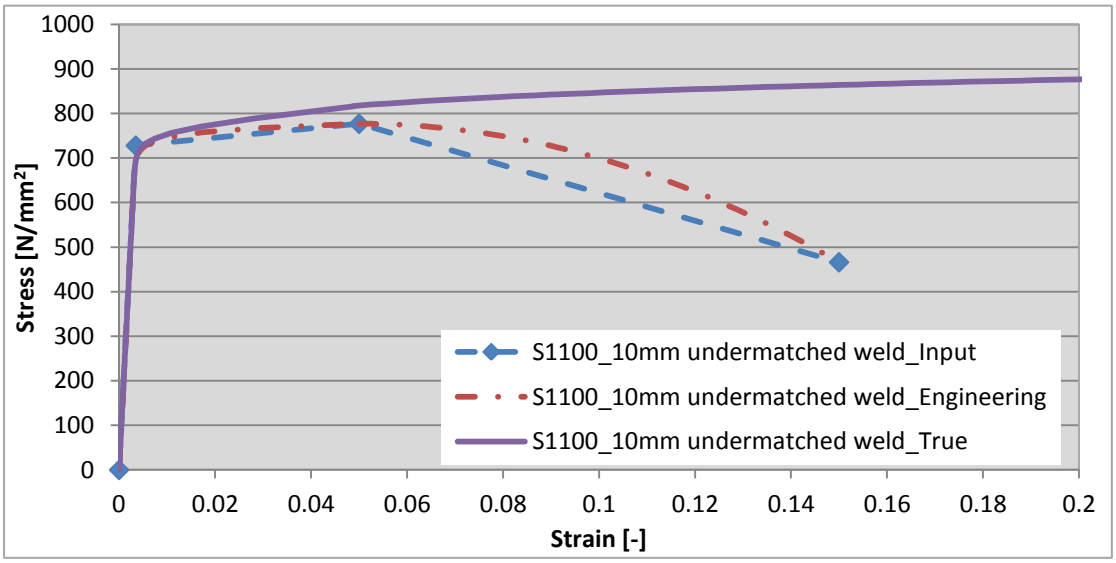

Figure B.21: Modified stress strain curves, S1100 10 mm undermatched weld

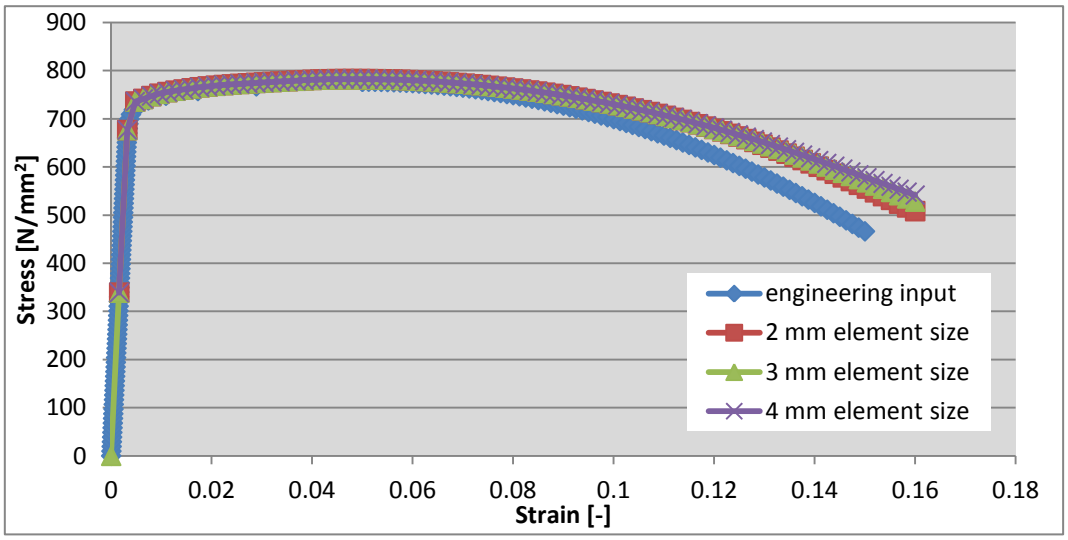

Figure B.22: Element size tests, S1100 10 mm undermatched weld

From the element size tests, it seems that for 2 mm, 3mm and 4 mm element sizes, only one calibration is enough.

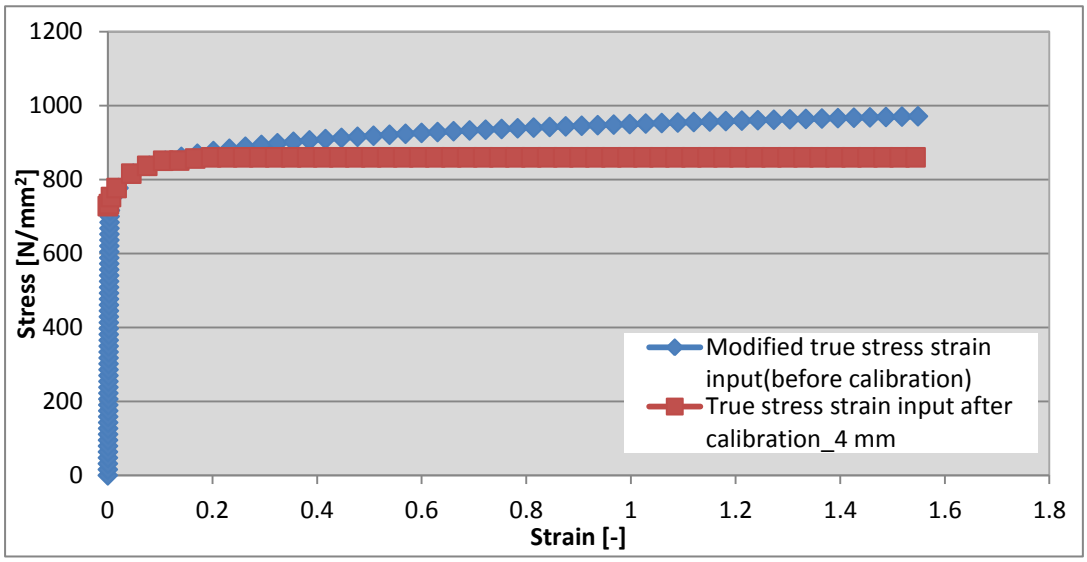

Figure B.23: Comparison of true stress strain input after calibration, S1100 10 mm undermatched weld

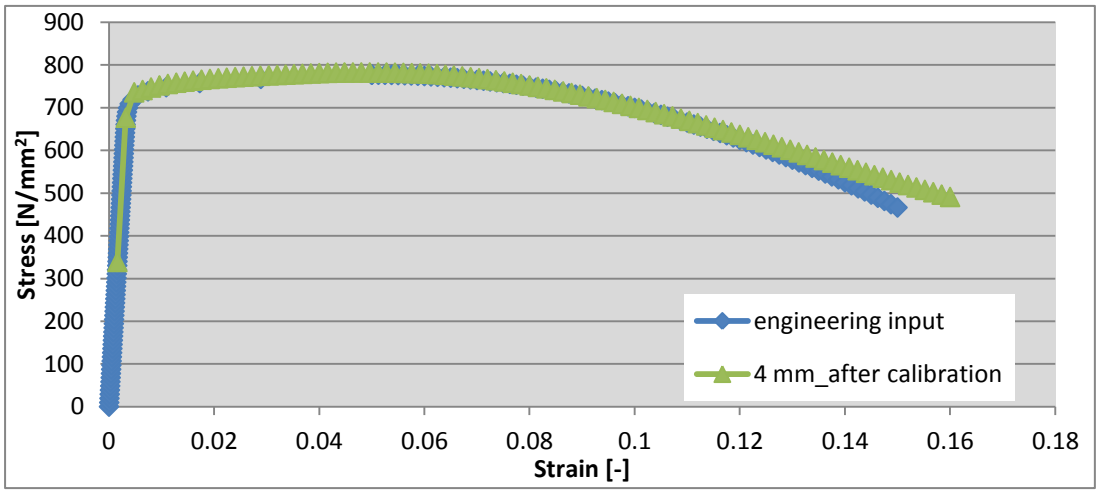

Figure B.24: FEM result after calibration, S1100 10 mm undermatched weld, mesh size: 4 mm

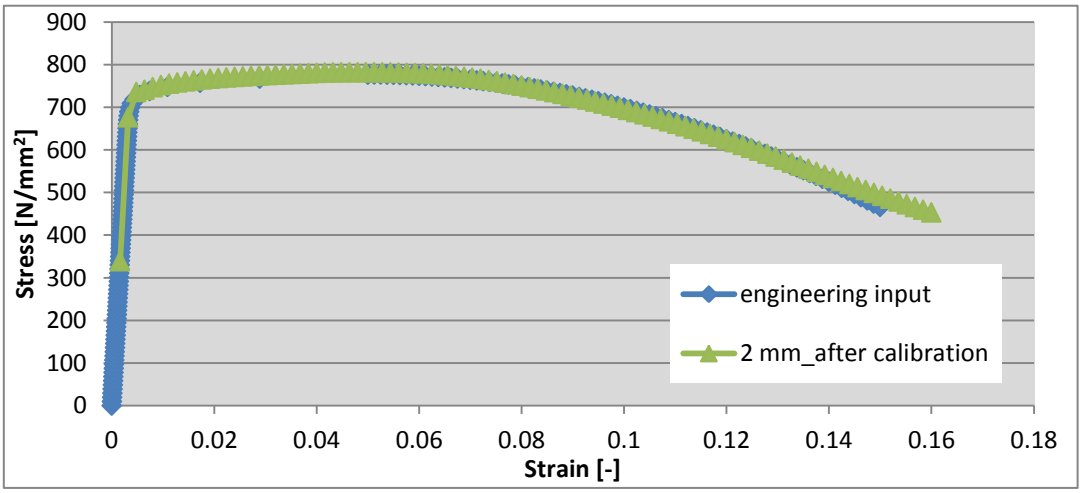

Figure B.25: FEM result after calibration, S1100 10 mm undermatched weld, mesh size: 2 mm

For any element sizes smaller than 4 mm, the 4 mm input is adapted for subsequent numerical simulations.

B.8 S1100 40 mm undermatched weld

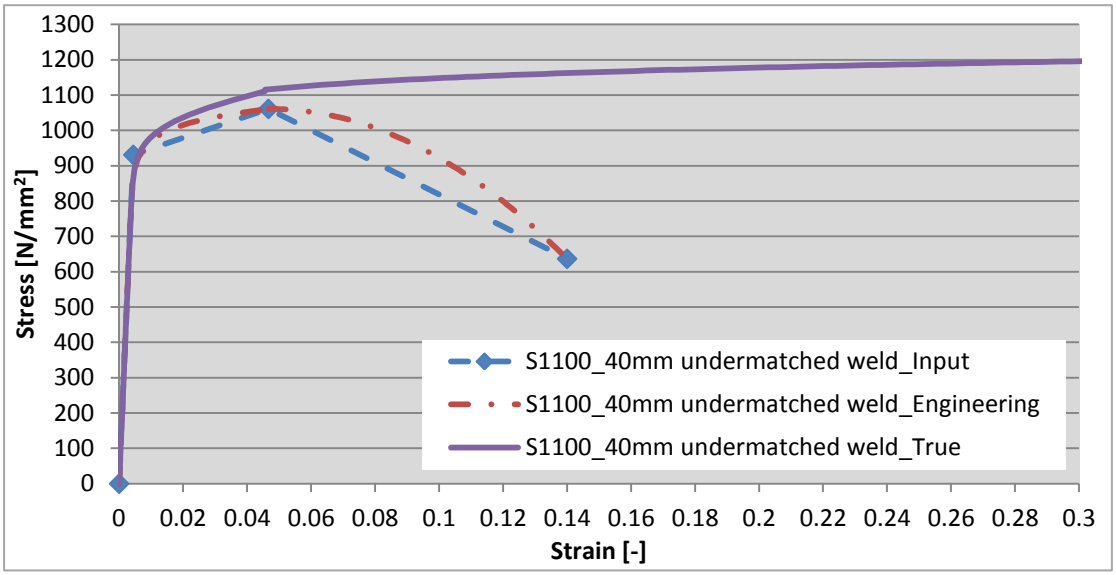

Figure B.26: Modified stress strain curves, S1100 40 mm undermatched weld

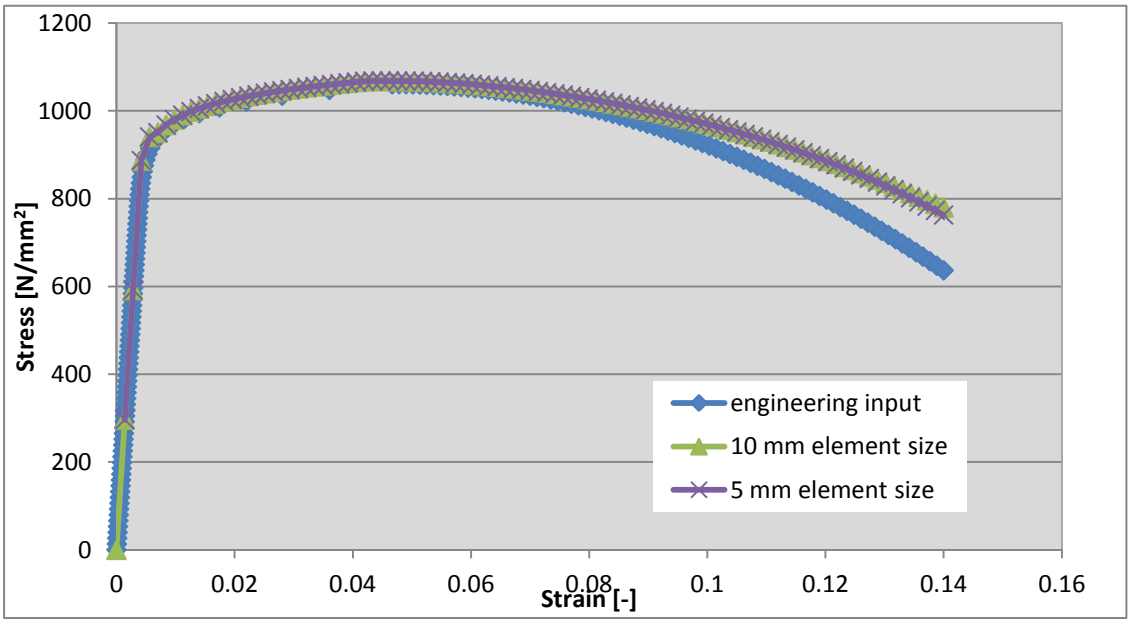

Figure B.27: Element size tests, S1100 40 mm undermatched weld

From the element size tests, it seems that for both 10 mm and 5 mm element sizes, only one calibration is enough.

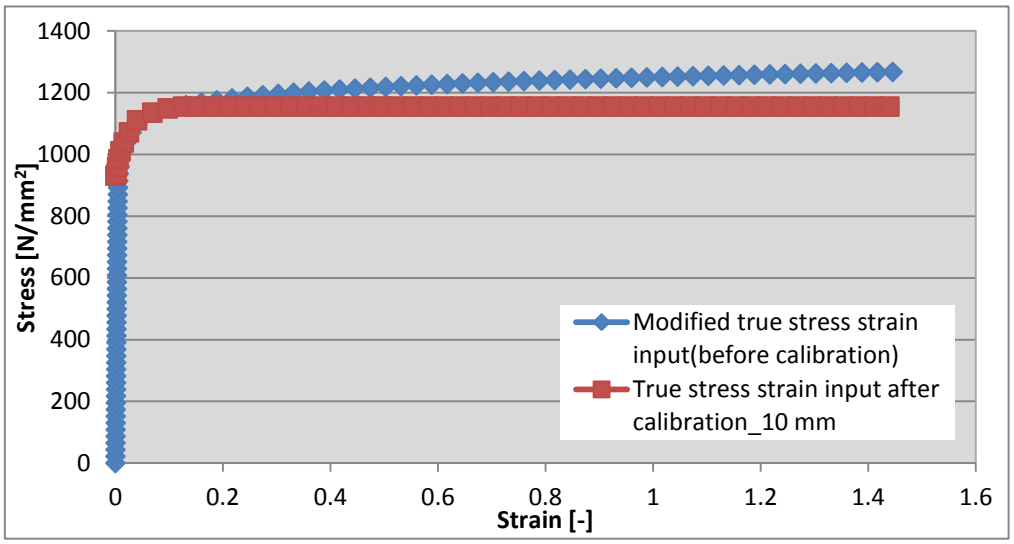

Figure B.28: Comparison of true stress strain input after calibration, S1100 40 mm undermatched weld

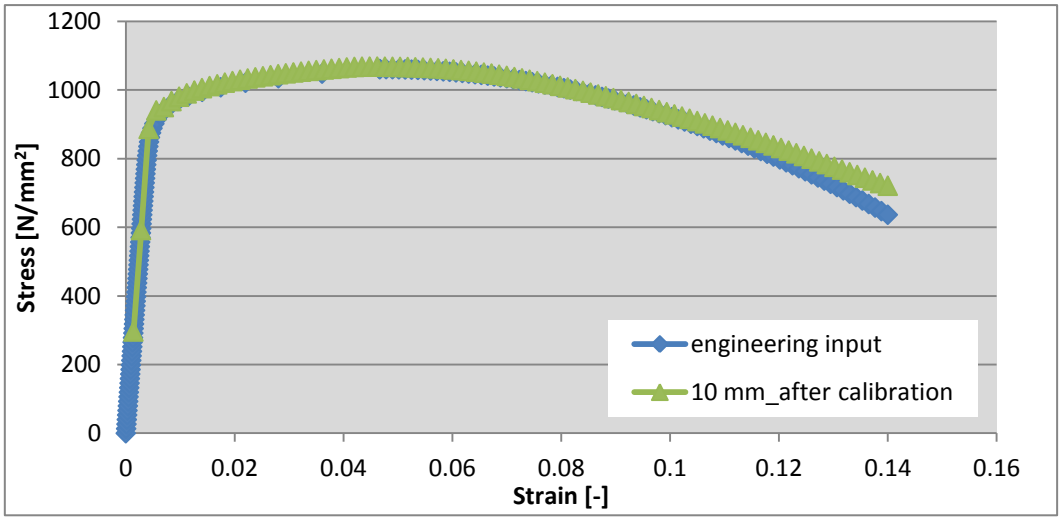

Figure B.29: FEM result after calibration, S1100 40 mm undermatched weld, mesh size: 10 mm

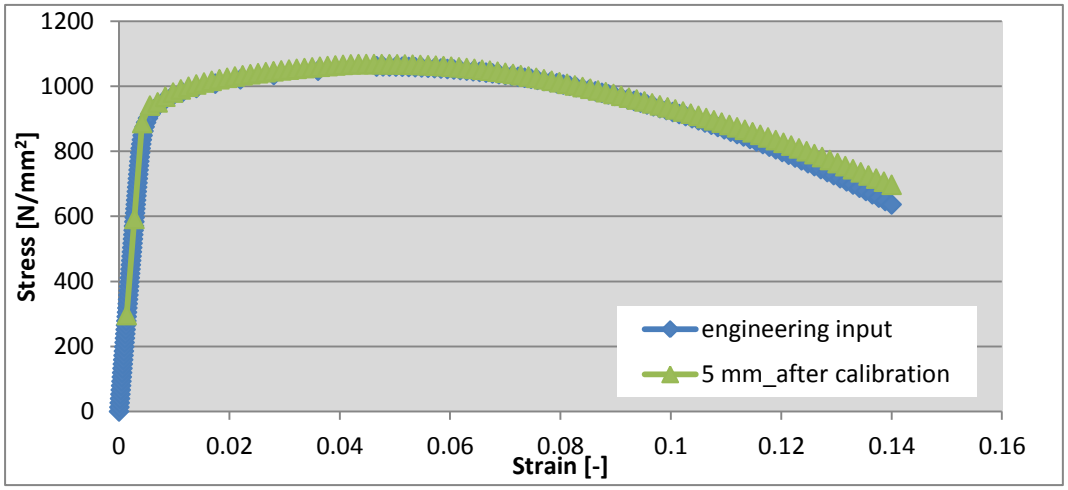

Figure B.30: FEM result after calibration, S1100 40 mm undermatched weld, mesh size: 5 mm

For any element sizes smaller than 10 mm, the 10 mm input is adapted for subsequent numerical simulations.

C. Parameter study

The parameter study was made in 2 ways: reduce the end plates' thickness and reduce the connection plate's thickness. The specimen 2C1 was used as an example.

C.1 Reduce the end plates' thickness

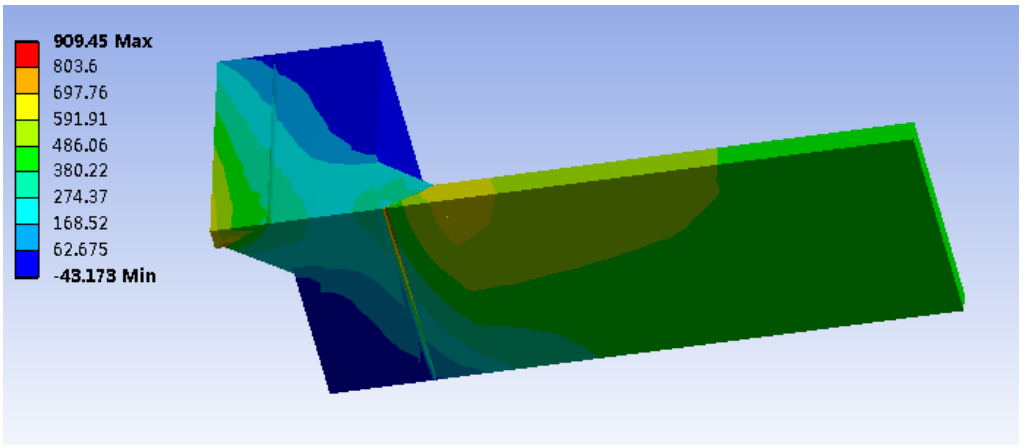

Figure C.1: Normal stress result, half of the end plates' thickness of specimen 2C1 (20 mm)

C.2 Reduce the connection plate's thickness

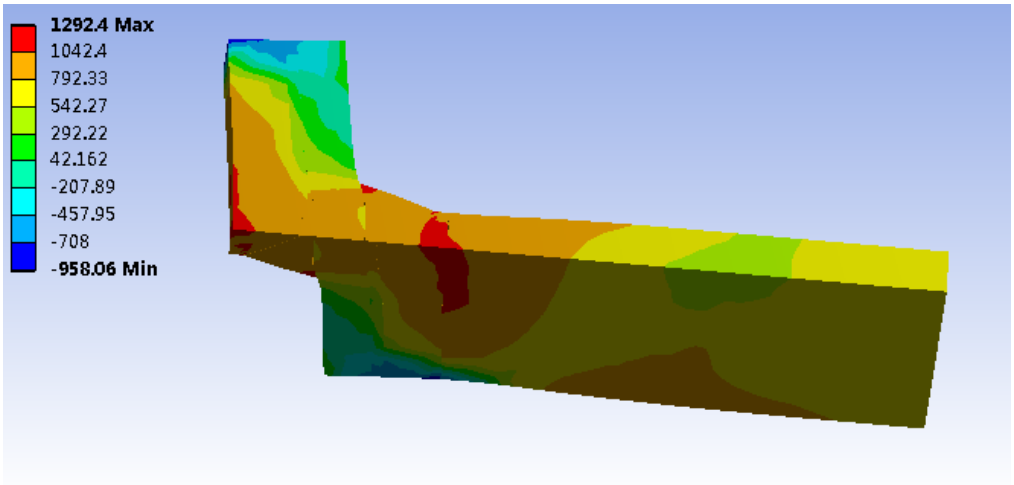

Figure C.2: Normal stress result, half of the connection plate's thickness of specimen 2C1 (20 mm)

From the parameter study we can see that the SCF is actually more pronounced, a more extensive parameter study is recommended.